Compression oriented enhancement of noisy images: Application to ultrasound images

Meriem Outtas

N° d'ordre : 10/2019-C/ELC

République Algérienne Démocratique et Populaire
Ministère de l'Enseignement Supérieur et de la Recherche Scientifique
Université des Sciences et de la Technologie Houari Boumediene
Faculté d'Electronique et d'Informatique

THESE

Présentée pour l'obtention du Diplôme de Doctorat
En : ELECTRONIQUE
Spécialité: Traitement du Signal et des Images
Par:

OUTTAS Meriem

Thème

Compression orientée restauration des images bruitées : application aux images échographiques

Soutenue publiquement, le **06.04.2019,** devant le jury composé de :

Mme A.KOURGLI	Professeur à l'U.S.T.H.B	Présidente
Mme A.SERIR	Professeur à l'U.S.T.H.B	Directrice de Thèse
M O.DEFORGES	Professeur à l'INSA Rennes	Co-Directeur de Thèse
M S.AOUAT	Professeur à l'U.S.T.H.B	Examinatrice
Mme F.SOUAMI	Maitre de conférences/A à l'U.S.T.H.B / F.E.I	Examinatrice
M S.A. FEZZA	Maitre de conférences/A à l'INTTIC Oran	Examinateur
M W.HAMIDOUCHE	Maitre de conférences à l'INSA Rennes	Invité

Dedicated to
my parents,
my brothers,
the memory of my uncle,
my nephews Kinane and Melina,
my two lovely children Nihel and Achraf,
and my dear husband and great support Lyes

Contents

Résumé

Le diagnostic médical est fortement basé sur différentes modalités d'imagerie médicale. En conséquence, la quantité de données d'images numériques à stocker ou à transmettre est considérable. Il devient nécessaire de développer des solutions de compression efficace et peu complexe. La compression d'images médicales "intuitivement " exige d'assurer une qualité de l'image diagnostique qui n'engendre pas de risques d'erreur. Par ailleurs, l'échographie est l'une des modalités les plus utilisées. Cependant, elle présente un inconvénient en terme de qualité visuelle causé par le bruit de speckle. Ce travail vise à réduire le bruit de speckle tout en effectuant une compression avec pertes des images échographiques. Aussi, le schéma de compression proposé a été appliqué à une seconde modalité, l'imagerie par résonance magnétique (IRM). En effet l'IRM est une modalité gourmande en termes de capacité de stockage. Durant cette thèse, nous avons proposé trois contributions principales : un filtre à sorties multiples pour la réduction du speckle des images d'échographie médicale, une mesure de la qualité d'image pour l'imagerie médicale (échographie et IRM) et un schéma de compression pour les images médicales.

Abstract

The medical diagnosis is strongly based on different medical imaging modalities. Consequently, the amount of digital image data to be stored or transmitted is huge. Hence, efficient and low-complexity compression becomes necessary. Medical image compression "intuitively" requires ensuring the quality of the diagnostic image while reducing the bit rate. Regarding the modalities, ultrasound is one of the most widely used one. However, it has a drawback of visual quality caused by the speckle noise. This work aims to achieve speckle noise reduction together with lossy compression in ultrasound medical images, where the losses are mainly the undesirable speckle noise. Furthermore, the proposed compression scheme is efficiently applied to Magnetic Resonance Images(MRI).

In this thesis we propose three main contributions: a multi-output filter for speckle reduction of medical ultrasound images, an image quality metric for medical context (ultrasound and MRI) and a scheme of compression for medical images. We perform a study on the usability of opinion-unaware no-reference natural image quality metrics in the context of medical images: filtered ultrasound and compressed Magnetic Resonance Images (MRI), as result of the study we propose a metric adapted to medical images. Then, we propose a multi-output speckle reduction filter based on MMD (MOF-MMD), which makes it possible to obtain three filtered images that help the radiologist's diagnostic needs. Indeed, the diagnostic task is based on different characteristics of the image. Since the end-user of the medical images is the radiologist, we believe that it is more reasonable to evaluate the algorithm using human observers. Thus, we conduct a subjective experiment involving three radiologists with different years of experience. The correlations between the subjective scores and the objective metrics outputs and the impact of the radiologists years of experience are presented and analyzed. The last contribution consists on developing a lossy coding scheme based on the MMD applied to ultrasound and MR Images.

Acknowledgements

Je tiens tout d'abord à remercier ma directrice de thèse Amina Serir et mon co-directeur Olivier Deforges, mes encadrants Lu Zhang et Wassim Hamidouche pour leur dévouement et leurs soutiens durant ces années de thèses. J'ai énormément appris à leurs côtés, ils m'ont permis de progresser et de m'améliorer. Cette expérience a été enrichissante tant sur le plan scientifique que sur le plan humain. Je remercie également Pr. Kourougli qui m'a fait l'honneur de présider le jury. Je remercie Dr Fezza, Pr Aouat et Dr Souami qui m'ont fait l'honneur d'evaluer et de valider mes travaux, et dont les retours ont permis d'améliorer la version finale de ce manuscrit. Je remercie aussi tous les membres de l'équipe VAADER: permanents, post-doctorants, doctorants et stagiaires pour la bonne ambiance de travail et les moments agréables durant les pauses café riches en discussions et CALORIES.

Je remercie chaleureusement les membres de ma famille pour leurs encouragements. En particulier, mon Docteur préféré, Lyes, mon époux pour son soutien, son aide, ses conseils et pour avoir supporté mes changements d'humeurs. Mes enfants Nihel et Achraf qui m'ont encouragé à leur façon.

Je tiens aussi à remercier mes frères Reda, Mohammed et Zaki ainsi que le personnel de l'USTHB, qui m'ont facilité les démarches administratives. Je tiens aussi à remercier tout le personnel de l'INSA de Rennes pour avoir mis à ma disposition tous les moyens nécessaires pour mener à bien ce travail.

Merci à tous ceux qui m'ont aidé et encouragé de près ou de loin.

Glossary

AD: Average Difference
ADC:Analog-to-Digital Converters
ASIC: Application-Specific Integrated Circuit
BIQES: Blind Image Quality Evaluathor based on Scales
BRISQUE: The Blind/Referenceless Image Spatial QUality Evaluator
CT: Computed Tomography
DSP: Digital Signal Processors
FID: Free-Induction Decay
FoM: Pratts Figure of Merit
FPGA: Field-Programmable Gate Array
FR: Full Reference
IQA: Image Quality Assessment
JPEG: Joint Photographic Experts Group
MMD:Multiplicative Multiresolution Decomposition
MOF-MMD: Multi-Output Filter based on Multiplicative Multiresolution Decomposition
MR: Magnetic Resonance
MRI: Magnetic Resonance Imaging
MSE: Mean Square Error
NIQE:The natural image quality evaluator
NIQE-K: Natural Image Quality Evaluator based on Kurtosis
NMSE: Normlized Mean Square Error
NR: No Reference
PET: Positron Emission Tomography
PSNR: Peak Signal to Noise Ratio
RF: Radiofrequency
SAR: Syntehtic Apertur Radar
SI: Speckle Index
SNR: Signal to Noise Ratio

SPECT: Single-Photon Emission Computed Tomography
SREM: Speckle Reduction Evaluation Metric SSIM: Structural Similarity Index measure
SSNR: Speckle-Signal to Noise Ratio
US: Ultrasound
USDSAI: Ultrasound DeSpeckling Assessment Index
VCA: Variable Controlled Amplifier

CHAPTER 1

Introduction

The medical diagnosis is strongly based on different medical imaging modalities,this is due to medical imaging technologies development. Regarding the modalities, there is a wide panel of imaging technologies such as: radiology which uses the X-ray, radiography, magnetic resonance imaging, medical ultrasound, endoscopy and nuclear medicine functional imaging techniques as Positron Emission Tomography (PET) and Single-Photon Emission Computed Tomography (SPECT). Besides, the amount of digital image data to be stored or transmitted becomes very huge. Thereby, efficient and low-complexity compression becomes necessary.

However, medical image compression "intuitively" requires maintaining the quality of the diagnostic by using the compressed and decompressed image while reducing the bit rate.

Ultrasound (US) is one of the most widely used medical imaging systems. It is used in nearly all hospitals and clinics for diagnostic purposes. Since six decades ultrasonography is visualizing internal body structures such as heart, kidney, tendons and blood vessels and can be used also as a guide in surgical procedures.

Nevertheless, US imaging has a main drawback of visual quality caused by the speckle noise that is inherent to ultrasound.

In this thesis, we aim to address this issue by reduction of speckle noise in join with lossy compression in ultrasound medical images, where the losses are mainly the undesirable speckle noise. Moreover, by conducting different tests on US, we figure out that the proposed method in this thesis can also be applied succesully to MRI. Therefore, we have additionaly expanded our study to MRI modality.

1.1 Contributions

In this thesis we propose three main contributions: a multi-output filter for speckle reduction of medical ultrasound images, an image quality metric for medical context(ultrasound and MRI) and a scheme of compression for medical images. At the begining we study a speckle reduction method for SAR images based on multiplicative multi-resolution decomposition (MMD) and we applied it to ultrasound images[OSK14]. The obtained results are promising. However, the validation method, even if widely used in the bibliography, is based on quality metrics with reference dedicated to natural images.

In our first contributions, we perform a study on the usability of opinion-unaware no-reference natural image quality metrics in the context of medical images: filtered ultrasound and compressed MRI, as result of the study we proposed a metric adapted to medical images [OZD+16].

Our second contribution, is a multi-output speckle reduction filter based on multiplicative multiresolution decomposition (MOF-MMD). Indeed, as long as we are able to assess the quality of the filtered and/or compressed images with a valid metric, it is possible to prorpopose algorithms on medical images. The MOF-MMD permit to obtain three filtered images that help the radiologist's diagnostic needs. Actually, the diagnostic task is based on different characteristics of the image texture, edges, global aspect [OZD+17]. Since the end-user of the medical images is the radiologist, we believe that it is more reasonable to evaluate the algorithm using human observers. Thus, we conduct a subjective experiment involving three radiologists with different years of experience to assess the final perceived quality of filtered in vivo abdominal liver US images. The correlations between the subjective scores and the objective metrics " outputs and the impact of the radiologists" years of experience on their way of scoring be discussed are presented and analyzed [OZD+18].

The last contribution consists on developing a lossy coding scheme based on the MMD applied to ultrasound and MR Images. The results are conclusive comparatively to those obtained with the wavelet-based scheme with the respect of the diagnostically need.

1.2 Organization of the dissertation

This dissertation is organized as described below.

Chapter 2 - Medical context and backgrounds we provide in this Chapter, information about medical context. Thus, we describe expectations of medical practitioners in terms of speckle reduction and lossy compression.

Chapter 3 - State of the art reviews of the literature methods regarding the studied topic. It relates non exhaustively subjective and objective quality assessment , speckle reduction in ultrasound images and compression in medical images methods.

Chapter 4 - An image quality assessment metric for medical images (NIQE-K) presents an evaluation of two metrics on assessment of medical images quality and describes a proposed metric NIQE-K more adapted to medical images more specifically the MRI and US.

Chapter 5 - The Multi-Output Filter based on MMD describes the algorithm based on Multiplicative Multiresolution Decomposition (MMD) dedicated to speckle reduction on ultrasound. In this chapter the proposed method is evaluated objectively and subjecively, we also provide analysis on the obtained results.

Chapter 6 -The compression scheme based on MMD presents a compression scheme based on the MMD and motivated by the expertise obtained from the study of the quality presented in chapiter 4.

Chapter 7 - Conclusions and Perspectives this last chapter concludes the dissertation and presents some perspectives for future work.

CHAPTER 2 Medical context

This chapter contains a brief presentation of the medical context of this work, the main principles of US and MRI and some aspects treated in image processing.

2.1 Ultrasound Imaging

Introduction

The use of ultrasound has many advantages such as [Sza04] [Jen07]:

- it is safe and painless for the patient,
- it does not use ionizing radiation so it is free of radiation risk,
- it is "real time" providing the instantaneous dynamics of the anatomy.
- it is portable and compact,
- it is relatively inexpensive when compared with other imaging modalities (CT or MRI).

Diagnostic ultrasound imaging build up non-invasively fine images of internal body structures. The resolution attainable is higher with shorter wavelengths, as the wavelength is inversely proportional to the frequency [LB13].

2.1.1 Generation of ultrasound images

The ultrasound is a vibration (Ultra, means that frequencies of the vibrations are higher than the upper audible limit of human hearing) transmitted through a medium (solid, liquid or gas) as mechanical pressure waves. Ultrasound propagates in soft tissue

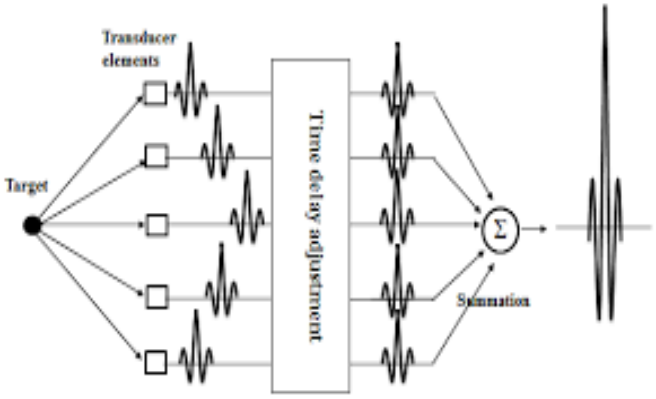

Figure 2.1: Receive beamforming in a medical ultrasound imaging system [MKAK]

(as it does in a fluid or gas) as longitudinal waves. In solids such as bone, ultrasound can be transmitted as both longitudinal and transverse waves. The velocity of waves depends on the density and compressibility of the medium [LB13]. As the ultrasound waves propagate, they reflect off on any object they encounter along their propagation path [AMD08]. The construction of images is based on the measurement of distances, which relies on the propagation velocity [LB13].

The piezoelectric effect (found in piezoelectric material) permits to convert mechanical pressure (which causes alterations in their thickness) into an electrical voltage on their surface. Conversely, the indirect piezoelectric effect is an alteration in thickness of piezoelectric material when a voltage is applied to the opposite side. If the applied electric voltage is alternating, it induces oscillations which are transmitted as ultrasound waves into the surrounding medium. The piezoelectric material, therefore, serves as a transducer, which converts electrical energy into mechanical energy and vice versa [LB13].

The resulting low voltage signals are scaled using a Variable Controlled Amplifier (VCA) before being sampled by Analog-to-Digital Converters (ADC) [AMD08]. Once the received signals reach the beamformer, the signals are scaled and appropriately delayed to permit a coherent summation of the signals. This new signal represents the beamformed signal for one or more focal points along a particular specific scan line. Figure 2.1 shows the beamforming technique used mostly in the US imaging scanners.

Various processings are carried out on the beamformed data, depending on the imaging modes. The diffrents operations and implementaions of the signals are typically performed by the US systems in Application-Specific Integrated Circuit (ASIC), Field-

Programmable Gate Array (FPGA) Digital Signal Processors (DSP) or a combination of these components [AMD08].

2.1.2 Ultrasound characteristics

Spatial resolution

Spatial resolution is defined as the ability to distinguish between two objects located at different positions in space.

Lateral resolution Lateral resolution depends on the diameter of the ultrasound beam. It varies in the axial direction, being best in the focus zone. As many array transducers can be focused in only one plane, because the crystals are arranged in a single line, lateral resolution is particularly poor perpendicular to that plane. The lateral resolution is a function of the beam width, it is defined by the ability of the system to separate two echoes located on the same plane, which is perpendicular to the axis of the same beam[Dah11].

Axial resolution The axial resolution determines the ability of the probe to differentiate between two targets located in the ultrasonic beam axis. It depends on the pulse length and improves as the length of the pulse shortens[Dah11]. In ultrasonic imaging, axial resolution is better than lateral resolution, besides showing less variation.

2.1.3 Speckle

The ultrasound image shows a granular structure called speckle making visual interpretation difficult. Speckle is an undesirable property of the image as it masks small differences in gray level [Bur78] [WSSL83a]. This kind of noise, that corrupts the image in a multiplicative manner, appears due to interference phenomena between the incident and reflected signals, and thus is inherent to ultrasound [FMYS97]. Many researchers investigated the statistical proprieties of speckle noise in ultrasound images since the seventies such as Burckhardt [Bur78] and Wagner and al [WSSL83a].

The grainy appearance of the image is due to the speckle pattern, which is typical of ultrasound images. This is due to the coherent summation of scattered ways from the numerous small structures in the tissue [Jen07]. This speckle noise limits the application of image processing such as segmentation, detection or even automatic

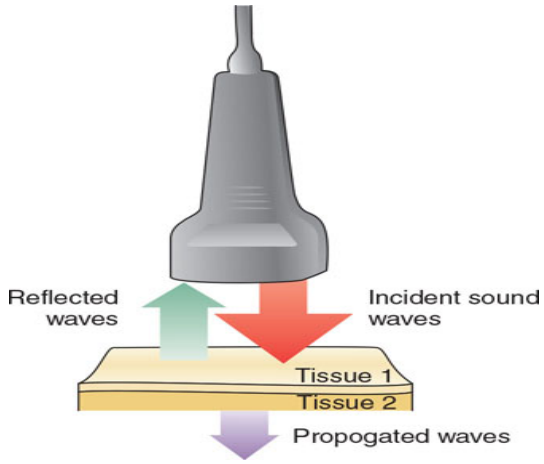

Figure 2.2: Illustration of interference phenomena in ultrasund transducer (Radiologykey.com/physics-of-ultrasound-2/)

diagnose appliance. This "granular" texture (speckle) also is not truly a noise in the typical engineering sense because its texture often carries useful information about the image being viewed [LPC+05]. In one hand, the speckle interferes with image interpretation such as diagnosis and analysis such as segmentation, registration, and computer aided detection [KLY16a], in the other hand "*the local brightness of the speckle reflects the corresponding echogenicity of the underlying scatterers, in the case ofliver ultrasound likely the hepatic lobules*"[GG14]. Hence, the challenge is to reduce speckle while preserving meaningful data.

Wagner [WSSL83b]:"*An ultrasound B-scan image is the result of a rather complicated set of physical phenomena, namely, the insonification and resulting absorption, reflection, and coherent scattering from a tissue medium of pulsed radio frequency ultrasonic pressure waves, and the electronic detection of the backscattered or echo pulses for display as an image* .

Speckle modeling in ultrasound images: The knowledge of the statistical properties of speckle is important to understand and develop filters for speckle noise reduction. Several works propose to study physical features and statistical properties to build a speckle noise modeling for both ultrasound and Syntehtic Apertur Radar (SAR) imaging. A largely accepted model for the speckle imaging is given by [MT06b]:

$$g_{i,j} = f_{i,j} \times u_{i,j} + \xi_{i,j} i, j \in N \tag{2.1}$$

where g, f, u and ξ stand for the observed envelope image, original image, multiplicative and additive components of the speckle noise, respectively. i and j denote the axial and lateral indices of the image samples, alternatively, they can denote the angular and range indices for sector images.

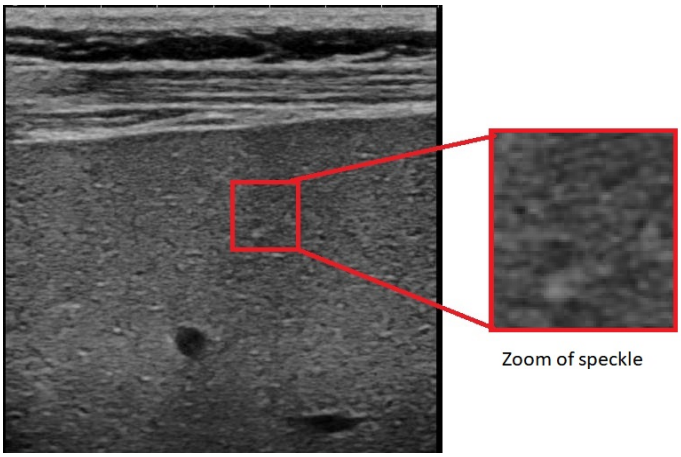

Figure 2.3: Clinical ultrasound image corrupted with speckle

2.1.4 Ultrasound and image processing

Medical applications involve image analysis tasks such as image segmentation, image feature extraction, image registration, storage and image retrieval, in the case of ultrasound images the specke impedes post-processing techniques. Hence, the image despeckling is an important preprocessing task.

A large amount of research has investigated speckle reduction and improved the quality of US images. There are two main categories of despeckling methods: compounding methods and post-processing ones. The compounding speckle reduction methods include both spatial and frequency compounding [WZX13a].

Post-processing speckle reduction techniques are widely used. These techniques decrease speckle after the US image is formed. In this work we proposed image processing on ultrasound. Hence, it is interesting to highlight some aspects of ultrasound image related to image processing.

This work aims to perform an image enhancement process, which reduces speckle and thus helps in the interpretation of these images with a reliable diagnosis. Moreover, we study the usaubility of quantitative quality evaluation metrics in ultrasound images assessment. For this task we have evaluated the quality of ultrasound imaging carried out by medical experts through subjective tests.

2.2 Magnetic Resonance Imaging

The MRI uses the quantum mechanical property of "spin". It is the atomic and subatomic property of (spin) angular momentum which correspond to angular momentum of a rotating object in classical physics. The H (hydrogen) nuclei have a non-zero spin. It can absorb and emit electromagnetic radiation and undergo "resonance" when placed in a magnetic field [Els]. The hydrogen is largely present in human body and biological tissues as there are composed of water molecules, each containing two hydrogen nuclei.

Oscillating magnetic waves are applied to these atoms, which, already subjected to a strong constant magnetic field $\vec{B_0}$, will enter into magnetic resonance (spin echo) [Taq11]. This phenomenon occurs at a particular frequency the Larmor frequency proportional to the field strength $\vec{B_0}$ As a result, the object's hydrogen nuclei align with the magnetic field. A second radiofrequency (RF) magnetic field $\vec{B_1}$, perpendicular to $\vec{B_0}$ is applied [GTC+15].

Once the RF signal is removed, the nuclei realign themselves and return to equilibrium, they lose energy by emitting their own RF signal. The energy emitted by the nuclei is referred to as the Free-Induction Decay (FID) (*cf.* Figure 2.4). It induces a voltage that can be detected by a suitably tuned coil of wire, amplified and displayed. In practice, multiple RF pulses are applied to obtain multiple FIDs, which are then averaged to improve the MRI. The signal-averaged FID can be resolved by a Fourier transformation, into either an image MRI or a frequency spectrum, providing biochemical information [GTC+15].

The Figure 2.5 illustrate the reconstruction process, where multiple phase-encode steps generate an array of different Magnetic Resonance (MR) signals from a slice through a spherical phantom. The first Fourier transformation of each of these signals provides a raw frequency projection of the object, modified by the phase shifts transmitted by each step. It should be noted that for low order phase encodings, the signal MR is strong. The frequency projection is close to the general shape of the object but lacks definition of the edges. Higher-order phase encoding steps have smaller signals MR but provide more information about spatial details, such as edge locations. To construct the final image, a second Fourier transform is performed using the data from this intermediate step grouped into columns of the same frequency[MRIquestions.com].

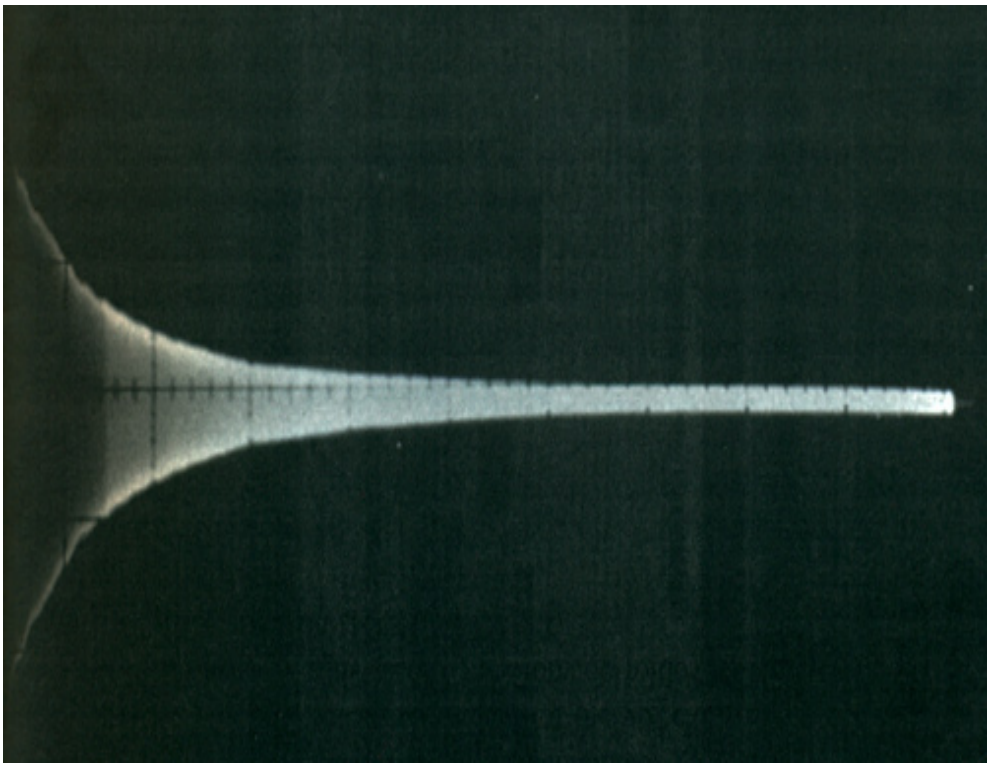

Figure 2.4: The free induction decay (Courtesy of Allen D. Elster, MRIquestions.com)

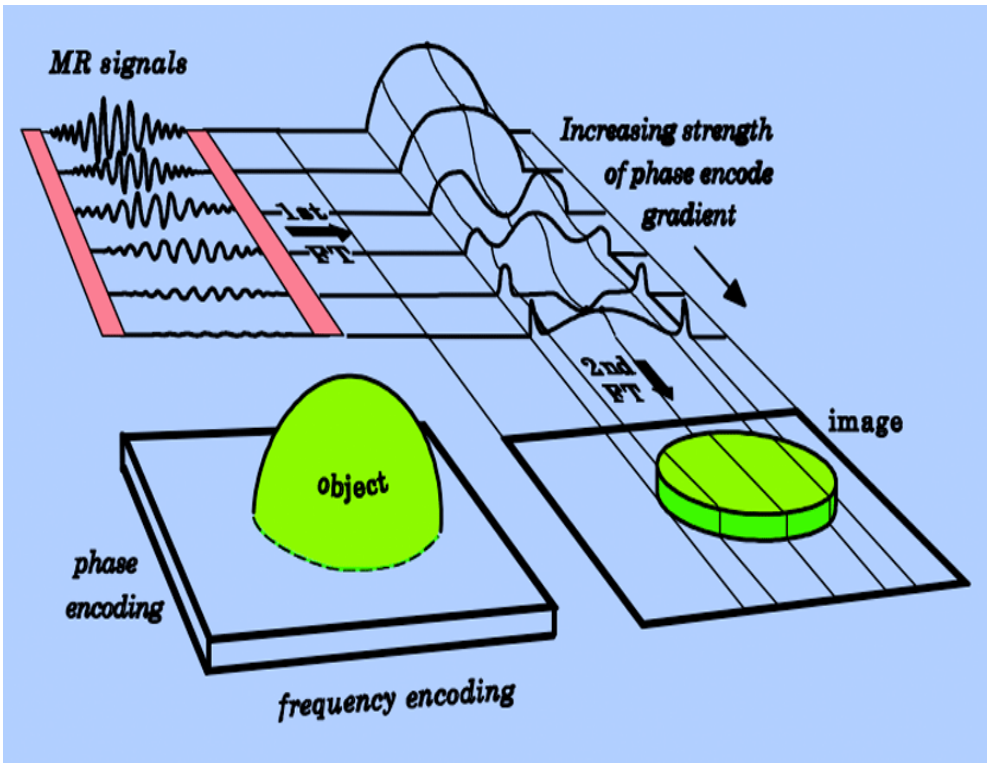

Figure 2.5: Graphic representation of MRI is frequecy and spatially encoded (Courtesy of Allen D. Elster, MRIquestions.com)

2.2.1 Image pocessing of MRI

The MRI offers a tool of quality for visualization of anatomical structures in vivo. However, it has, like any imaging modality, shortcomings that degrade the quality and rendering of acquisitions. The most harmful defects are in particular noise and drift phenomenon. It can be very constraining to reduce noise in MRI without any significant gain ultimately. Indeed, these defects are corrected by the eye of the specialist that corrects image defects on its own [Cap02].

However, for the medical field, the MRI is one of the most demanding modality in terms of storage space (with Computed Tomography (CT)). For ethical considerations related to diagnosis, the medical data are compressed in lossles mode. This permit to keep an identical copy of the original one. Therfore, compression algorithms are easy to implement but with less compression rates and more computationnal time [Taq12]. Consequently, the lossy compression could be preferable.

2.2.2 Image quality constraints and lossy compression

Even if lossy image compression is not widely accepted by medical expert, lot of contributions, in medical compression image context, present a lossy version of their compression algorithms. To support this, ther is a study conducted by [KBB+09] that assess the impact of irreversible compression on visual quality with sufficient scale and rigour to stand up to scientific and clinical scrutiny. This study provides a table of recommended compression ratios for each modality and anatomical area investigated.

Furthermore, the Canadian Association of Radiologists (CAR) proposes guidelines that integrate the use of lossy compression in medical imaging [Can08]. The CAR argues the use of lossy compression by citing the position of American College of Radiology (ACR):"Data compression may be performed to facilitate transmission and storage. The type of medical image, the modality, and the objective of the study will determine the degree of acceptable compression. Several methods, including both reversible and irreversible techniques (lossless and lossy are also common terms), may be used under the direction of a qualified physician or practitioner, with minimal if any reduction in clinical diagnostic image quality" [Can08]. Therefore, regarding the compression in medical imaging, the major constraint is the diagnostic accuracy of the compressed image. It is important to evaluate the quality of the compressed images and the reliability of diagnosis.

Conclusion

We have presented in this Chapter the medical context of our work. We have described briefly the generation of the US and MRI images including some important charatiristics of these studied modalities. Finally, we have presented some specific needs in terms of image processing on the US and MRI.

CHAPTER 3

State-of-the-art: Medical images quality assessment, despeckeling and compression

Introduction

In this thesis we treate the topic of ultrasound images in three image processing fields image quality assessment, speckle's filtering and compression. Image quality assessment and compression have been extended to MRI images for reasons explained previously. The rest of the chapter reviews the state of the art in these fields in medical context.

3.1 Image quality assessment for medical images

In medical image processing, the goal is not to create visually pleasing images: a medical image has a specific purpose to allow the physician to diagnose a diseas [Goo10]. The purpose of the assessment, in the case of despeckeling, is to express how well the algorithm has despeckled the image while preserving the important details.Furthermore, in compression scheme, the goal is is to express how well the used coder increases the compression rates without compromising diagnostic quality. Besides, the image quality assessment could quantify the preservation of details in the case of despeckling or compression process. Thereby, in some image processing methods an Image Quality

Assessment (IQA) can be used to tune the parameters of used algorithms. In other words, in the case of denoising based on setting thresholds, the IQA could be used in an iterative process, where the thresholds are modified. The iterative process when the quality reaches its maximum. Similarly, in compression scheme the quantification coefficient or the thresholds of embedded zero trees EZW are tuned in relation with the obtained image quality scores. For above cited reasons, image quality assessment is needed for medical image processing. Preferentially, determining the image quality of medical images is done by a panel of human observers: a group of experienced physicians with a well-chosen protocol are asked about the quality of the image in terms of diagnostic. This process is the more reliable, however, it is time-consuming and difficult to perform because of unavailability of medical observes, in fact the agenda of medical experts is always overloaded and it is very difficult to find volunteer experts for subjective test. Hence, we propose to provide an efficient IQA metric to evaluate the post processing algorithms in medical applications. The aim is to beforehand select algorithms to involve in the subjective tests.

Currently, to evaluate the performance of the medical despeckled images, several quality metrics originated from natural IQA are adopted.

This section describes and reviews available objective and subjective quality assessment methods used for the evaluation of medical content and in particular for the evaluation of speckle reduction in ultrasound medical imaging

3.1.1 Subjective assessment

The subjective assessment involves human beings to obtain the perceived quality score. The methods used to collect perceived quality scores first depends on the constraints of availability of radiologist and second affects the accuracy and reliability of the data collected. In fact, the subjective testing methodology impacts both the accuracy and the reliability of the collected perceived quality scores. For the subjective quality assessment of the medical images, various testing methods have been used through the literature. The methodologies used to assess the perceived quality of medical content is have been recommended by International Telecommunication Union Radiocommunication Sector (ITU-R) [BT.00]. This section reviews protocols used to conduct subjective tests on quality assessment for medical contents mainly for US imaging.

According to the number of stimulus (2D image or short video) presented to the observer, the testing methods can be divided into two groups: single stimulus (SS) and multi stimulus (MS). The observer (medical expert or physicians) scores the stimulus using a discrete or continuous scale, typically containing five descriptors: Bad, Poor,

Fair, Good, and Excellent quality. In SS methods, one stimulus is presented and scored. In MS methods, two or more stimuli are presented for reference but only the stimulus of interest is scored [LLM+18].

Absolute Categorical Rating (ACR)-Single Stimulus

The Absolute Categorical Rating (ACR) [IL08] is a SS method and it consists of consecutive trials in which an observer views and scores a stimulus. The stimulus is displayed to the observer, then the display is set to a constant gray background and the observer is immediately requested to provide an opinion score of the viewed stimulus [RPCH10].

The reference stimulus is included in the test trial evaluated by the observer. However, the observer is unaware if a stimulus is a processed or reference stimulus. The stimuli are randomly presented and vary for each observer. The rating scale used for ACR is discrete scoring one. Each category is labeled by the adjectives "Bad", "Poor", "Fair", "Good", and "Excellent". A mean opinion score (MOS) is computed for each stimulus by averaging the corresponding observer opinion scores.

Kara et al. [LLM+18] used the ACR method on 3D heart images. They study the effects of angular resolution and light field reconstruction involving 20 observers: 8 medical experts and 12 non-experts. In [LP13], the authors investigated the effects of blurring, gamma modification, adding noise, color saturation, and JPG compression on animal pathology slides. The test was conducted with: 6 pathology experts, 7 pathology students and 11 imaging experts.

Single-Stimulus Continuous-Quality Scale (SSCQS)

The Single stimulus continuous quality evaluation (SSCQS) procedure is also SS method. It consists of consecutive trials in which an observer views and scores a stimulus. The testing is similar to that of the ACR method, with a continuous rating scale. The SSCQS method has been used by Tulu and Chatterjee in the study of impairment's effect on clinical decision capability. They investigate the effects of packet loss, packet delay, and jitter on the transmission of ophthalmology videos in telemedicine context [TC08].

Double-Stimulus Continuous-Quality Scale (DSCQS)

The double stimulus continuous quality scale (DSCQS) procedure is also a recommendations from ITU-R for the subjective assessment of pictures [Rec02]. A test session

comprises a number of sequences. According to the number of observer, there are two variants. The main difference between the two variants is that the assessor is allowed to switch between the A and B signals until the assessor has the mental measure or the signals are shown one or more times before asking the assessor to give a measure.

The DSCQS was used to evaluate speckle reduction filter on ultrasound images in [LPC+05] and [LMP+14]. In [HPN+10] the authors propose a methodology for clinical evaluation of image quality using DSCQS procedure, particularly in assessing clinical ultrasound image quality. In the other hand Loizou[LMP+14] performs a comparative evaluation of several despeckle filtering methods applied to ultrasound images of the common carotid artery. The comparison was based on a quantitative and a qualitative evaluation. For the objective evaluation of the quality of the images the NIQE index assessment tool is used. For the visual assessment two clinical experts: a cardiovascular surgeon and a neurovascular specialist were asked to judge the quality of the despeckled images. The test was carried out according to the International Telecommunication Union(ITU) recommendations which suggest the DSCQS procedure[BT.00]. Chaabouni et al.[CGL+14] studied the question of medical subjective quality assessment using the DSCQS method. The subjective tests were conducted on compressed video sequences with a panel of experts from different ages, sex and ranks (intern, extern, resident, doctor, professor) according to the DSCQS procedure.

Razaak et al. [RMS14] choose DSCQS method to study the quality of medical processed ultrasound videos in terms of predicting the diagnostic. They also study the impact of the Quantization Parameter (QP) on HEVC compressed medical ultrasound videos. According to this study the subjective scores are less sensitive with DSCQS methodology.

Subjective assessment methodology for video quality (SAMVIQ) - Double Stimulus

In a recent study Zhang and al.[ZWC15] compare eleven despeckle filters performances by using full reference image quality metrics, No-reference image quality metrics and visual evaluation of experts. They invited three experts with a different work age to evaluate the filtered images where the observer freely views and scores a collection of test stimuli associated with an explicitly identified reference stimulus [RPCH10].

In the SAMVIQ protocol the images are presented to the observer (assessor) such that he can evaluate all processed versions of the image as well as against the reference. SAMVIQ offers the possibility to visualize each image several times and re-evaluate a

previously scored image. The explicit and the hidden are used as quality anchors that stabilize the results and improve the consistency of the scores.

The stimuli are randomized in order to prevent the assessors from attempting to vote in an identical way according to an established order [FK05]. A training session is conducted by a test supervisor in order to make the assessor familiar with image artifacts and the user interface [FK05].

3.1.2 Objective assessment

Objective image quality assessment methods use mathematical modeling for "automatically" providing measures that estimate the perceived image quality. These methodes can be classified, according to the availability or not of an original image, as Full-Reference (FR) or No-Reference (NR) methods.

Full Reference (FR) image quality metric

A large number of Full Reference (FR)image quality metrics are used to evaluate medical processing algorithms.

The signal to noise ratio (SNR) The Signal to Noise Ratio (SNR) is a fundamental parameter widely used to assess quality of image. Many authors use the SNR in dB as a quantitative performance measure for speckle suppression in US image. As a definition of the SNR, some authors [PPLA03] [GCS05] [KKJ+10] use the ratio of the reference noise-free image variance σf to the noise variance σn.

$$SNR = \frac{\sigma f}{\sigma n} \tag{3.1}$$

Pizurika [PPLA03] uses the SNR not only as an assessment metric but also for tunning the optimal value of the parameter's method (the one that maximizes the signal-to-noise ratio).

A second definition of the SNR as follows :

$$SNR = \frac{\sum_{x=1}^{M}\sum_{y=1}^{N} f_{xy}^2}{\sum_{x=1}^{M}\sum_{y=1}^{N}(f_{xy} - \hat{f}_{xy})^2} \tag{3.2}$$

is used by Gupta [GSP05] and Wang [WFC+13] to measure the despeckling performances.

The speckle- signal to noise ratio (Speckle-SNR) The speckle-SNR is defined as being a ratio of the mean to the standard deviation of the speckled images [Bur78]. For a fully developed speckle (Rayleigh statistics) the speckle-SNR is known to be approximately equal to 1.91 [WSSL83a]

The speckle-SNR is expected to increase as the amount of the speckle decrease. [MT06a] and [GBS14] used the specifications of this metric to evaluate the performance of their despeckling methods. It is measured in a fully formed region and expressed by

$$SSNR = \frac{\mu}{\sigma} \tag{3.3}$$

where μ is the mean intensity value and σ is the standard deviation in the region of fully formed speckle. A higher value of the SSNR indicates less speckle.

The Mean square error (MSE) The mean square error is defined as:

$$MSE = \frac{1}{MN} \cdot \sum_{x=1}^{M} \sum_{y=1}^{N} (f_{xy} - \hat{f}_{xy})^2 \tag{3.4}$$

where f is the original noise-free image , $\hat{f}$ is the denoised image, M and N are the width and height of the image, respectively.

Easy to calculate MSE, measures the average square differences between the original and the denoised image. MSE is largely used to evaluate enhancement algorithm for noise reduction of ultrasound images[LMA89] [ABT01] [LPC+05] [ZWC15].

- The root of MSE (RMSE)

$$RMSE = \sqrt{\frac{1}{MN} \cdot \sum_{x=1}^{M} \sum_{y=1}^{N} (f_{xy} - \hat{f}_{xy})^2} \tag{3.5}$$

- Signal to mean square error (SMSE)

$$SMSE = \frac{\sum_{x=1}^{M} \sum_{y=1}^{N} f_{xy}}{\sum_{x=1}^{M} \sum_{y=1}^{N} (f_{xy} - \hat{f}_{xy})^2} \tag{3.6}$$

  According to Achim[ABT01] the (Smse) ratio, is more adequate to evaluate the noise suppression in case of multiplicative noise. It corresponds to the classical SNR used for additive noise [ABT01]. [KKJ+10] and [VS08] used this criterion to quantify the performance improvements of speckle reduction methods in medical ultrasound images.

- The normalized mean square error Normlized Mean Square Error (NMSE)

  Defined as being the reciprocal of the SMSE, this criterion is used in the coherent imaging in which the standard definition of the SNR might be inadequate considering the multiplicative nature of speckle noise [MT06a].

The Average Difference (AD) AD is the mean difference between original and filtered image divided by the size of the image[WZX13b]. The higher value corresponds to dissimilar image. The AD is defined by:

$$AD = \frac{1}{MN} \cdot \sum_{x=1}^{M} \sum_{y=1}^{N} \left| (f_{xy} - \hat{f}_{xy}) \right| \tag{3.7}$$

The peak signal to noise ratio (PSNR) The peak signal to noise ratio is given by :

$$PSNR = 10 \log_{10} \frac{L^2}{MSE} \tag{3.8}$$

where L is the number of the image gray levels. The PSNR is among the widest quantitative No-reference IQA used to assess despeckeling methods in US images. For instance PSNR is adopted by [TC11] [AAC+12] [LPC+05] and [ZWC15]

Edge preservation measure β The edge preservation measure is defined as:

$$\beta = \frac{\Gamma(\Delta f - \overline{\Delta f})(\widehat{\Delta f} - \overline{\widehat{\Delta f}})}{\sqrt{\Gamma(\Delta f - \overline{\Delta f}, \Delta f - \overline{\Delta f}) \cdot \Gamma(\widehat{\Delta f} - \overline{\widehat{\Delta f}}, \widehat{\Delta f} - \overline{\widehat{\Delta f}})}} \tag{3.9}$$

where Δf and $\widehat{\Delta f}$ are the high-pass filtered versions of f and $\hat{f}$, obtained with a 3×3 pixel standard approximation of the Laplacian operator, and

$$\Gamma(f_1, f_2) = \sum_{x=1}^{M} \sum_{y=1}^{N} f_1(x, y) \cdot f_2(x, y) \tag{3.10}$$

β aims to assess the ability of the despeckeling methods to preserve sharp details of the original images that often constitute features of interest for diagnostic [ABT01] [MT06a]. Of interst [TC11] [ABT01] [MT06a] [GCS05] [WFC+13] use β as an image quality assessment in despeckling of ultrasound medical imaging in addition to other metrics of noise reduction.

coefficient of correlation ρ Sattar [SFSL97] proposed a performance evaluation based on correlation defined as:

$$\rho = \frac{\Gamma(f - \overline{f})(\widehat{f} - \overline{\widehat{f}})}{\sqrt{\Gamma(f - \overline{f}, f - \overline{f}) \cdot \Gamma(\widehat{f} - \overline{\widehat{f}}, \widehat{f} - \overline{\widehat{f}})}} \tag{3.11}$$

This metric is used as a supplementary performance evaluation based on correlation by [GCS05] [VS08]. ρ is close to unity when the despeckled image is similar to the reference image.

Structural Similarity Index measure Some above cited metric like SNR and PSNR are globally simple to calculate and they have a mathematical meaning but are not correlating well with perceived quality measurement. As the human visual perception extract structural information from an image Wang [WLB04] propose an objective metric close to human perception that assess the perceptual image quality, the Structural Similarity Index measure (SSIM) which compares local patterns of normalized pixel intensities.

$$SSIM = \frac{(2\mu_f \mu_{\widehat{f}} + c_1)(2\sigma_{f,\widehat{f}} + c_2)}{(\mu_f^2 + \mu_{\widehat{f}}^2 + c_1)(\sigma_f^2 + \sigma_{\widehat{f}}^2 + c_2)} \tag{3.12}$$

where μ_f,$\mu_{\widehat{f}}$,σ_{f^2} and $\sigma_{\widehat{f}}^2$ are the means and variances of reference noise-free image f and despeckled image $\widehat{f}$. $\sigma_{f,\widehat{f}}$ is the covariance between image f and $\widehat{f}$. c_1 and c_2 are constants which can be changed.

This index is widely used for assessing enhanced or despeckled medical ultrasound images [RV12] [LPC+05] [AAC+12] [ZWC15] [GBS14].

Furthermore, [KUBW+14] show that SSIM provides the closest match to the subjective assessments by the radiologists in term of quality factor performance when applied MR Image compression.

Pratts figure of merit FoM Proposed by[Pra77] FoM measures edge pixel displacement between filtered and reference noise-free image :

$$FoM = \frac{1}{max(N_f, N_{\widehat{f}})} \cdot \sum_{i=1}^{N_f} \frac{1}{1 + \alpha d^2} \tag{3.13}$$

where N_f and $N_{\widehat{f}}$ represent the numbers of edge pixels in the edge maps of reference and filtered images. α is a constant.d is the Euclidean distance between the ith detected edge pixel and the nearest ideal edge pixel.

This metric was adopted by [GBS14] [ZWC15] [FGJ11] where the ideal edge pixels and detected edge pixels are binary maps, which are calculated from the noise-free image and the denoised image. The authors extract the edge maps using Canny edge detector algorithm.

Speckle Reduction Evaluation Metric (SREM) In [MRC14] a speckle reduction evaluation metric, the SREM, is proposed. It is based on the computation of the contrast similarity map (CSM) and gradient similarity maps (GSM) between two images. The overall similarity between images $f(i,j)$ and $\hat{f}(i,j)$ can be calculated by :

$$SREM = \frac{\sum CSM(i,j) \cdot \sum GSM(i,j)}{\sum GSM(i,j)} \tag{3.14}$$

Ultrasound Despeckling Assessment Index (USDSAI) Tay and al.[TAH06] defined a performance metric Q called the ultrasound despeckling assessment index (USDSAI) as:

$$USDSAI = \frac{\sum_{k \neq l} (\mu_{C_k} - \mu_{C_l})^2}{\sum_{k=1}^{K} {\sigma_{C_k}}^2} \tag{3.15}$$

where

$$\mu_{C_k} = \frac{1}{|C_k|} \sum_{(n,m) \in C_k} \widehat{f}(n,m) \tag{3.16}$$

and

$${\sigma_{C_k}}^2 = \frac{1}{|C_k|} \sum_{(n,m) \in C_k} (\widehat{f}(n,m) - \mu_{C_k})^2 \tag{3.17}$$

where $|C_k|$ denotes the number of pixels in class C_k.

This modified Fisher discriminant contrast metric determines how well a despeckling algorithm reduces variances in homogeneous classes while keeping the distinct classes well separated and preserving edges. USDSAI seems to be helpful to [RLVSFMF+14] and [CHKB09] for assessing their algorithms.

No Reference image quality metric

TheNo Reference (NR) metric can be further divided into two categories: Opinion-Aware (OA) if it needs to be trained on a database of distorted images with associated subjective opinion scores; and Opinion-Unaware (OU) if it is free of training. Several OA NR metrics are proposed such as DIIVINE [MB11] , CBIQ [YD12] , LBIQ [TJK11], BLIINDS [SBC12], BRISQUE [MMB12] and the newest one ILNIQE [ZZB15] which is

an enriched form on an OU NR metric the NIQE studied in this section. Nevertheless in medical domain, it is much more difficult to obtain collections of distorted images with co-registered radiologists' scores. Thus OU NR metrics are of greater interest to us. The OU NR metrics have not been extensively studied yet, even for natural images. In this section we present the more appropriate IQA method, already applied or that can be applied for medical images.

Speckle Index Shibin and al. [WZX13c] use the Speckle Index (SI) to evaluate speckle reduction filters. The SI is defined as follows:

$$SI = \frac{1}{MN} \cdot \sum_{x=1}^{M} \sum_{y=1}^{N} \frac{\sigma_(x,x)}{\mu_(x,y)} \tag{3.18}$$

where$\sigma_(x,x)$ and $\mu_(x,y)$ are the standard deviation and the mean. This metric measures the reduction of speckle in terms of average contrast of the image. Lower value of SI corresponds to improved image quality.

The natural image quality evaluator The The natural image quality evaluator (NIQE) [MSB13] is a perceptual metric proposed for evaluating the quality of a natural image. It is based on constructing a collection of features from a corpus of natural images, and fitting them to a multivariate Gaussian (MVG) model. the NIQE is both opinion- and distortion-unaware. It is expressed as the distance between constructed features and features extracted from the assessed image:

$$NIQE = \sqrt{\left((\nu_1 - \nu_2)^T \left(\frac{\sum_1 + \sum_2}{2}\right)(\nu_1 - \nu_2)\right)} \tag{3.19}$$

where ν_1, ν_2 and $\sum_1, \sum_2$ are the mean vectors and covariance matrices of the reference image's MVG model and the distorted image's MVG model, respectively. It estimates the image quality only from spatial domain. Lower value of NIQE corresponds to better image quality. In [LMP+14] and [ZWC15] the NIQE is used to assess quality of despeckled medical images.

BRISQUE The Blind/Referenceless Image Spatial QUality Evaluator: Natural scene statistic-based distortion-generic (BRISQUE) [MMB12] which operates in the spatial domain. It uses scene statistics of locally normalized luminance coefficients to quantify the presence of distortions in the image.

BIQES The Blind Image Quality Evaluathor based on Scales (BIQES) [SW15] uses intrinsic features of the image. It transforms the test image into a scale-space representation, and measures the global dissimilarity with the co-occurrence histograms of

the original and its scaled images (*i.e.,*the dissimilarity between the image itself and its lower resolution versions). The first dissimilarity, called low pass error Q_L, is calculated by comparing low pass versions across scales with the original image. The second dissimilarity, called high pass error Q_H, is computed from the variance and gradient histograms, weighted by the contrast sensitivity function in order to make it perceptually effective. These two dissimilarities are combined together to derive the final quality score:

$$BIQES = \frac{k}{\sigma}\overline{Q_L} + \sigma\overline{Q_H} \tag{3.20}$$

where $\bar{\cdot}$ denotes the mean operation, k and σ are the *kurtosis* and the **standard deviation** of log amplitude of the image's Fourier spectra, respectively. Lower value of BIQES corresponds to better image quality.

3.2 Speckle reduction methods in ultrasound

The speckle noise is inherent to US images as presented previously, however this kind of noise is also present in coherent electromagnetic wave such as radar and synthetic aperture radar(SAR), and in acoustic images of the sea floor (sonar image). Since the seventies, several speckle reducing filters were proposed dedicated to SAR. Hence, many speckle reducing filters used for US images are originated from the SAR community especially. In this chapter we will review the speckle reduction algorithms proposed for US images

3.2.1 Adaptive filters

The adaptive filters uses the local statistics of the image, these techniques often perform calculation of statistics in subregion of the image to estimate statistical behavior over different pixel. Almost of these techniques assume that the speckle noise model has a multiplicative form [LPC+05]. This category of filters is widely present in literature such as:

Median filter [RNR84]

This basic filter based on the principle of replace the gray level of neighborhood's center pixel with the median gray level of the considered neighborhood.

Lee filter

[Lee80] [Lee] Lee proposed algorithms to filter images corrupted by additive noise, multiplicative noise and combined additive and multiplicative noise. These filters are based on local statistics of the image and the minimum mean square error (MMSE) criterion.

For the speckle reduction, the multiplicative LEE filter is the more appropriate. The formulation of [YA02a] is:

$$\hat{I}_{Lee} = \bar{I}_s + K_s(I_s - \bar{I}_s)$$

where $\bar{I}_s$ represent the mean value of the intensity within the filter window η_s, and K_s is the adaptive filter coefficient calculated by:

$$W(x,y) = 1 - \left(\frac{C_u^2}{C_s^2}\right)$$

with,

$$C_s = (1/|\eta_s|)\Sigma(I_p - \bar{I}_s)^2/(I_p - \bar{I}_s)^2$$

and $C_u^2 = \frac{var(z')}{(\bar{z})^2}$

$var(z')$ and $(\bar{z})^2$ are the intensity variance and mean over a homogenous area of the image, respectively

Kuan filter [KSSC85]

This filter is similar to the previous filter, it proposes a more general approach by using the exact LLMMSE, avoiding the Taylor approximation made by Lee.

Frost filter

[FSSH82] The Frost filter as well as Lee and Kuan filters uses local statistics of the image. It uses an exponentially damped convolution kernel that adapts to regions containing edges by exploiting local statistics[YA02a]. The filter output expression is given by

$$\hat{I}_s = \sum_{p \in n_s} m_p I_p$$

where

$$m_p = exp(-KC_s^2 d_{s,p}) / \sum exp(-KC_s^2 d_{s,p})$$

$$d_{s,p} = \sqrt{(i - i_p)^2 + (j - j_p)^2}$$

where K is the damping factor, (i, j) the grid coordinates of pixel s and (i_p, j_p) are those of pixel p.

Its main advantage is inhibiting filtering process at the edges by choosing the factor K. The image is then estimated using the minimum mean-square error criterion (MMSE). .

Lopes et al. filter [LTN90]

This filter combines the Lee and Frost filter with a preleminary step to classify the pixels. Thus, the local image statistics are used to determine Heterogeneous Class and Homogeneous class.

Wiener filter

This filter utilizes the second-order statistics of the Fourier decomposition, by minimizing the MSE between the estimated signal and the desired one. Wiener filtering assumes that the noise is mainly additive with known spectral characteristics. Hence, it is not adequate for multiplicative noise suppression such as speckle. Jain developed a homomorphic approach to address this issue, which by taking the logarithm of the image, converts the multiplicative into additive noise, and applies the Wiener filter[ABT01].

SBF filter

[TAH06] The squeeze box filter (SBF), is a stochastically driven method that iteratively removes outliers by determining the local mean and standard deviation from an adaptively varying window. The adaptively determined mean is used to replace the outlying values of an ultrasound image causing homogeneous regions to be aggressively smoothed while preservation of edges is profoundly respected. This filter method reduces the local variance at each pixel by squeezing the stochastically distributed pixel values to a limiting value.

3.2.2 Anisotropic diffusion filter

Average Difference (AD) process was introduced firstly by Perona and Malik [PM90] for filtering images while preserving significant details of the image typically edges, lines, structures. Also called Perona,ÄìMalik diffusion, this approach is widely present in the literature with different extensions and improvements:

Speckle reducing anisotropic diffusion filter

Yu and Acton [YA02b] introduce Speckle Reducing Anisotropic Diffusion filter (SRAD), that was the first application of anisotropic diffusion filtering to speckle noise. This is done by introducing the instantaneous coefficient of variation for an edge-sensitive speckle reduction.

Details preserving anisotropic diffusion

An improved version of the SRAD is then proposed with the Detail Preserving Anisotropic Diffusion (DPAD) [AL06]. This improved version of the SRAD involves estimation of the coefficient of variation of both signal and noise based on Kuan's filter.

Oriented speckle reducing anisotropic diffusion

In [KWKV07] the authors extended the SRAD and DPAD methods to an Oriented Speckle Reducing Anisotropic Diffusion (OSRAD). This method is combined with matrix anisotropic diffusion, allowing different levels of filtering in the gradient and the principal curvature directions.

Anisotropic Diffusion filter with Memory based on Speckle Statistics

In [RLVSFMF$^+$14], an Anisotropic Diffusion filter with Memory based on Speckle Statistics (ADMSS) was proposed. This recent method embeds a memory mechanism that speeding-up the diffusion process in meaningless regions and adaptively preserves relevant structures.

The anisotropic diffusion approach was firstly applied to speckle removal by Yu and Acton in [YA02a] with the speckle reducing anisotropic diffusion filter (SRAD). An improved version of the SRAD is proposed with the detail preserving anisotropic diffusion (DPAD) [AL06]. In [KWKV07], the authors extended the SRAD and DPAD methods to an oriented speckle reducing Anisotropic diffusion (OSRAD). More recent work proposes a speckle filter based on anisotropic diffusion paradigm with a memory mechanism that aim to preserve relevant information during the filtering process [RLVSFMF$^+$14].

3.2.3 Multi-scale based filters

Another approach used in speckle reducing is the multi-scale based filters. Most of these filters use the wavelet transform [ABT01] [PPLA03] [GSP05]. The wavelet based speckle reduction filters include three main steps : wavelet decomposition, modification of wavelet coefficients, reconstruction of the modified wavelet coefficients "noise free coefficient" by invert wavelet transform. Some works proposed multi-scale based speckle reduction methods using pyramid transform [ZYKK07] [KLY16b].

Several multi-scale based methods were proposed for speckle reduction in ultrasound imaging mainly based on Wavelet, Curvelet or Contourlet transforms. Most of these filters use the wavelet transform, as the wavelet theory provides a powerful representation of the image and is widely used for image processing such as image compression, segmentation and noise reduction.

The wavelet-based speckle reduction filters include three main steps: wavelet decomposition, modification of wavelet coefficients, reconstruction of the modified wavelet coefficients and "noise free coefficient" by invert wavelet transform. The wavelet shrinkage denoising was first proposed by [Don95], later this thresholding method was applied to medical imaging for speckle reduction [ABT01]. Most of the shrinkage method used ByayesShrink proposed in [CYV00] in order to calculate an adaptive threshold for wavelet thresholding. The authors in [PPLA03] proposed to balance the degree of noise reduction for the preservation of relevant details. Extension of wavelet transform are also involved in despeckling: dual tree complex wavelet transform in [VA18] or monogenic wavelet transform [GZYY18]. Other multi-scale approaches based on the pyramid transform were suggested to reduce speckle in US images as in [ZYKK07, KLY16b, SiVS+18]

3.2.4 Non-local means filter

The Non-Local (NL) approach is a new paradigm that proposes to replace the local comparison of pixels by the non-local comparison of patches [CHKB09]. Firstly introduced in [BCM05], NL-means methods were used for US noise reduction with a Bayesian formulation by Coupé et al. [CHKB09] in the Optimized Bayesian NL-means (OBNLM) filter. The OBNLM introduces a Pearson distance to compare non-local patches and select the most relevant, and uses it as features for denoising images. Related hereto, [SPR+16] propose to incorporate a Gamma model in the NL-means denoising. In [CCY+11] and [CYH+12], Yang et al. found that increasing the searching region can lead to improved noise-suppression performance in low dose CT image pro-

cessing. In [CZS+18], they incorporated a structure-adaptive fuzzy estimation into iterative NL-means for random-valued noise estimation. It was also found that NL-means estimation can be used to build the regularization term for medical image reconstruction [CMF+08]. The main drawbacks of these methods are the over-smoothing of the images, and the computational complexity.

The review of the state-of-the art methods shows that: first, the speckle reduction methods either oversmooth the ultrasound or do not reduce speckle significantly in some regions; second, all the algorithms provide only one viewing possibility, while doctors may have different requirements of image features in different situations. These motivate us to propose an improved speckle filtering method without oversmoothing effect and with multiple viewing possibilities.

3.3 Compression in medical images

Archiving medical imaging and/or their transmission for telemedicine while preserving data integrity increase the need for an efficient method of compressing medical images. In order to preserve the data integrity and for ethical considerations related to diagnosis, the medical data are mostly compressed in lossles mode. However, Koff et al. [KBB+09] studied the impact of irreversible compression on visual quality with respect of an accurate diagnostic. They suggest a range of compression levels that can be applied with confidence in diagnosis. The study involves different imaging modalities and anatomical areas. In [KUBW+14] the authors presented a work on acceptable compression ratios for lossy compression of medical images. They were able to determine a threshold level, in terms of objective quality measurement, of confidence such that the quality of the compressed image is diagnostically acceptable. Another possibility is to perform what is called near-lossless compression, which enables to limit the type and amount of distortion introduced on the compressed image. Near-lossless techniques use a quality criterion to guide the compression algorithm [AMC98].

Therefore in this section we will review non-exhaustively the methods of compression used for medical images. We will interested mainly to MRI and ultrasound modalities. But first of all, we will quickly provide some tools on which the compression algorithms are based.

3.3.1 Overview of components of image compression

Image compression needs some tools; this section relates the mains components of image compression. The use and importance of each component depends on the compression technique. Figure 3.1 shows general scheme of lossy compression.

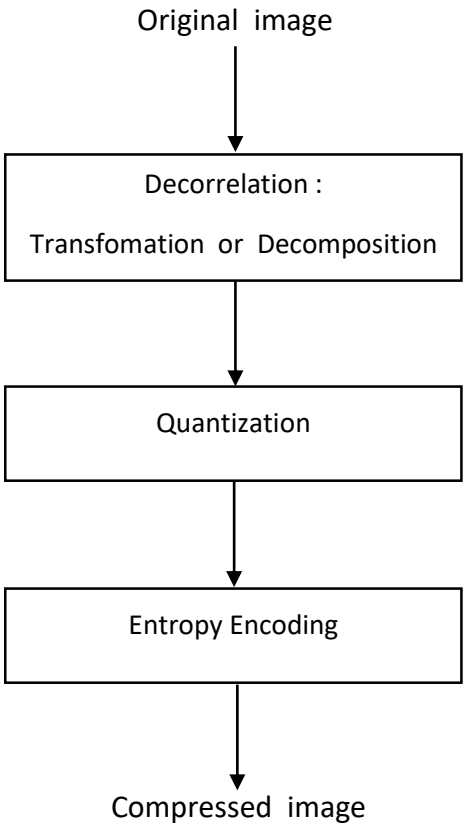

Figure 3.1: Lossy compression scheme

Decorrelation

Intuitively the compression means reduction of information, this occurs in the first step of the compression process. The redundancy of information presents in the image is used to this aim [RJ91]. Typically, there is two ways to reduce this redundancy:

- Using the property of correlation between adjacent pixels, the **predictive coding** where the purpose is to predict the value of a given pixel based on knowledge of the values of the surrounding pixels

- Using the time/frequency property to reduce the dynamic range of the signal, the **transformation of the signal**. The most widely used transforms are the Discret Cosine Transform (DCT) and the Discret Wavelet Transform (DWT).

Quantization

This step is the main difference between the lossy and lossless compression schemes. The quantization of the data reduce the number of output symbols. The bit rate and the distortion is directly driven by the quantization choice. Once the output sequence achieved, the symbols are encoded by the next step.

Entropy and entropy encoding

In the theory of information developped by Shannon [Cla48], he defines the *entropy* which permits to calculate the minimum number of bits required to code a sequence of symbols. The entropy H is defined by

$$H = -\sum_{\nu} P_\nu \log(P_\nu) \tag{3.21}$$

where P_n is probability distribution of the variable n (the probability that $\nu_i = \nu$).

The *entropy encoding* is a lossless compression scheme of data based on probability occurrence of the symbols in a sequence. Hence, each symbol will be encoded to ensure that the source encoding is the closest to its *entropy*. The code length associated to a considered symbol depends on the symbol frequency or probability of occurrence. More it is frequent, more the length is reduced. There are two main categories of entropy encoding Variable Length Code (VLC) with the well-known Huffman and Golomb codes, and the arithmetic coding which permits to encode an entire sequence of symbols.

3.3.2 Lossless compression algorithms for medical images

Compression scheme based on predictive coding technique

The predictive approach is suitable for lossless compression.It is based on the difference between the original and predicted values. Therefore, it is fully independent of the transform-based coding, and employs a differential coding: Differential Pulse Code Modulation (DPCM), to form the residuals which are then coded using either the Huffman or arithmetic coding methods.

Lossless Joint Photographic Experts Group (JPEG) The well-known JPEG standard offers two schemes a lossless and lossy scheme. The lossless mode of JPEG uses a predictive coding technique. The JPEG is recognized by Digital Imaging and Communications in Medicine (DICOM) standard which is used for storing and transmitting medical images. DICOM allows the integration of medical imaging devices such as scanners, servers, network equipment and Picture Archiving and Communication Systems (PACS) from several equipment and entities. The prediction residual is estimated from the neighboring samples previously encoded in the image [SVCK97].

Context Based, Adaptive, Lossless ImageCodec (CALIC) Proposed by [XM96], CALIC is based on the pixel context, by selecting a predictor from previously known pixels, with an adaptive improvement of the predictions. This technique has been studied in a medical context by [KOK+98].

The Low Complexity Lossless Compression for Images (LOCO-I) known as JPEG-LS [WMSS00] It is based on context modeling and predictive coding combined with an adaptation of Golomb coding. Golomb coding allows a dynamic update of the code tables which could be more suitable for an adaptive mode. The JPEG-LS allows a near lossless mode where the maximum absolute error can be limited. The lossless mode of this technique, also has been studied by [KOK+98] in a medical context.

Compression scheme based on least-squares method

In [WRA+13] the authors used the least-squares prediction with arithmetic coding for compression of MRI and CT medical images. The artithmetic coding is parallelized in oder to reduce the complexity.

Compression scheme based on Discret/Integer Wavelet Transform

In the JPEG 2000 compression the block DCT transformation has been replaced by the Discrete Wavelet Transform (DWT), which is used for its reversibility that allows lossless coding. The implementation of the DWT, know as the lifting scheme and greatly recognized as faster developed by [DS98] is the one used in the JPEG 2000. The other advantage of the lifting scheme is that it permit the construction of Integer-to-integer DWT. ZHANG et al. [ZW04] proposed an Embedded Multiple Subband Decomposition and Set Quadtree Partitioning (EMSD-SQP) based on Integer Wavelet Transform

(IWT). The subband decomposition is multiplied and scaled according to significance, and then the subbands are partitioned into four subsets. The EMSD-SQP was dedicated to medical images and compared to state of the art methods initially proposed for natural images. Shirsat et al. [SB13] were also inspired by lifting scheme with predictive coding to perform lossless compression. The Set Partitioning in Hierarchical Trees (SPIHT) compression is also a widely used technique. It uses the multiresolution representation of the image: the "S" transform. This transformation is an integer multiresolution transformation, similar to the wavelet subband decomposition. SPIHT is commonly used for comparison method as it is the case in [KOK+98] for medical context.

3.3.3 Lossy compression algorithms for medical images

Lossy compression in the medical context should be used with particular attention to ethics and diagnosis, it can be used also for specific needs such as transmission. In fact, through the literature, lossy compression for the medical image is not widely used.

One could find lossy compression for US modality combined with speckle reduction in [GSP05]. Gupta et al. propose the following method:

- Calculate the logarithm of the image
- Decompose the corrupted image using DWT
- Estimate the threshold level of the noise using BayesShrink (*cf.* 3.2.3).
- Classify the subband in order to distinguishing the noisy data
- Quantize each class using adaptive quantization
- perform entropic coding

Another study in [KUBW+14] where the authors apply a lossy JPEG or JPEG2000 compression and intend to determine a SSIM and Mean Square Error (MSE) thresholds for acceptable compression ratios without compromising diagnostic quality. Hence, a subjective test was conducted on as set of compressed CT images presented to radiologists, who were asked to assess the quality.

Conclusion

In this Chapter we have identify and analyze metrics for quantitatively assessing the speckle reduction in ultrasound medical images. Through the literature related to speckle and noise reduction in ultrasound medical imaging one could conclude that the full-reference IQA are widely used in comparison to No-reference one. In reality a genuine noise-free image is not available which compromises the evaluation.

In the other hand studies involving medical experts and quantitative methods suggest that the new objective quality metric NIQE proposed by [MSB13] can correlate with perceived quality by the human "medical expert". The NIQE seems to be a promising metric for IQA of ultrasound medical imaging particularly for evaluation speckle reduction.

Furthermore, the lossy compression is not widely used for medical imaging; nevertheless, one could investigate the possibility to perform a lossy compression controlled by an adapted quality measure which is correlated with the diagnosis performance.

CHAPTER 4

An image quality assessment metric for medical images NIQE-K

Introduction

In this chapter, we propose a new metric called Natural Image Quality Evaluator based on Kurtosis (NIQE-K) for assessing quality of medical images. It is base on NIQE and inspired by some BIQES features and is more adapted to medical images. The NIQE-K combines some low level features of the image with the NIQE to assess the quality of processed medical images. This study, based on evaluating concurrently the three methods, first encompasses tests conducted on natural IQA database (LIVE-Release2 and CSIQ). The second experiment is conducted on an ultrasound image with noise distortions. The last experiment includes tests on Magnetic Resonance images with compression distortions analyzed with quality scores evaluated by radiologists.

The opinion unaware NR metrics have not been extensively studied yet, even for natural images. In this chapter, we will focus on two state-of-the-art opinion unaware NR metrics: the natural image quality evaluator NIQE [MSB13] and the blind image quality evaluator based on scales BIQES [SW15]; more details about NR metrics are given in 3.1.2. While the NIQE has been used in [ZWC15, LMP$^+$14] for medical IQA, its competitor BIQES has not been tested in the context of medical images.

4.1 The NIQE-K for medical images

Trough the literature ($c.f 3$), two metrics are more interesting for medical field the first one is the NIQE used efficiently to asses ultrasound medical image in [LMP$^+$14] and [ZWC15]. The second one BIQES [SW15], has not been used for medical image

assessment, however this metric is not trained neither with human scores nor with pristine/distorted images.

4.1.1 Limitation of existing IQA metrics in medical images assessment

Intuitive tests, summarized in the next section, were conducted to evaluate the NIQE. It was noticed that when an image presents repeated local variations (high frequencies), the NIQE generally indicates that the image is of *good quality*. The more the local variations are, the better the quality is indicated by the NIQE. Thus the quality of a corrupting image with noise could be scored as good by the NIQE as the noise increases the local variation. This inspired us to enrich or modify the NIQE to make it more sensitive to distortions existing in medical images, such as noise. Let us show an illustration about limitation of NIQE. The Fig. 4.1 show an original image in 5.14(a) and its corrupted version with noise encountered in ultrasound image, the quality score attributed by NIQE and BIQES are indicated below each image. It should be noted that a higher value of these scores represents a lower quality of the image. Hence, the image corrupted with noise is noted as better quality by the both metric.

4.1.2 Formulation of NIQE-K

It was revealed in [SW15] that the Fourier spectra show remarkable change due to different types of distortions of the same image. The local kurtosis as well as the standard deviation of log amplitude of the Fourier spectra change significantly. The ratio of kurtosis to standard deviation is higher for blury and noisy images.

Based on the observation of BIQES formulation, we tried frequency-domain analysis to improve the perceptual evaluation of the NIQE. The $kurtosis(k)$ and the **standard deviation** σ of log amplitude of the image are use in that aim. Indeed, by multiplying the ratio $(\frac{k}{\sigma})$ by the NIQE, we obtain the named metric as NIQE-K:

$$NIQE - K = NIQE \times \frac{kurtosis\left(log\left|FFT\left(image\right)\right|\right)}{\sigma\left(log\left|FFT\left(image\right)\right|\right)} \tag{4.1}$$

(a) NIQE=2.65, BIQES=0.052

(b) NIQE=2.58, BIQES=0.048

Figure 4.1: Quality assessment comparison betwwen pristine image and noisy version 5.14(a): original image; 4.2(b): Image corrupted with Sattar's noise.

4.2 Experiment and validation of niqe-k

4.2.1 Test on Live and CSIQ IQA database

The NIQE and the BIQES have showed good performances on natural IQA databases [MSB13, SW15]. Thus we firstly compare the performances of the NIQE-K with those of the NIQE and the BIQES on natural IQA databases. The results of this experiment would help provide clues as to whether or not an opinion unaware NR natural IQA metric behaves the same for medical images as for natural ones.

We compared the three metrics on two well-known databases:

1. LIVE [SWCB05]: one of the most widely used databases for IQA algorithm validation. It consists of 29 reference images with their degraded versions, using the following distortion types: JPEG2000 (Wavelet compression), JPEG (DCT compression), White Noise in the RGB components (WN), Gaussian blur in the RGB components (GBLUR), and bit errors in JPEG2000 bitstream when transmitted over a simulated fast-fading Rayleigh (FF) channel. Each distorted image has a difference mean opinion score (DMOS) value.

2. CISQ [LC10]: It consists of 30 reference images and their degraded versions with six different types of distortions: JPEG2000 compression, JPEG compression, Additive White Gaussian Noise (AWGN), Additive Pink Gaussian noise called $1/f$ noise, Gaussian blurring (Blur), and global contrast decrements (Contrast). The DMOS of all the distorted versions of an original image is provided. Generally, only four types of distortions are used, since most IQA methods perform poorly in the case of Contrast and $1/f$ noise.

We used the Spearman's Rank-Order Correlation Coefficient (SROCC) and the Pearson's Linear Correlation Coefficient (PLCC) as evaluation measures for performance comparison. Results on the LIVE and CSIQ databases are shown in Table 4.1 and Table 4.2.

It is noticeable that the NIQE-K performs better than the NIQE and the BIQES for the AWGN distortion. Concerning the 1/f noise distortion, the NIQE-K is more correlated with human scores than the NIQE and the BIQES. Among the various noises known to commonly deteriorate the quality of medical images, the one introduced by specific reconstruction technique as that of CT images has $1/f$ frequency characteristic [GPL+11]. The performance of the considered metric on the 1/f noise distortion shows thus the potential of the NIQE-K to assess the quality of medical images. In

Table 4.1: Performance comparison in the LIVE database

	NIQE		BIQES		NIQE-K	
	SROCC	PLCC	SROCC	PLCC	SROCC	PLCC
JPEG 2000	0.89	0.90	0.88	0.88	0.66	0.70
JPEG	0.86	0.89	0.93	0.94	0.84	0.87
WN	0.97	0.97	0.97	0.97	0.97	0.98
GBLUR	0.93	0.94	0.90	0.92	0.85	0.91
FF	0.86	0.89	0.81	0.83	0.86	0.87

Table 4.2: Performance comparison in the CISQ database

	NIQE		BIQES		NIQE-K	
	SROCC	PLCC	SROCC	PLCC	SROCC	PLCC
AWGN	0.81	0.81	0.78	0.80	0.83	0.83
JPEG	0.88	0.93	0.86	0.90	0.85	0.90
JPEG 2000	0.90	0.92	0.86	0.89	0.84	0.87
1/f noise	0.29	0.34	0.25	0.26	0.55	0.56
Contrast	0.21	0.33	0.33	0.31	0.21	0.27
Blur	0.89	0.92	0.85	0.90	0.78	0.89

addition, the NIQE and the NIQE-K have the same performance on the FF distortion, which may reflect the distortion encountered in the telemedicine. While the NIQE-K's performances are close to those of the NIQE and the BIQES on most remaining distortion types, they are poorer on the JPEG2000 distortion. On this point, a further study on JPEG2000 distortion in medical context will be given in section 4.2.3.

4.2.2 Tests on simulated medical images

As a first simple step to test the three considered methods in medical context, we considered some particular distortions present in medical images, but not present in the above mentioned databases. We tested them on corrupting ultrasound images with various simulated noises, as shown in Fig. 4.2. We also included the median filtering, widely used as noise removal technique. The objective quality scores of NIQE, BIQES and NIQE-K are calculated and shown in Table 4.3 (a higher value of these scores represents a lower quality of the image).

From Table 4.3, we can see that the performance of the NIQE is consistent for the filtered images, while the performance of the BIQES is consistent for the original and the two noisy images. The NIQE-K offers a trade-off between the two metrics. Furthermore, the NIQE ranks the original image as the last (poorest quality), which is not logical. In this sense, the BIQE and the NIQE-K are comparable. Even if the

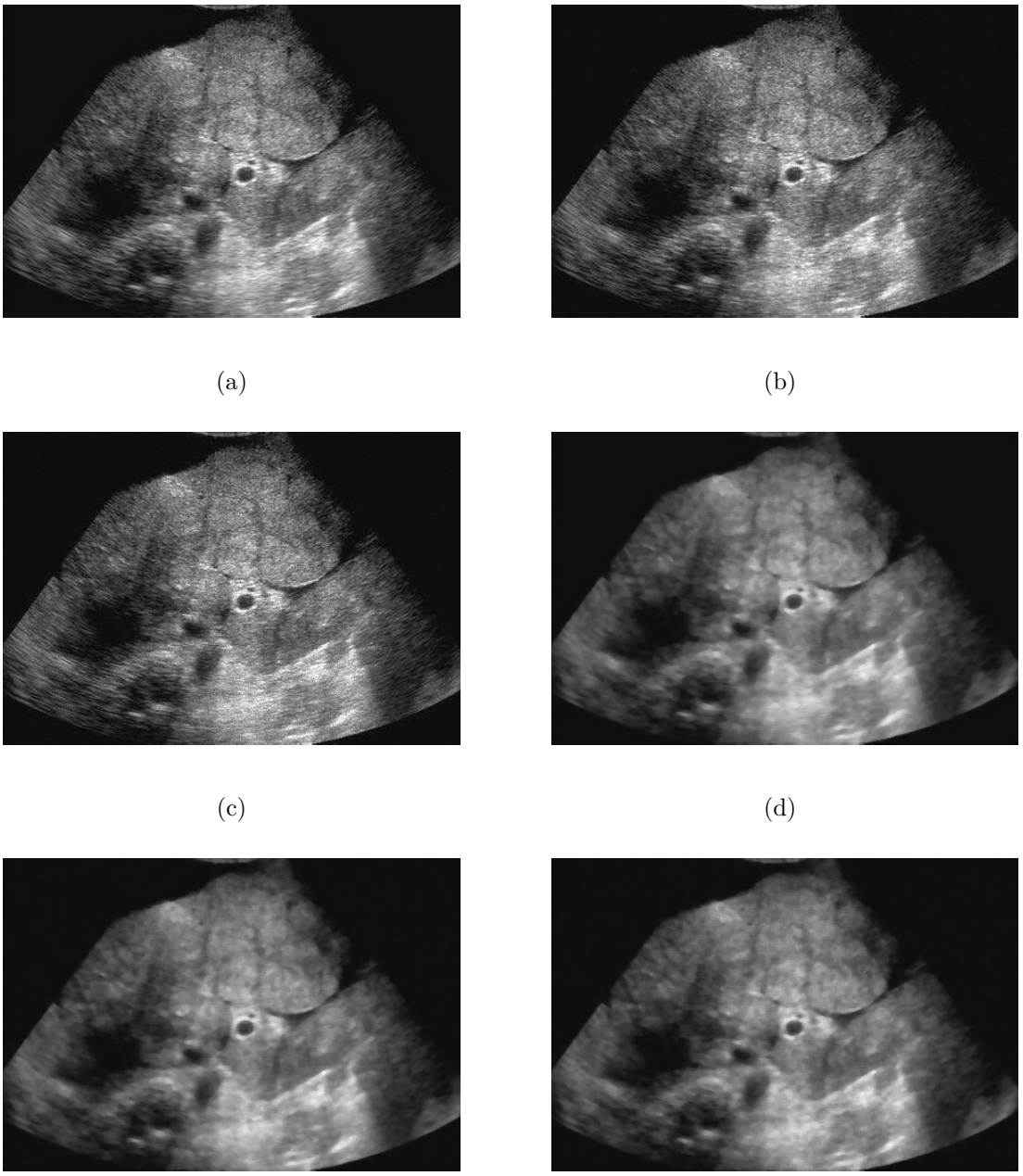

(a) (b)

(c) (d)

(e) (f)

Figure 4.2: Quality comparison of different noisy images and their filtered versions images 5.14(a): original one; 4.2(b): with Sattar's noise; 4.2(c): with Speckle noise; 4.2(d): Median filtering of 5.14(a); 4.2(e): Median filtering of 4.2(b); 4.2(f): Median filtering of 4.2(c)

Table 4.3: Quality evaluation scores of simulated images (the rankings from *best to worst* quality are given in parentheses)

Image/distortion	NIQE	BIQES	NIQE-K
Original image	6.65 (6)	0.044 (1)	19.82 (2)
Sattar's noise	4.61 (1)	0.047 (2)	18.08 (1)
Speckle noise	6.51 (5)	0.052 (3)	41.31 (6)
Original image + Median filter	5.54 (4)	0.060 (4)	27.74 (4)
Sattar's noise + Median filter	5.24 (2)	0.062 (5)	26.82 (3)
Speckle noise + Median filter	5.40 (3)	0.063 (6)	29.17 (5)

NIQE-K places a noisy image before the original one, it could be explained by the fact that an image quality (or abnormality perception) could be enhanced by adding suitable noise under certain conditions. An example is that adding stochastic resonance noise in spatial domain enhanced the quality of the X-ray mammogram in [RV13], or in wavelet domain to enhance the quality of the ultrasound images [Ral08]. It chanced that the experimental results in section 4.2.3 gave another example of medical image quality enhancement by distortion.

4.2.3 Visual evaluation of experts

In the context of medical images, the radiologist is the end-user, thus is still the ultimate reference for evaluating image quality. Thus in this last experiment, we will compare the studied three metrics' performances with those of radiologists.

Dataset from LARIS laboratory

A study was conducted by the LARIS laboratory in the University Hospital of Angers in France, of which the test images are 162 cerebral MR images of the T2 FLAIR sequence in Digital Imaging and Communication in Medicine (DICOM) format. These images were compressed by JPEG 2000, the standard recommended by DICOM, at three compression ratios: 1/1 (no compression), 1/7.5 (lossly average compression) , 1/20 (lossly high compression). The subjective evaluation of these images was made by radiologists with different years of experience: the first radiologist (denoted by Expert 1) is an expert in neuroradiology; the radiologist 2 and 3 (denoted by Resident 1 and 2) are residents in radiology with respectively 4 and 5 years' experience. The diagnostic purpose of this study was the detection-localization of Multiple Sclerosis (MS) lesions, while Resident 1 had theoretical knowledge about the MS and Resident 2 had analyzed 30 MS images per month for 6 months.

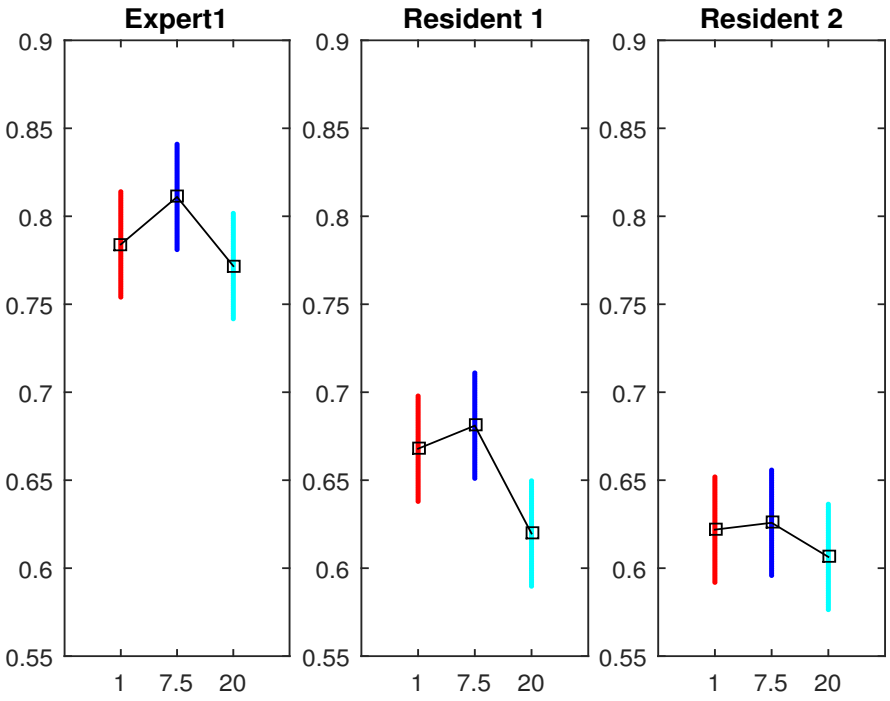

Figure 4.3: Quality score (the ordinate) evaluated by each radiologist for each compression ratio (the abscissa), a higher value represents a better quality here.

In this study, the question was not *how well the image was pleasing*, but *how well the image allowed the radiologist to diagnose the disease*. The detection-localization task performances of the radiologists were then characterized/quantified by the JAFROC figure of merit [Cha11] to get their final quality scores ranging from 0 to 1.

Discussion

The final quality score of each radiologist for each compression ratio is shown in Fig. 4.3. It is interesting to find that the quality appears best for the images compressed at the compression ratio 1/7.5, and worst at the compression ratio 1/20 for all the radiologists. This reveals that a slight compression may promote the abnormality diagnosis by a radiologist, while a heavy compression would substantially deteriorate the radiologist's diagnostic performance. Other distortions (e.g. noise) may have the same effect, as mentioned in section 4.2.2.

Fig. 4.4 shows the BIQES, NIQE and NIQE-K scores calculated for each of the test images at three compression ratios. Since a higher value of the three metrics represents a lower quality, we show the multiplicative inverse for the score (consequently a higher

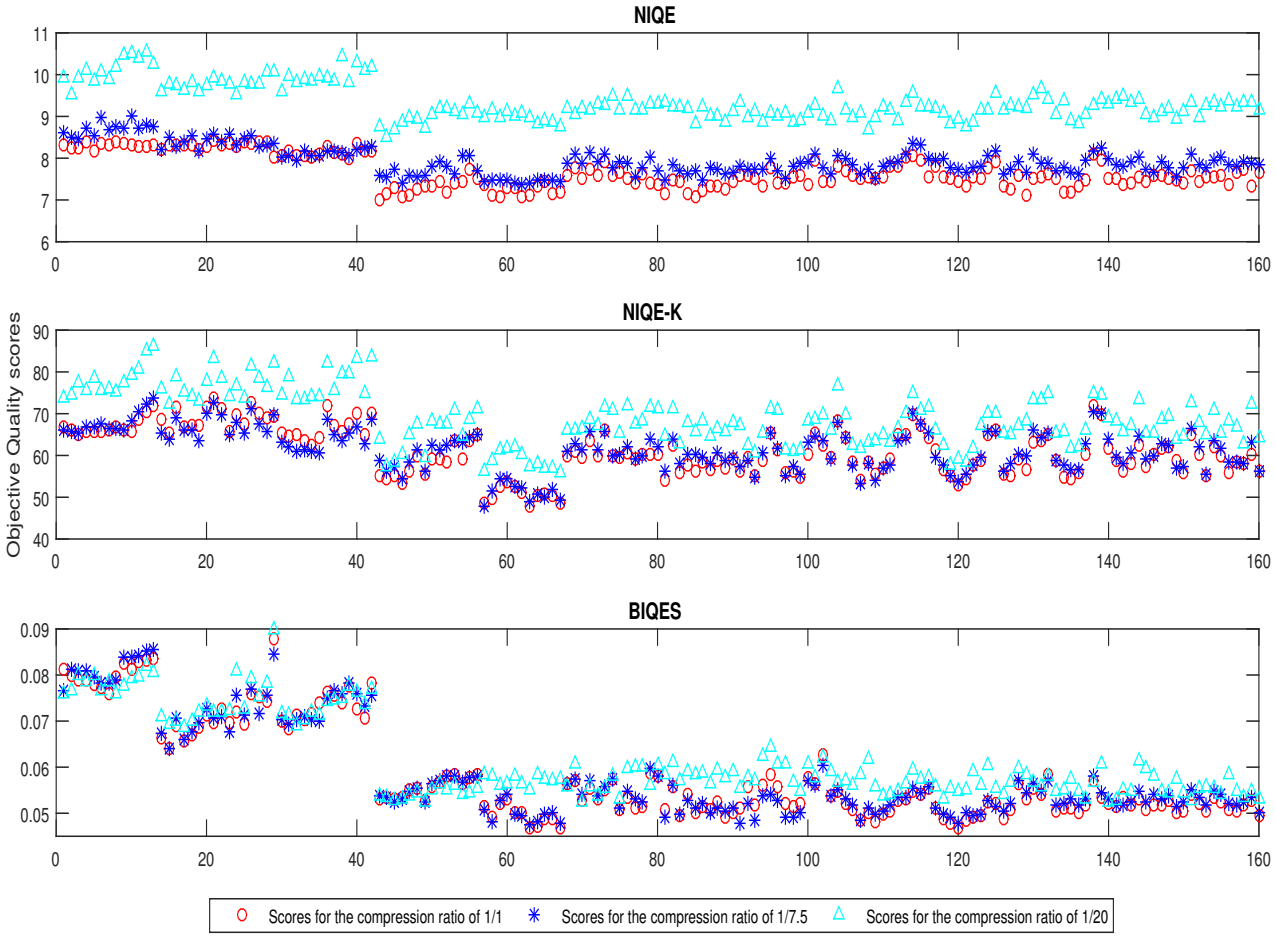

Figure 4.4: Objective scores of BIQES, NIQE and NIQE-K for each image (a higher value represents a lower quality)

value represents a better quality here) in Fig. 4.5 to facilitate the comparison with human scores in Fig. 4.3. By comparing Fig. 4.5 to Fig. 4.3, we observe that while the BIQES does not distinguish well the qualities of images compressed at three different ratio (i.e. similar scores for the three ratios), the NIQE and the NIQE-K do. However, the NIQE rates the qualities of images compressed at the ratio of 1/1 much better than those at the ratio of 1/7.5, and the NIQE-K rates the qualities of images compressed at the two ratios almost the same. We also counted the percentage of the images rated by the three metrics in the same way as the radiologists: 39% for the NIQE-K, 7% for the NIQE and 28% for the BIQES. That means that on these images the objective metrics rank the ratio 1/7.5 as the best, followed by the ratio 1/1, and the ratio 1/20 as the worst. From this point of view, the NIQE-K's behavior is the closest to that of radiologists.

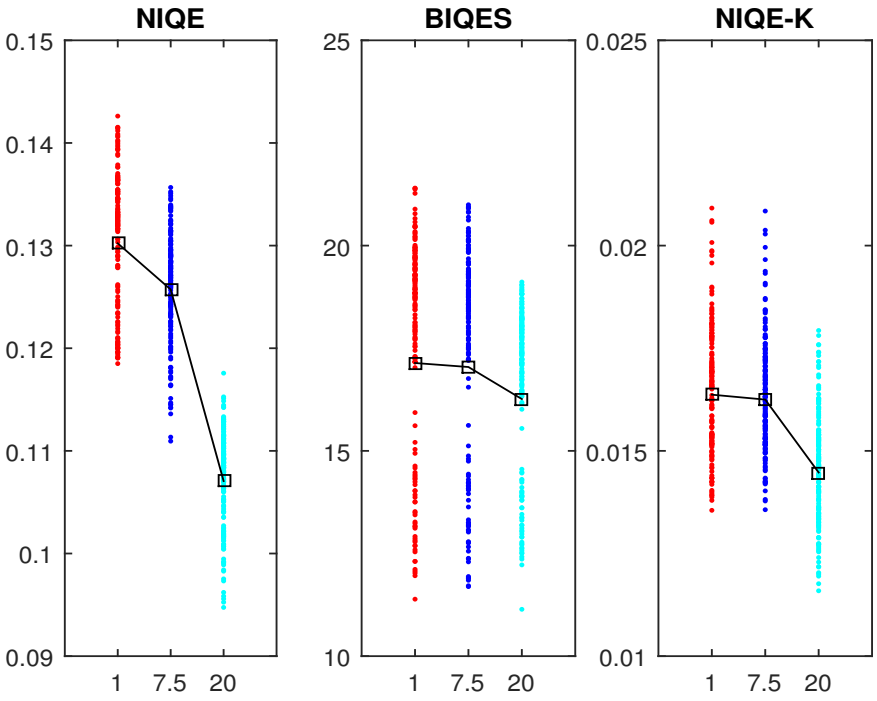

Figure 4.5: Objectives scores of BIQES, NIQE and NIQE-K for each compression rate (a higher value represents a better quality), each point corresponds to an image, and the mean of their scores are linked by a black straight line.

Conclusion

We have presented in this chapter our proposed OU NR IQA metric NIQE-K proposed for medical image assessment. Moreover, it involved a study of the usability of 2 others OU NR IQA metrics in the context of medical images: NIQE and BIQES. Results show that the IQA metrics for natural images could potentially be modified and applied for medical IQA. When the modification considers the specificities of medical images, we can approach satisfyingly radiologists' perception. Experiments conducted on MR images with specific diagnostic tasks highlight a greater potential of the NIQE-K. More analysis and experiments, over US images modalities are presented in the next chapter.

CHAPTER 5

The Multi-Output Filter based on MMD

Introduction

A large number of researches were proposed in order to reduce speckle and/or improve the quality of US images. We have presented in section 3.2 a review of post-processing speckle reduction techniques. These techniques present some limitations such as texture over-smoothing, loss of subtle details during the filtering process or moreover edge blurring. Some filtering methods also give artificial appearance to the enhanced images [ZWC15]. Moreover, all the speckle reduction works propose a unique viewing possibility, while the interpretation of an US is based on multiple evaluation tasks: general aspect, echo patten, outer contour/border and size. To address this issue, we propose in this chapter the Multi-Output Filter based on Multiplicative Multiresolution Decomposition (MOF-MMD) [OZD+17] [OZD+18] , which performs speckle reduction in order to enhance the relevant structures and textures (edges, texture and the global image) according to different diagnosis needs. The MOF-MMD permits to enhance distinctively three outputs: edges, texture and and the global image.

5.1 Multi-Output Filter based on Multiplicative Multiresolution Decomposition (MOF-MMD)

The proposed MOF-MMD is schematically represented in Fig. 5.1. It consists of five steps[OZD+18]:

- Preliminary step of features-like segmentation achieved using morphological operators;
- Calculation of noise level on local window;

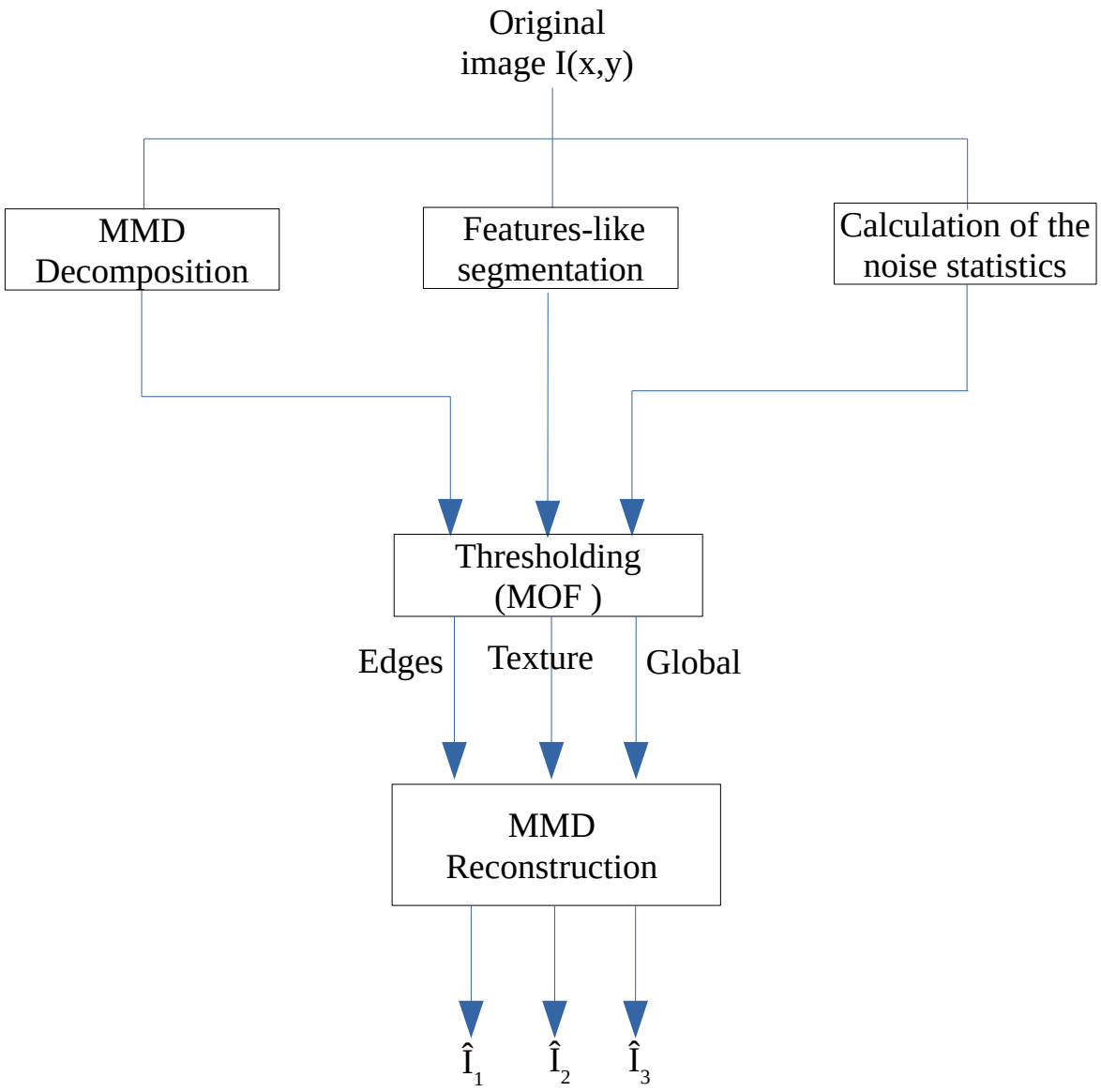

Figure 5.1: MOF-MMD Diagram

- Multi-scale decomposition using MMD;
- Thresholding process according to the features;
- Reconstruction of enhanced images using MMD synthesis.

The details of each step are given below.

5.1.1 Multiplicative multiresolution decomposition

Multiplicative decomposition

The nonlinear multiplicative decomposition is a multi-scale analysis/synthesis representation of 2D signals [SB04]. This nonlinear decomposition is suitable for multiplicative noise reduction and has been used to reduce multiplicative noise in Synthetic Aperture Radar [SB04] and medical US images [OSK14]. It uses filter banks with critical sub-sampling and perfect reconstruction (reversible). In [SB04] the authors consider a description of the analysis and the synthesis inputs-outputs systems with equal symbol rates at both the input and the output. The image is decomposed into an approximate output subband y_1 and three detail images y_{2h}, y_{2v} and y_{2d} characterized by horizontal, vertical and diagonal directions. The desired structure is obtained by performing a polyphase decomposition of the 2D signal (the image) [SBK13]. To avoid division by zero, the value 1 is added to the original image to provide the input image (I). The four poly-phase components x_{11}; x_{12}; x_{21} and x_{22} of the input image I of size $N \times M$ are defined by:

$$x_{ij}(n,m) = I(2(n-1)+i, 2(m-1)+j) \quad i,j \in \{1,2\} \tag{5.1}$$

where $n = 1, ..., \frac{N}{2}$ and $m = 1, ..., \frac{M}{2}$

The multiplicative decomposition could be used within its undecimated version, with an equal number of coefficients at each resolution scale. The four polyphase components for practical implementation of this undecimated algorithm are defined by:

$$x_{ij}(n,m) = I(n+i-1, m+j-1) \quad i,j \in \{1,2\} \tag{5.2}$$

where n = 1,...,N and m = 1,...,M

For $(i,j) \in \{1,2\}$, the linear filter h_{ij} and f_{ij} are given by:

$$\begin{cases} h_{ij}(k,l) = h((2k+1)+i, 2(l+1)+j) \\ f_{ij}(k,l) = \frac{1}{h_{ij}(k,l)} \end{cases} \tag{5.3}$$

where h and f are bi-dimensional linear filters. The approximation y_1 is given by

$$y_1 = \sum_{i=1}^{2}\sum_{j=1}^{2} h_{ij} x_{ij}. \tag{5.4}$$

The nonlinear analysis filters D illustrated in Fig. 5.2, is defined by the following equations:

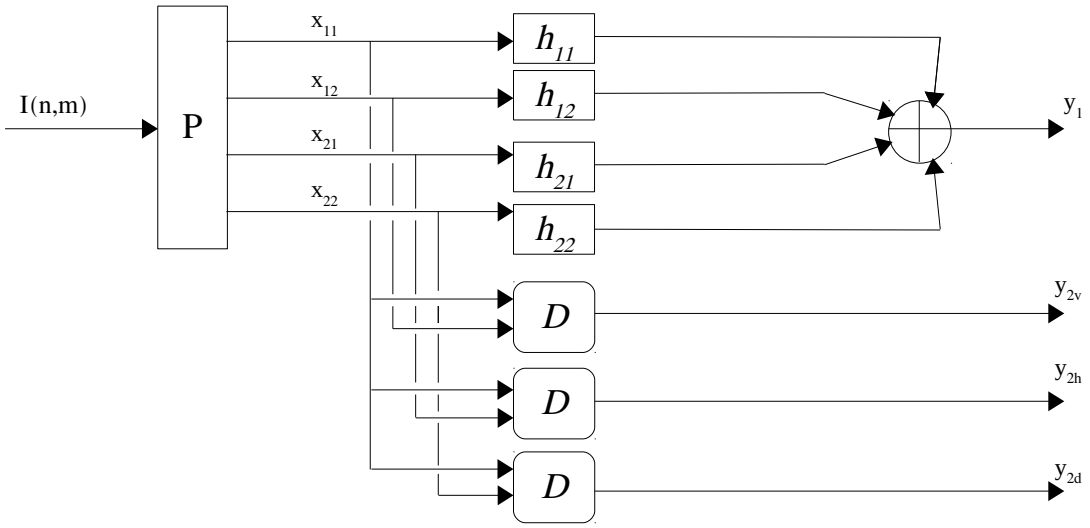

Figure 5.2: The 2D MMD analysis scheme

$$y_{2v} = \begin{cases} \beta \frac{x_{12}}{x_{11}}, & x_{11} \geq x_{12} \\ \beta \left(2 - \frac{x_{11}}{x_{12}}\right) & otherwise \end{cases} \tag{5.5}$$

$$y_{2h} = \begin{cases} \beta \frac{x_{21}}{x_{11}}, & x_{11} \geq x_{21} \\ \beta \left(2 - \frac{x_{11}}{x_{21}}\right) & otherwise \end{cases} \tag{5.6}$$

$$y_{2d} = \begin{cases} \beta \frac{x_{22}}{x_{11}}, & x_{11} \geq x_{22} \\ \beta \left(2 - \frac{x_{11}}{x_{22}}\right) & otherwise \end{cases} \tag{5.7}$$

where β is a positive scalar fixed to 0.5. The details y_{2h}, y_{2v} and y_{2d} vary within the interval $[0; 1]$. It should be noted that high contrasted details correspond to values far from β, whereas, values close to β correspond to smooth regions.

Multi-resolution decomposition

Multi-resolution decomposition is based on subband decomposition using analysis filter bank that operates at different stages of the outputs. The approximate output subband y_1 is decomposed into one or more coefficient outputs of the preceding stage. In the subband, y_1 is split into its polyphase y_{11}, y_{12}, y_{21} and y_{22} and then filtered. At the first resolution $j = 1$:

$y_{11}^{(j)} = x_{11}$, $y_{12}^{(j)} = x_{12}$, $y_{21}^{(j)} = x_{21}$ and $y_{22}^{(j)} = x_{22}$.

At the highest resolution J, the original discrete image is represented by the set R defined by

$$R = \left({y_1}^{(j)}, \left({y_{2h}}^{(j)}, {y_{2v}}^{(j)}, {y_{2d}}^{(j)} \right) \right)_{2 \leq j \leq J} . \tag{5.8}$$

Fig. 5.3 illustrates the undecimated multiplicative multi-resolution decomposition for one resolution level of an US image of an agar gel phantom.

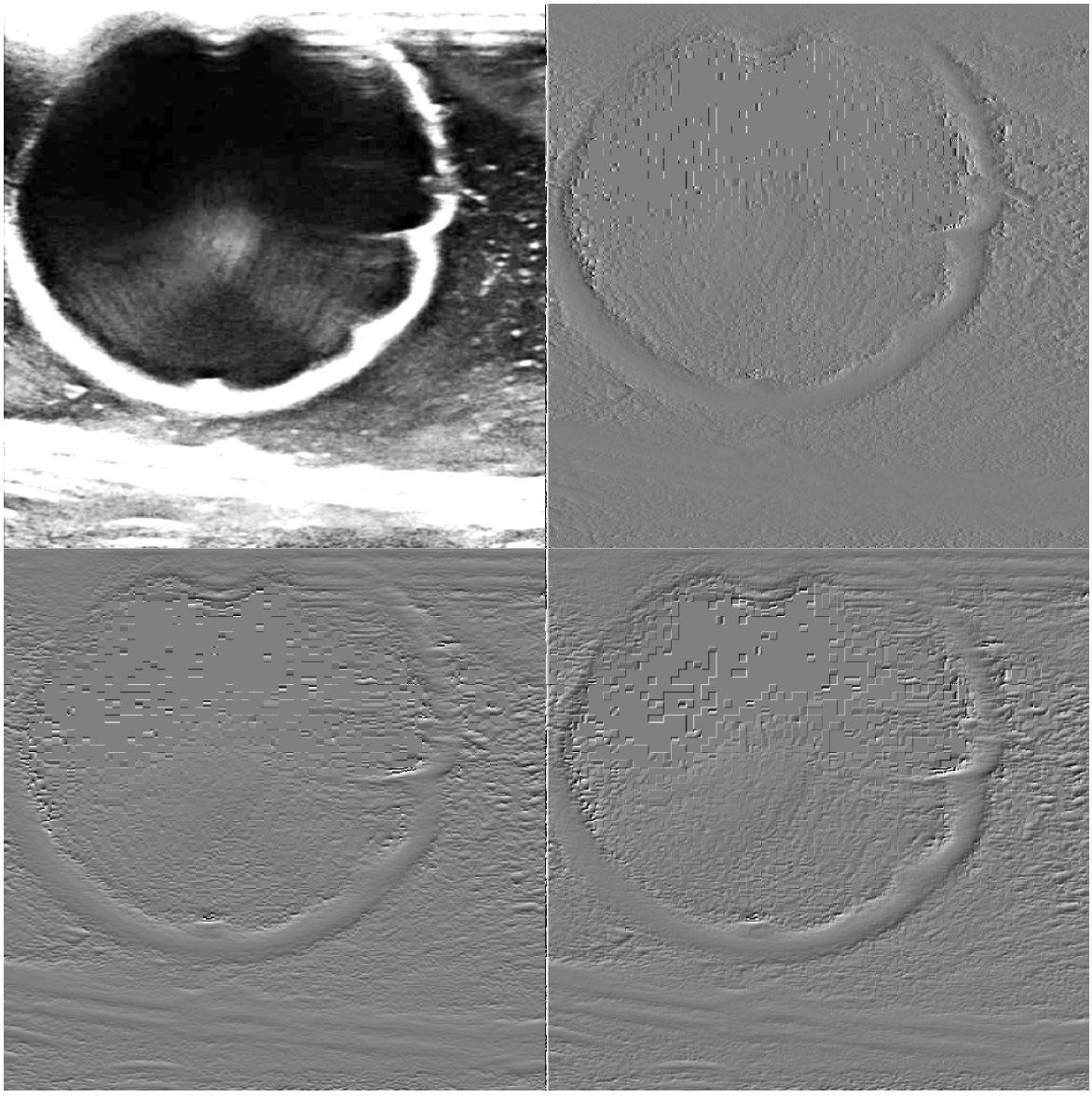

Figure 5.3: 2D MMD undecimated decomposition of US image of an agar gel phantom: approximation image (upper left), detail images vertical, horizontal and diagonal

MMD reconstruction

Lets $\hat{D}_{C,1}^{(J)}, \hat{D}_{C,2}^{(j)}, \hat{D}_{C,3}^{(j)}$ the three obtained MMD's coefficients according to the above-mentioned criteria. The thresholding process will be presented in the next section. These coefficients are reconstructed by MMD synthesis into the enhanced images $\hat{I}_1, \hat{I}_2, \hat{I}_3$. It should be noted that the approximate component y_1 is the same for the three outputs and that $\hat{D}_{C,j}^{(J)}$ are computed as follows:

$$\hat{D}_{C,1}^{(J)} = (y_{2H}^{(J)}, y_{2V}^{(J)}, y_{2D}^{(J)})_1$$

$$\hat{D}_{C,2}^{(J)} = (y_{2H}^{(J)}, y_{2V}^{(J)}, y_{2D}^{(J)})_2$$

$$\hat{D}_{C,3}^{(J)} = (y_{2H}^{(J)}, y_{2V}^{(J)}, y_{2D}^{(J)})_3$$

Here, we will describe a reconstruction on an image $\hat{I}$ from $(y_1, y_{2H}^{(J)}, y_{2V}^{(J)}, y_{2D}^{(J)})$. Let us consider one resolution of the reconstructed signal: the nonlinear synthesis filters r_{ij} represented on Fig. 5.4, are defined by the following equations:

$$r_{11}\left(y_{2h}, y_{2v}, y_{2d}\right) = \frac{1}{1 + \frac{h_{12}}{h_{11}}\gamma_v + \frac{h_{21}}{h_{11}}\gamma_h + \frac{h_{22}}{h_{11}}\gamma_d} \tag{5.9}$$

$$r_{12}\left(y_{2h}, y_{2v}, y_{2d}\right) = \gamma_v r_{11}\left(y_{2h}, y_{2v}, y_{2d}\right) \tag{5.10}$$

$$r_{21}\left(y_{2h}, y_{2v}, y_{2d}\right) = \gamma_h r_{11}\left(y_{2h}, y_{2v}, y_{2d}\right) \tag{5.11}$$

$$r_{22}\left(y_{2h}, y_{2v}, y_{2d}\right) = \gamma_d r_{11}\left(y_{2h}, y_{2v}, y_{2d}\right) \tag{5.12}$$

where

$$\gamma_v = \begin{cases} \frac{y_{2v}}{\beta}, & y_{2v} \leq \beta \\ \frac{1}{2 - y_{2v}/\beta} & otherwise \end{cases} \tag{5.13}$$

$$\gamma_h = \begin{cases} \frac{y_{2h}}{\beta}, & y_{2h} \leq \beta \\ \frac{1}{2 - y_{2h}/\beta} & otherwise \end{cases} \tag{5.14}$$

$$\gamma_d = \begin{cases} \frac{y_{2d}}{\beta}, & y_{2d} \leq \beta \\ \frac{1}{2 - y_{2d}/\beta} & otherwise \end{cases} \tag{5.15}$$

According to equations (5.9)-(5.12), the nonlinear response filters r_{ij} are expressed as a function of the nonlinear outputs y_{2h}, y_{2v} and y_{2d}. The reconstructed polyphase components $\hat{x}_{kl}$ are expressed as follows:

$$\hat{x}_{11} = f_{11} \times y_1 \times r_{11}\left(y_{2h}, y_{2v}, y_{2d}\right) \tag{5.16}$$

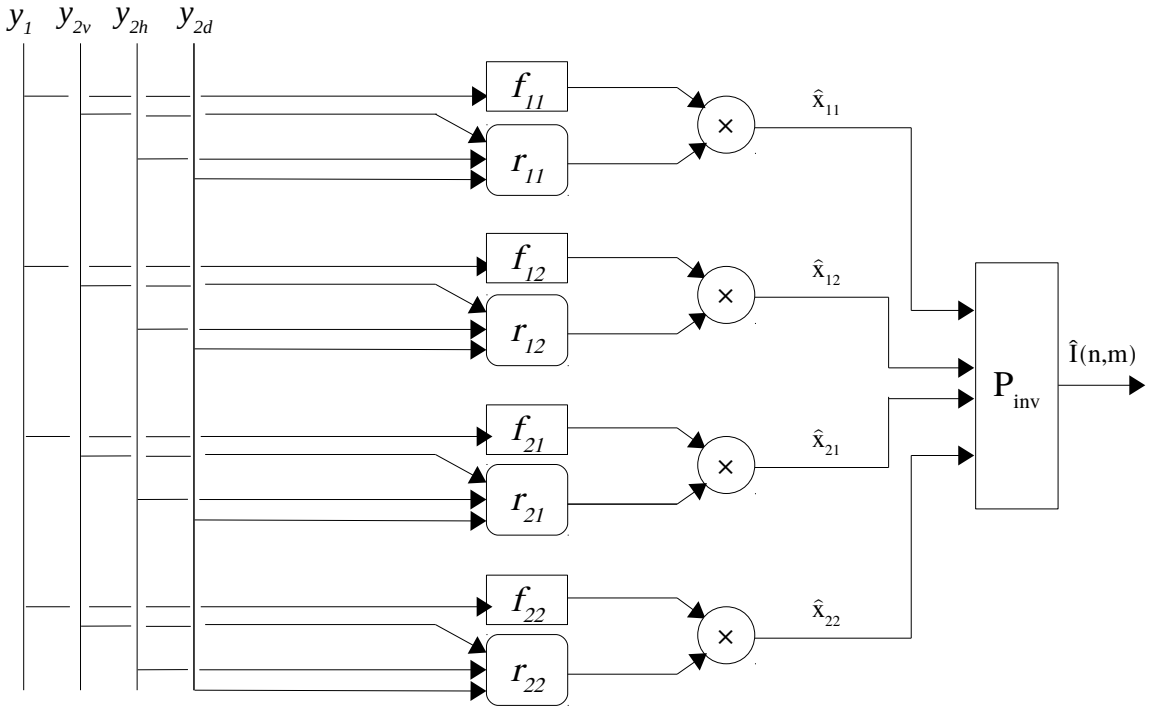

Figure 5.4: The 2D MMD synthesis scheme

$$\hat{x}_{12} = f_{12} \times y_1 \times \gamma_v \times r_{11}\left(y_{2h}, y_{2v}, y_{2d}\right) \tag{5.17}$$

$$\hat{x}_{21} = f_{21} \times y_1 \times \gamma_h \times r_{11}\left(y_{2h}, y_{2v}, y_{2d}\right) \tag{5.18}$$

$$\hat{x}_{22} = f_{22} \times y_1 \times \gamma_d \times r_{11}\left(y_{2h}, y_{2v}, y_{2d}\right) \tag{5.19}$$

These equations represent the reconstructed signal as a product of a smooth component $fij \times y_1$, and a component containing all the signal variations expressed as localized directional ratios y_{2h}, y_{2v}, y_{2d}. Then, the reconstructed image $\hat{I}$ by MMD synthesis, is obtained by subtracting the value 1 from the result of the reconstructed polyphase components as follows:

$$\hat{I}\left(n+i-1, m+j-1\right) = \hat{x}_{ij}\left(n, m\right) \quad i, j \in \{1, 2\} \tag{5.20}$$

where n = 1,...,N and m = 1,...,M

For the multi-resolution synthesis, the reconstructed process is iterated to produce successive approximations based on the set R (cf. equation 5.8). The final synthesized image is obtained at resolution $j = 1$.

5.1.2 Features-like segmentation by morphological operators

We proposed a speckle reduction algorithm where, the features-like segmentation enables the enhancement of the different features and structures of the image. It is performed using mathematical morphology.

Morphological Operators

Morphological operators are used here to segment features-like structures. Indeed, mathematical morphology is a well established domain used for image analysis. Based on the algebra of non-linear operators, it performs better and faster than the standard approaches in many tasks such as pre-processing, segmentation using object shape and object quantification [SHB07]. We will define some basic morphological operators. Firstly, a shape parameter called structuring element, characterized by its shape and size, is used to perform morphological techniques. Depending on the type of morphological transformation, the pixel value is set to the minimal or maximal value of the pixels [DNB13].

Let A be the grayscal image and B the structuring element. The two fundamental operations erosion and dilation are respectively given by :

$$A \ominus (B) = min\left\{(A)_p \mid P \in B\right\} \tag{5.21}$$

$$A \oplus (B) = max\left\{(A)_p \mid P \in B\right\} \tag{5.22}$$

Two other operators opening/closing are obtained by combination of erosion and dilation operations. An erosion (resp. dilation) by B followed by a dilation (resp. erosion) by $\tilde{B}$, the symmetrical element of B, is called an opening (resp. closing) operation:

$$A \bullet (B) = (A \ominus B) \oplus \tilde{B} \tag{5.23}$$

$$A \circ (B) = (A \oplus B) \ominus \tilde{B} \tag{5.24}$$

where $\oplus$, $\ominus$, $\circ$ and $\bullet$ denote dilatation, erosion, opening and closing operators, respectively.

Features-like segmentation

As medical images generally contain more round shapes than straight lines and angles, the disk-shaped structuring element is a more appropriate choice. An algorithm for the efficient computation of morphological operations for gray images with a circular structuring element has been proposed in [DNB13].

Let I be the original US image and C the circular structuring element with a radius of eight pixels. The features-like segmentation is obtained as follows:

$$I_{(o)} = I \circ C \tag{5.25}$$

$$I_{(oc)} = I_{(o)} \bullet C \tag{5.26}$$

$$I_{(e)} = I_{(oc)} \ominus C \tag{5.27}$$

$$I_{(d)} = I_{(oc)} \oplus C \tag{5.28}$$

$$S = I_{(d)} - I_{(e)} \tag{5.29}$$

where $\oplus$, $\ominus$, $\circ$ and $\bullet$ denote dilatation, erosion, opening and closing operators, respectively. S represents the contour image obtained by morphological treatment and illustrated in Fig. 5.5(b).

5.1.3 Calculation of Noise Statistics

The MOF-MMD is sensitive to noise statistics, indeed the thresholding step depends on the knowledge of these statistics. Therefore, we propose an automatic method to select a homogeneous window H_{area} to calculate the noise. The speckle filtering framework proposes an automatic estimation of the noise variance [RDM99]. In the case of homogeneous areas H_{area}, where the signal component can be considered constant and the image variation is only attributable to noise, the standard deviation of the speckle noise is given by:

$$R = \frac{Std_{H_{area}}}{\mu_{H_{area}}} \tag{5.30}$$

where $Std_{H_{area}}$ and $\mu_{H_{area}}$ stand for standard deviation and mean values of H_{area}, respectively. First, in order to avoid the black part of the ultrasound, the H_{area} must be inside the contour S extracted in the previous Section 5.1.2. Second, in order to detect H_{area} we use MMD's coefficient properties (described in Section 5.1.1). In smooth regions, the values of the MMD's coefficient components are close to β. H_{area} corresponds

(a) Original image

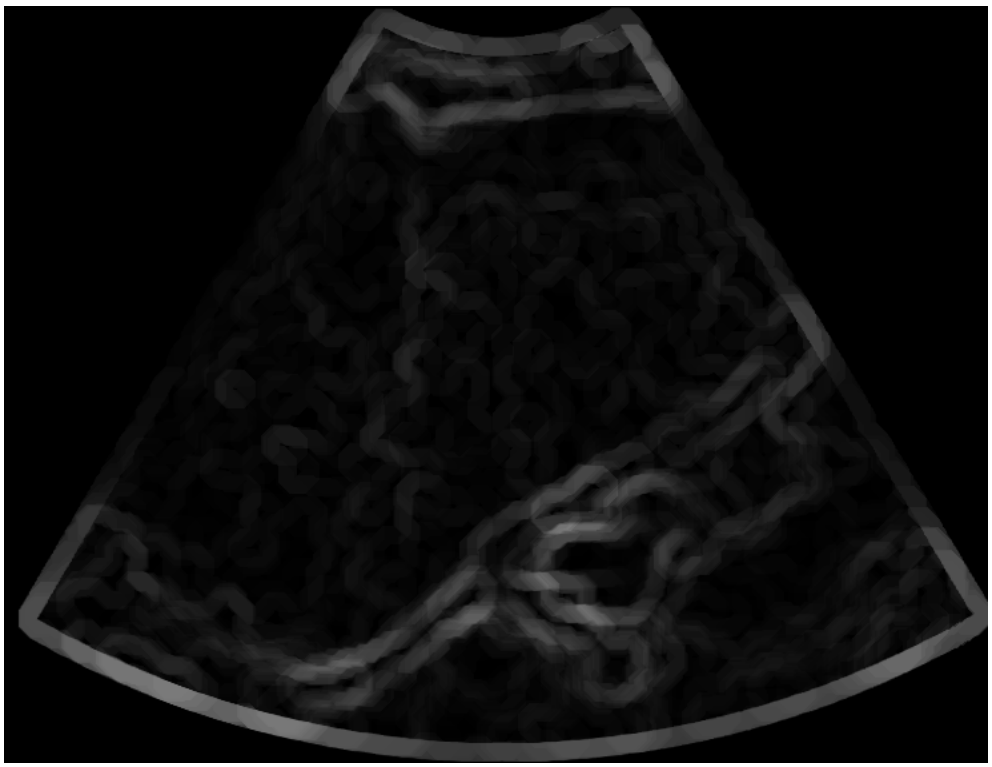

(b) Contour image

Figure 5.5: Features-like segmentation

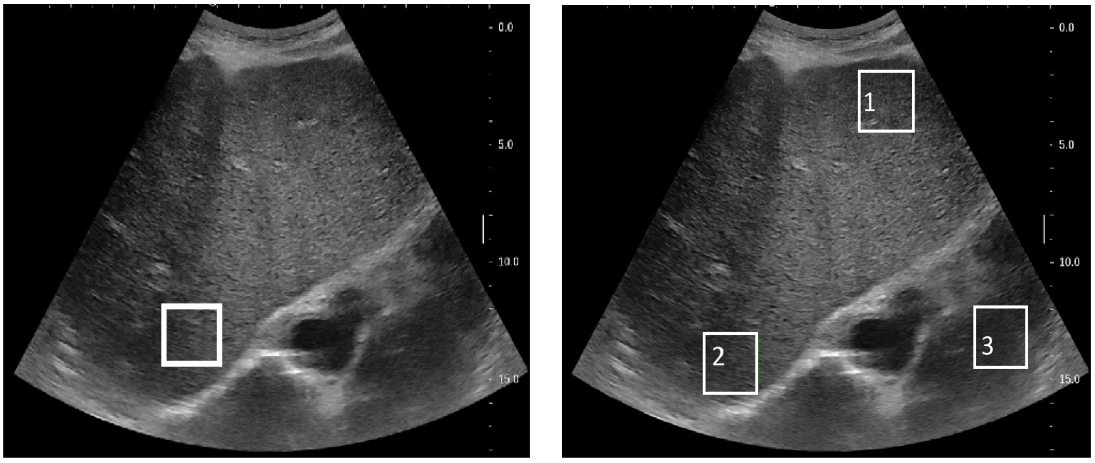

(a) Auomatic selection (b) Manual selection

Figure 5.6: Local window selection for calculation of C_n and T

to the one that minimized the median absolute deviation mad around β

$$mad = \frac{1}{n}\sum_{i=1}^{n}\left|y^1_{2(h,v,d)}(i) - \beta\right|_{i\in H_{area}} \tag{5.31}$$

The noise level is then calculated within the selected window $W = H_{area}$. So, at each resolution, one could estimate the normalized standard deviation $C_n = \sqrt{\frac{var_W}{\mu_W}}$ by using the variance var_W and the mean value μ_W of the selected window. The manual selection of multiple windows W is possible, thanks to the quality criterion selection (cf. Section 5.1.1). Fig. 5.6(a) and Fig. 5.6(b) depict the results of obtained areas by using automatic and manual processes, respectively. A good agreement is obtained by automatic calculation of noise statistics. This automation makes it possible to divide the length of the manual selection process by at least N (number of manually selected windows).

5.1.4 Thresholding: Multi-Output filter

The existing speckle reduction methods propose a unique enhancement for the overall image. Sometimes a stopping criterion is applied for specific structures of the image. Nevertheless, there is only one viewing possibility. Herein, we propose a new method that allows to the medical observer to view multiple enhancement possibilities of the original US image. This can respond to the specific need for a diagnosis, according to which it is **more relevant** to examine edges, texture, thickness, etc.

As indicated in Section 5.1.1, in smooth regions the values of the MMD's coefficient components are close to β. This property helps to enhance the image while preserving

structural details and avoiding a blurring effect. In the rest of this section, we will refer to MMD coefficient details y_{2H}, y_{2V}, y_{2D} by D_C where C stands for $'H'$ horizontal, $'V'$ vertical and $'D'$diagonal details.

The selection of the optimal threshold is the main limitation of the thresholding filter. To overcome this we propose to adapt thresholding to the local context. Thus, this is done according to the pixel intensity of the images obtained from features-like segmentation. This allows multiple enhancement possibilities of the original US image.

In this aim, at each resolution j, the MMD's coefficient $D_C^{(j)}$ is thresholded in three ways to provide the thresholded coefficient $\hat{D}_{C,k}^{(j)}$ with $k = 1, 2, 3$.

Filter first output - Sharp edge enhancement

This first output of the filter is an image with enhanced edges. It is pertinent for measures conducted in US images such as lesion size, distance and so on. For each pixel of the contour image, a thresholding is applied as follows:

$$\hat{D}_{C,1}^{(j)} = \begin{cases} \beta \quad if \qquad \beta - \beta_t \leq D_C^{(j)} \leq \beta + \beta_t \\ D_C^{(j)} \times \nu - (\gamma \times \alpha \times S) \quad if \quad D_C^{(j)} + \tau \leq \beta \\ D_C^{(j)} \times \nu + (\gamma \times \alpha \times S) \quad if \quad D_C^{(j)} - \tau \geq \beta \\ \beta \quad otherwise \end{cases} \tag{5.32}$$

where $D_C^{(j)}$ and $\hat{D}_{C,1}^{(j)}$ represent the MMD's coefficients at scale j of the original noisy image I and its thresholded version, respectively. β_t is a threshold that aims to reduce the speckle of the coefficient components in the smoothest pixels. β_t is set experimentally to 0.0016. $\tau = (T \times \nu \times \alpha \times S)$, with $T = C_n \times j/J$ is the threshold calculated from the noise level at each scale j while J represents the number of scales. α is set to 0.25 to avoid the displacement of edge pixels in the filtered images. ν and γ are given by $\nu = \frac{1}{\sqrt{1+{C_n}^2}}$ and $\gamma = 1 - \frac{1}{\sqrt{1+{C_n}^2}}$. Notice that the thresholding is proportional to the contour images *i.e.,* the thicker is the edges the more it is enhanced. Fig 5.7 shows the MOF-MMD first's output after MMD reconstruction of 5.32

Filter second output - Texture enhancement

This second output of the filter is an image with enhanced texture. It is pertinent to enhance texture by reducing speckle while preserving the texture pattern. Let $\bar{S}$ denote the image of pixels that belong to the original image and do not belong to the contour S. The second output results from the following thresholding:

Figure 5.7: MOF-MMD 1st OUTPUT

$$\hat{D}_{C,2}^{(j)} = \begin{cases} \beta \quad if \qquad \beta - \beta_t \leq D_C^{(j)} \leq \beta + \beta_t \\ D_C^{(j)} \times \nu - \left(\gamma \times \bar{S}\right) \quad if \quad D_C^{(j)} + \xi \leq \beta \\ D_C^{(j)} \times \nu + \left(\gamma \times \bar{S}\right) \quad if \quad D_C^{(j)} - \xi \geq \beta \\ \beta \quad otherwise \end{cases} \tag{5.33}$$

with $\xi = T \times \nu \times \bar{S}t$, Fig 5.8 shows the MOF-MMD second's output after MMD reconstruction of 5.33

Filter third output - Global image enhancement

The third output of the filter is a global enhancement of the image. Based on the complement of the image contour (Co_S), which is obtained by subtracting the pixel value of the contour image S from the maximum pixel value of (S), S_{max} is as follows:

$$Co_S = S_{max} - S \tag{5.34}$$

Figure 5.8: MOF-MMD 2nd OUTPUT

The MMD's coefficients are thresholded according to the Co_S image values, as follows:

$$\hat{D}_{C,3}^{(j)} = \begin{cases} \beta \quad if \qquad \beta - \beta_t \leq D_C^{(j)} \leq \beta + \beta_t \\ D_C^{(j)} \times \nu - (\gamma \times Co_S)\, if D_C^{(j)} - (\gamma \times Co_S) \leq \beta \\ D_C^{(j)} \times \nu + (\gamma \times Co_S)\, if D_C^{(j)} + (\gamma \times Co_S) \geq \beta \\ \beta \quad otherwise \end{cases} \tag{5.35}$$

where n = 1,...,N and m = 1,...,M

Fig 5.9 shows the MOF-MMD third's output after MMD reconstruction of 5.35

5.2 Experiment and validation of mof-mmd

In order to evaluate the performance of the proposed MOF-MMD, two kinds of tests are conducted: quality assessment using objective metrics and qualitative visual evaluation by medical experts. The proposed filter performance is compared with two recent and efficient speckle reduction filters, OBNLM [CHKB09] and ADMSS [RLVSFMF$^+$14].

Figure 5.9: MOF-MMD 3rd OUTPUT

5.2.1 Image dataset

The original clinical US images of *in vivo* abdominal liver were obtained from a retrospective database of the University Hospital of Angers in France. The 21 experimental images of different liver with different resolutions ($1080 \times 810, 1024 \times 768$) were captured by SuperSonic Aixplorer and the Siemens Acuson S2000 system. The images are of granular, smooth, cirrhotic and non-cirrhotic liver. The ethical approval to use image after anonymization was obtained from the University Hospital of Angers. The images were registered in an external PC and processed offline.

5.2.2 Evaluation methods

The evaluation is carried out, on the 21 ultrasound images, in terms of speckle reduction capacity and the improvement of image quality. To quantify the speckle reduction achieved by different filters, the speckle's signal-to-noise ratio (SSNR) is measured [KLY16b]. For the quality evaluation metrics, three Image Quality Assessment (IQA) metrics were also chosen to assess the quality of the filtered images. As there is no genuine reference image in our cases, we consider blind objective metrics. For evaluating our proposed method, we use the two state-of-the-art no-reference metrics

NIQE [MSB13] and BIQES [SW15], presented in 3, and our proposed blind metric NIQE-K [OZD+16].

5.2.3 Subjective experiment

Human observer

Three radiologists with different years of experience (3 years, 7 years and more than 10 years experience) were asked to score the perceived quality of the filtered images, based on four criteria: the image contrast, the ability to diagnose, the texture conspicuity and the edge sharpness. The radiologists are from the affiliated Hospital of Nanjing Medical University in China, thus they haven't seen the test images before. The assessment was conducted in an environment similar to the one in which radiologists practice daily.

Subjective test methodology

The test according to SAMVIQ is conducted task by task. Each task includes an explicit reference, a hidden reference and all processed versions: MOF-MMD OUTPUT1-2-3, ADMSS and OBNLM.

According to [KBP+17] Simple Stimulus (SS) protocols perform better than Double Stimulus (DS) ones in terms of subject fatigue and avoidance of mistakes due to accidentally reversing scores in DS. Additionally, SAMVIQ scores with greater accuracy compared to ACR for the same number of observers (on average 30% fewer observers were required) and is more reliable for the perceived quality scores of the collected data [RPCH10]. For the above cited reasons, we choose the SAMVIQ method in this test since it provides more accurate and reliable perceived quality scores on collected data.

Fig. 5.10 shows the graphical user interface (GUI) of the experiment. The observer is asked to score each stimulus using a continuous rating scale from 0 to 100. The rating scale is categorized according to the adjectives Low, Medium and High. The observer is allowed to view a stimulus multiple times in a task and change the score, which lengthens the duration of the test session.For our subjetcive test, the number of reference images is limited to 12 as the subjective test, particularly with the SAMVIQ protocol, is intrinsically time-consuming. Accordingly, evaluators are asked to evaluate a total of 72 images on four criteria.

In the purpose avoiding observer fatigue, the test is divided into 2 sessions. In each session, 2 criteria are evaluated by asking the following questions to assessors:

Figure 5.10: Graphical User Interface

- Session 1
  - Diagnosis: Please score how well the enhanced image helps the diagnosis.
  - Contrast: Please score the contrast improvement of the enhanced image (difference between the tissue and the background).
- Session 2
  - Texture conspicuity: Please score the general clarity of the texture.
  - Edge sharpness: Please score the visibility of the tissue border

Representative images for each criterion with associated score are shown in Fig. 5.11 and 5.12.

The image 5.11(a) has less difference in brightness between the light and dark parts (*i.e.,* contrast) than image 5.11(b). On the other hands some edges are depicted in Fig. 5.11, and are more visible inside the blues circles than inside the reds ones.

The images 5.12(a) and 5.12(b) show more clearly the difference in texture enhancement. The red and blue circles represent two areas where the grain pattern is smooth and raised, respectively.

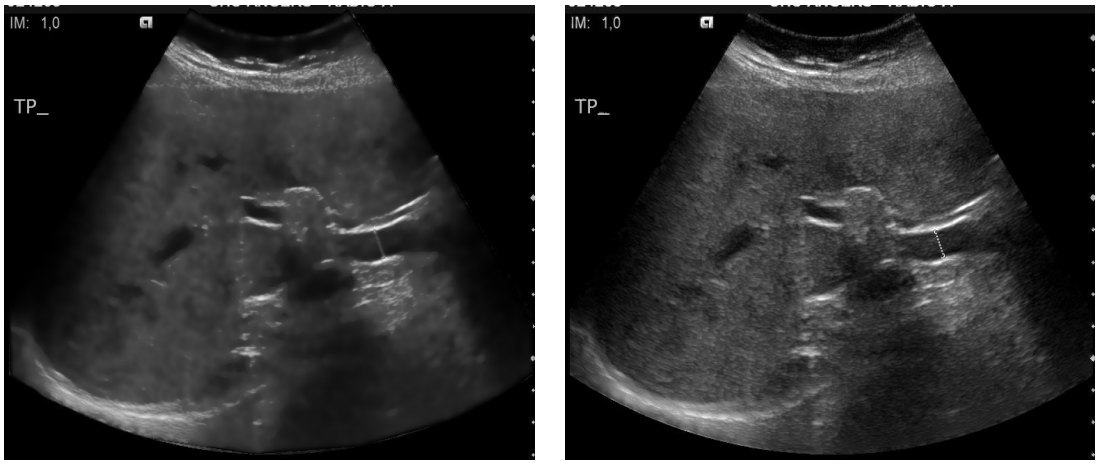

(a) Contrast score=16.66 Edge score=23.33 (b) Contrast score=80 Edge score=80

Figure 5.11: Illustration of evaluated contrast and edge criterion with associate subjective score.

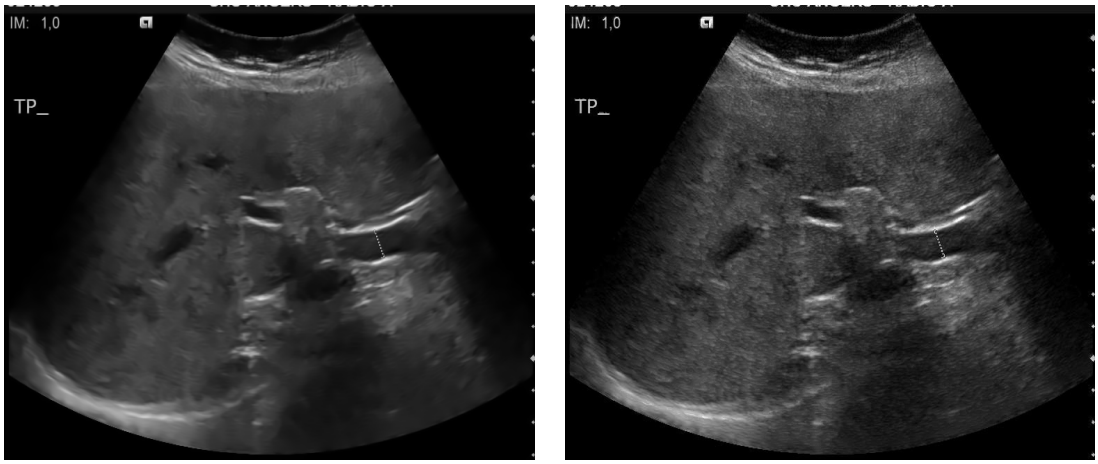

(a) Texture score=16.66 (b) Texture score=86.66

Figure 5.12: Illustration of evaluated texture criterion with associated subjective score

5.2.4 Objective evaluation results

For objective comparison, the SSNR and the three quality metrics are calculated and depicted with a box plot in Fig. 5.13. Considering the speckle reduction capacity shown by the SSNR in Fig. 5.13(a), the proposed method as well as the OBNLM and ADMSS reduce the speckle while the OBNLM filter has a slightly better performance. However, the OBNLM filter offers a bad image quality due to the over-smoothing effect, cf. Fig. 5.13(b)and 5.13(d).

Regarding the three outputs of the proposed method, the NIQE, NIQE-K and BIQES indicate that they render a higher quality compared to the OBNLM and the ADMSS. Moreover, the standard deviations of the three outputs are lower than those of the ADMSS and OBNLM, which indicates a lower dispersion and a higher uniformity of the processed images. The MOF-MMD substantially reduces the speckle while improving the quality of the image. It provides three outputs that are useful for the diagnosis of general aspect, echo pattern and outer border.

5.2.5 Subjective evaluation results

Table 5.6 shows the MOSs given by radiologists for five sets of processed images shown in Fig. 5.14. For the four considered criteria (contrast, texture conspicuity, edge sharpness and diagnostic) the three medical experts mostly scored the proposed method as better. The OBNLM method has relatively lower scores due to the artificial appearance and the oversmoothing texture which is unnatural for the radiologists. Considering the texture conspicuity, the three radiologists find Output1 more noticeable, meaning that the features-like segmentation based on mathematical morphology is also valuable for texture enhancement. For contrast enhancement, according to three radiologists, the MOF-MMD Output1 improves contrast. Considering the edge sharpness and the diagnostic parameters, radiologist 1 indicates a better diagnostic and sharpness of the edges on output3, radiologist 2 scores output1 as that which best enhances the edges and radiologist 3 finds output2 as the best one. This result suggests that the edge sharpness coincides with the diagnostic facility and that the years of experience of the radiologist may be an important factor for making a diagnosis. The great interest of the proposed method is that it provides radiologists with the possibility of choosing an output as they wish according to their experiences and needs in different circumstances.

Another observation from the subjective scoring is the difference between the initial hypothesis and the results. In fact, the multi-output filter supposes initially output 1 for edge sharpness, output 2 for texture enhancement and output 3 for general improve-

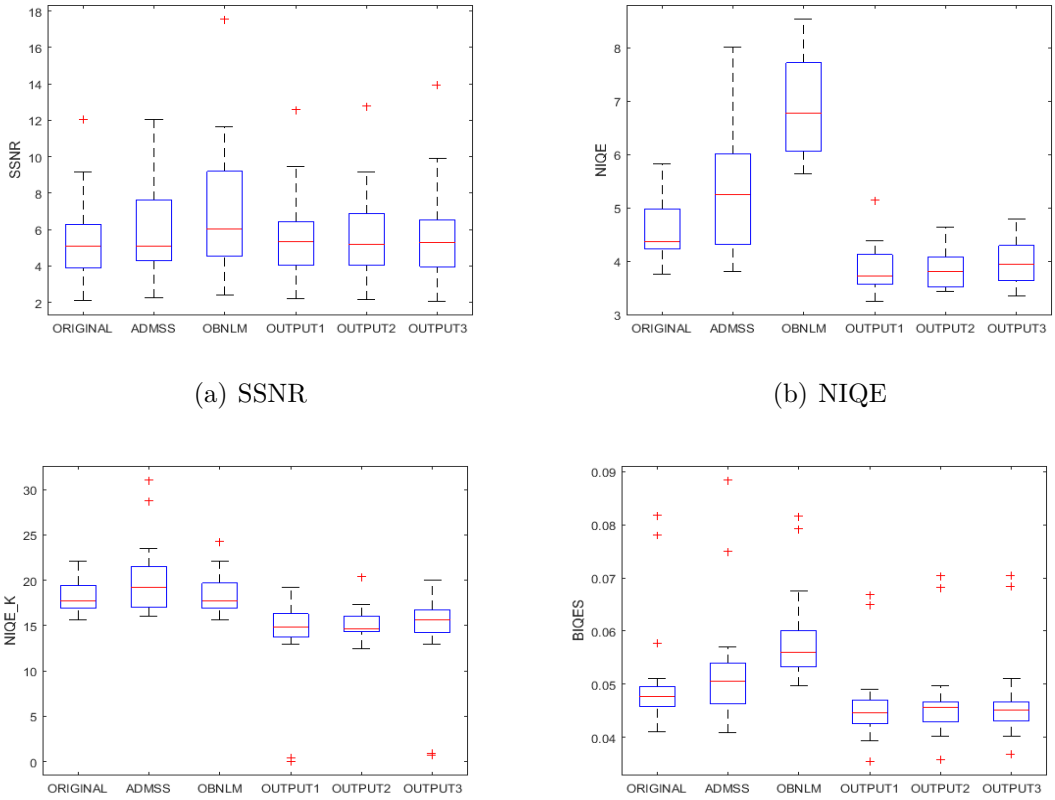

(a) SSNR (b) NIQE

(c) NIQE-K (d) BIQES

Figure 5.13: Box plots of SSNR and quality assessment metrics of US images and their filtered versions: ADMSS, OBNLM, proposed OUTPUT1-3. (A higher SSNR indicates less speckle. The lower values of metrics means higher performances)

ment of the image quality supposed to facilitate the diagnostic task. This experiment shows that output 1, considering the scores of radiologists and all criteria (contrast, texture conspicuity, edges sharpness and diagnostic), is generally the most adequate as it is ranked best most often, all parameters combined. Finally, this latter finding about output 1 suggests that the features-like segmentation by morphological operators is a very interesting step for enhancing, and could help the application of image processing techniques in US images.

Statistical analysis

The collected scores are further analyzed statistically with ANOVA (Analysis of Variance) using MATLAB's *ANOVA* function. For each test, the perceived quality is selected as the dependent variable. The image content's, the despeckleing algorithms and the observers are selected as independent variable. The results are summarized in Table 5.2, and show that there is no significant difference between observers (P-

(a) Original

(b) ADMSS

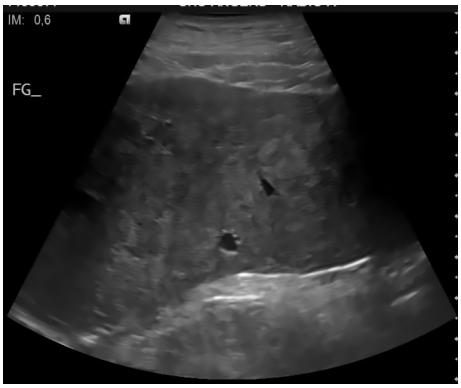

(c) OBNLM

(d) Proposed Output1: Edges

(e) Proposed Output2: Texture

(f) Proposed Output3: Global

7

Figure 5.14: Subjective comparison of speckle reduction of liver US image

Table 5.1: Subjective mean scores of speckle filtering methods

	Radiol1				Radiol2				Radiol3			
	Contrast	Texture	Edges	Diagn.	Contrast	Texture	Edges	Diagn.	Contrast	Texture	Edges	Diagn.
ADMSS	43.33	50	43.33	39.16	46.66	52.5	50.83	48.33	55.83	56.66	52.5	51.66
OBNLM	45.45	34.54	32.72	37.27	49.09	40.83	47.27	41.81	33.63	38.18	30.91	26.36
Proposed Output1	50	76.66	79.16	77.5	55.83	66.66	79.16	64.16	76.66	78.33	69.16	69.16
Proposed Output2	39.16	75.83	79.16	80.83	55	65	69.16	55.83	75.45	70	72.73	79.09
Proposed Output3	42.5	75.83	81.66	81.66	53.33	66.66	76.66	56.66	74.16	66.66	70.83	75.83

value>0.05) in scoring the image quality. Furthermore, the image content and despeckling method both have a significant effect on perceived quality (P-value<0.05). The impact of image content is probably due to the fact that the original images are different in terms of parenchymal tissue echogenicity (*i.e.,* the tissue ability to bounce an echo). A statistical T-test is further performed for pairwise comparisons with hypothesis testing between the despeckling algorithms. The results are summarized in Table 5.3, and indicate that the perceived quality is significantly better for the proposed method (OUTPUT1, OUTPUT2 and OUTPUT 3). For the pairwise comparisons: OUTPUT1 vs OUTPUT2, OUTPUT2 vs OUTPUT3 and OUTPUT1 vs OUTPUT3 the difference is not statistically significant for each case.

Table 5.2: Results of ANOVA to evaluate the effect of the observer, content and despeckling on the perceived quality

Factor	dF	F	P-value
Observer	2	2.25	0.106
Content	11	2.27	0.009
Despeckling algorithms	4	68.04	<0.001

Correlation analysis

In this section we briefly analyze the correlation between objective metrics and the collected perceived scores. Being able to predict the perceived image quality would help to shorten the times of the subjective tests. The two well-known correlation coefficients: PLCC (Pearson Linear Correlation Coefficient) and SROCC (Spearman Rank Order

Correlation Coefficient) are used as correlation metrics. PLCC requires constructing nonlinear mapping between objective metrics and subjective scores using Logistic regression [SBC05].

Table 5.3: T-Test of statistical significance for pairwise comparisons of despeckling method. Three symbols: "1" means that the method for the row is significantly better than the method for the column, "-1" means that it is significantly worse, and "0" means that it is statistically indistinguishable

	ADMSS	OBNLM	OUTPUT1	OUTPUT2	OUTPUT3
ADMSS	0	-1	1	1	1
OBNLM	1	0	1	1	1
OUTPUT1	-1	-1	0	0	0
OUTPUT2	-1	-1	0	0	0
OUTPUT3	-1	-1	0	0	0

$$M_P = \beta_1 \left(\frac{1}{2} - \frac{1}{1 + exp(\beta_2 (M - \beta_3))} \right) + \beta_4 M + \beta_5 \tag{5.36}$$

where M and M_p are the original and the fitted objective NR-IQA scores respectively. $\beta_1, \beta_2, \beta_3, \beta_4, \beta_5$ are the regression parameters of the logistic function. The results of

Table 5.4: PLCC after nonlinear regression and SROCC between MOS and NR-IQ metrics

	PLCC			SROCC		
Criterion	NIQE	NIQEK	BIQES	NIQE	NIQEK	BIQES
Contrast	0.34	0.30	0.23	0.25	0.10	0.37
Diagnostic	0.82	0.50	0.33	0.56	0.38	0.30
Texture	0.79	0.43	0.65	0.46	0.34	0.56
Edges	0.88	0.61	0.72	0.61	0.54	0.60

correlation between the three metrics and the perceived quality of contrast, diagnostic, texture and edges, are summarized in Table 5.5. One can conclude that the $NIQE$ metric is reliable to predict the perceived quality by radiologists for the diagnostic task. Moreover, the characterization of the lesion is well predicted by the $NIQE$ as edge and texture perception by radiologists is highly correlated with the $NIQE$. However, the contrast perceived by the radiologists is far from the one assessed by the three objective metrics used.

Subjective scores

the subjective evaluation was done by three radiologists, with different years of experience (3 years, 7 years and more than 10 years experience). They subjectively rated the images based on their perceptual assessment considering four criterion: the contrast, diagnostic, edges sharpness and texture conspicuity. The radiologists are from Nanjing Yike Medical University Affiliated Hospital in China. The obtained scores were averaged across despeckling methods to yield a mean opinion scores for each image:

$$MOS_{i(criterion)} = \frac{1}{S}\sum_{i=1}^{S} r_{ij(criterion)} \tag{5.37}$$

Where S is the total number of the subject, $r_{ij(criterrion)}$ represents the raw score of the i-th image given by the j-th subject considering a criterion.

5.3 Correlation between subjective and objective scores

Fig 5.15 shows the scatter plots of MOS versus original (OR) and filtered images ADMSS (AD),OBNLM (NLM) and three MOF-MMD (MS1, MS2, MS3) for contrast, diagnostic, edges and texture, respectively. Comparing the MOS of the original ultrasound images and filtered by different methods, we see that filtering, depending on the method used, can slightly improve the quality perceived by medical experts. Regarding the evaluation based on the contrast criterion, MOS indicates a clear improvement through Multi-Scale (MS) filtering. In terms of diagnostic criterion, the disparity of MOS indicates a significant improvement for some images. However, the average of the MOS shows that on overall images the improvement is not significant. Moreover, the quality can be impaired by unsuitable filtering. For edges assessment criterion the improvement is noticeable, according to the MOS, with multi-scale filtering. The MOS depicted in Fig5.15(c) shows the last criterion considered subjectively. The texture is slightly improved only by MS1, and deteriorated by the rest of the despeckling processes. This is due to the fact that the pattern of speckle changes with parenchymal texture in the presence of steatosis and fibrosis at microarchitectural levels and may be imperceptible to the eye on a conventional ultrasound image[GG14].

Table 5.5 shows the PLCC and SROCC values respectively, between the four NR-IQA metrics and perceived MOS. The best-performing metric in each row is highlighted. One can see that the NIQE metric is consistently high correlated with the subjective scores. In particular for the assessment in term of diagnostic, texture and edges. The

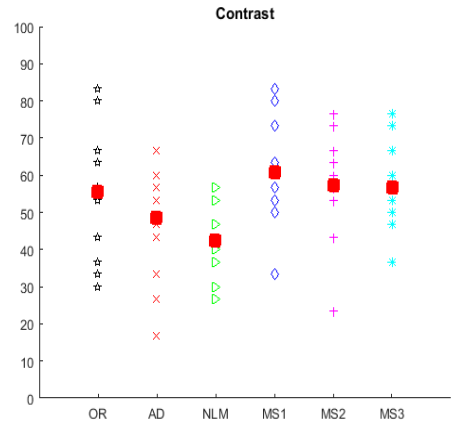

(a) Conrast

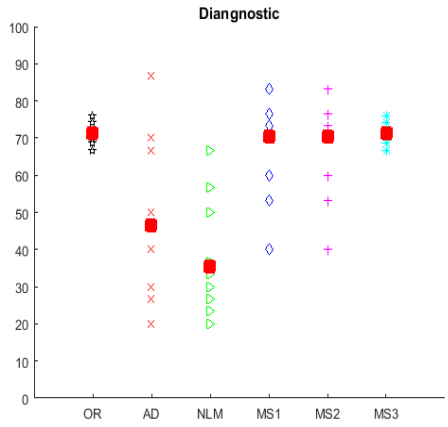

(b) Diangnostic

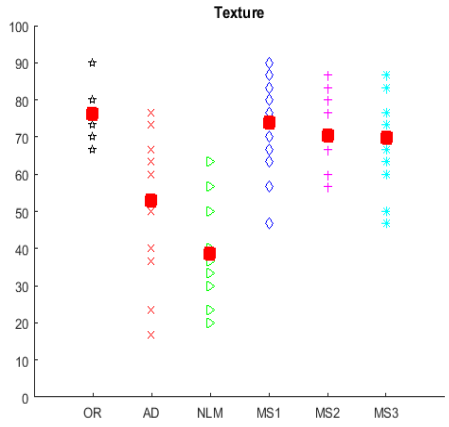

(c) Texture

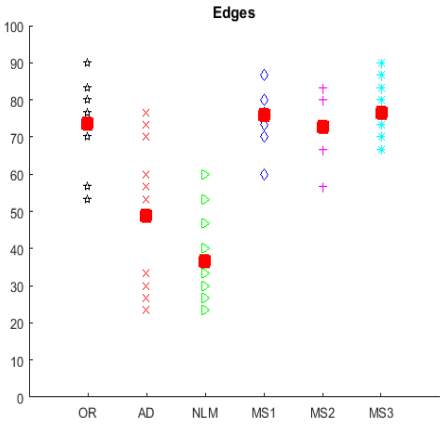

(d) Edges

Figure 5.15: Scatter plots of MOS versus original and filtered images for Contrast, Diagnostic, Texture and Edges

BRISQUE metric has also good performances when assessing the quality considering diagnostic, texture and edges. The best correlation performances are obtained for edges quality assessment. Therefore, the NIQE and BISQUE metric are suitable in term of perceptual quality perceived during the diagnosis. Indeed, the edges of an US image represent a crucial part of the image and has its importance when performing a diagnosis [RM16].

It can be observed that for the assessment of contrast the BRISQUE is slightly correlated to the subjective scores. Nevertheless the four metrics have insufficient performance to evaluate the quality of contrast as perceived by expert.

A plot with a best fitting logistic curve is shown in the Fig 5.16. It shows NIQE and BRISQUE versus MOS of contrast, diagnostic, edges and texture respectively. One

Table 5.5: PLCC between MOS and NR-IQ metrics after nonlinear regression

Criterion	NIQE	NIQEK	BIQES	BRISQUE
Contrast	0.34	0.30	0.23	**0.37**
Diagnostic	**0.82**	0.50	0.33	0.72
Texture	**0.79**	0.43	0.65	0.72
Edges	**0.88**	0.61	0.72	0.80

Table 5.6: SROCC between MOS and NR-IQ metrics

Criterion	NIQE	NIQEK	BIQES	BRISQUE
Contrast	0.25	0.10	**0.37**	0.28
Diagnostic	**0.56**	0.38	0.30	**0.56**
Texture	0.46	0.34	0.56	**0.64**
Edges	0.61	0.54	0.60	**0.67**

can observe that the majority of NIQE and BRISQUE scores are close to the adjusted curve. That indicates that the NIQE and BRISQUE score the quality of image close to the one perceived by medical experts. With the only exception of contrast evaluation which is not correlated between metrics and experts.

Conclusion

In this chapter, we addressed a fully automatic multi-output filter based on multiplicative multiresoution decomposition (MOF-MMD). The aim is to improve the ability of interpreting the ultrasound image for the medical user. The MOF-MMD permits enhancement of the image in multiple ways, according to the structure that needs to be viewed. We use both the specificity of the multi-scale decomposition (MMD) and the advantage of mathematical morphology to delimit the undesirable structures. To evaluate the performance of the proposed method, the SSNR and three blind quality metrics are used to quantify the speckle reduction and quality improvement of the US image. Moreover, a subjective evaluation is carried out according to the recommendation with the SAMVIQ protocol. Furthermore, we analyze the recorded scores in terms of correlation with the objectives metrics used in this thesis. The visual evaluation shows that the proposed method with its various outputs is more or less valuable according to the different years of experience of the radiologists. The correlation analysis shows that

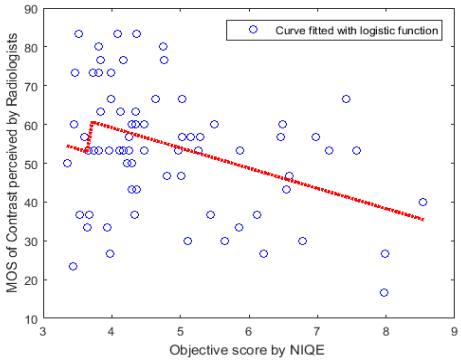

(a) NIQE vs MOS Conrast

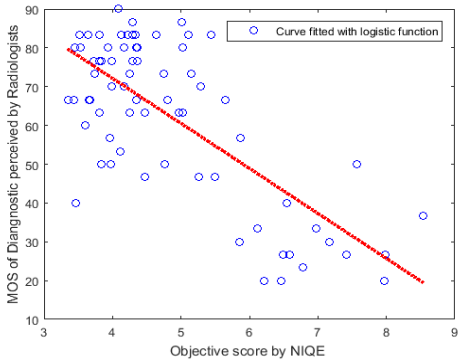

(b) NIQE vs MOS Diangnostic

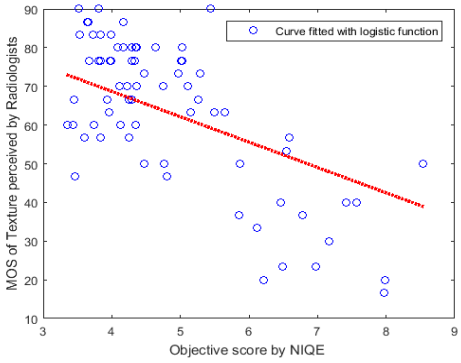

(c) NIQE vs MOS Texture

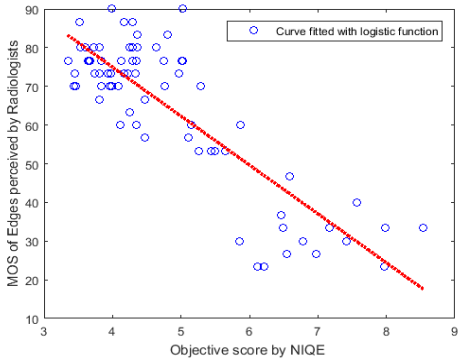

(d) NIQE vs MOS Edges

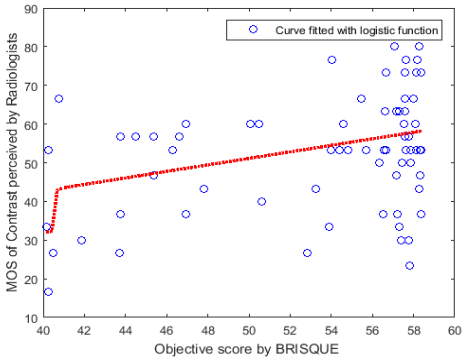

(e) BRISQUE vs MOS Conrast

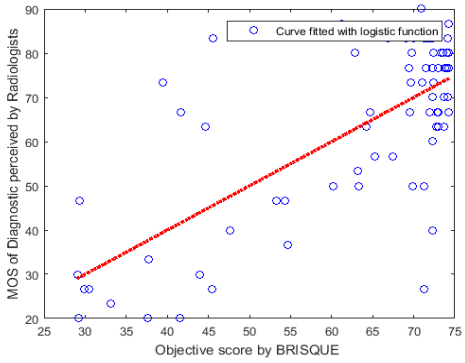

(f) BRISQUE vs MOS Diangnostic

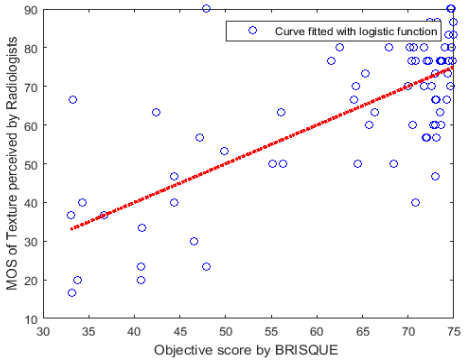

(g) BRISQUE vs MOS Texture

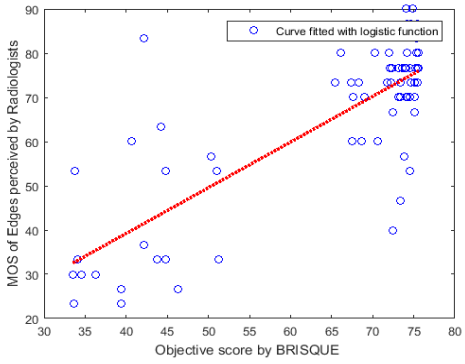

(h) BRISQUE vs MOS Edges

Figure 5.16: Scatter plots of NIQE versus MOS of Contrast, Diagnostic, Texture and Edges

the subjective scores are correlated to the NR-IQA NIQE metric which alternatively allows comparison of the medical ultrasound.

CHAPTER 6

The compression scheme based on MMD

Introduction

The compression of medical images is of great interest in the current conjuncture of development of medical data. The great challenge is to preserve data integrity, as the medical data and doctors opinions are very sensitive, for obvious reasons, to confidence. In this chapter, we will propose a lossy compression method based on our previous works and knowledge about quality assesment of medical images. Koff et al. [KBB+09] conduct a study on irreversible compression and its impact on visual quality for ensure accurate diagnostic. Another work on this topic presented in [KUBW+14] where the authors present a concept of "diagnostically lossless" compression by setting a threshold in terms of FR quality metric, will be also introduced. The proposed method is with respect of these fulfills. However, the lack of time did not allow us to perform tests on a consistent database. Nonetheless, the obtained preleminary results suggest that the proposed method is valuable for medical image compression.

6.1 Compression scheme based on MMD

The proposed compression scheme is based on the Multiplicative Multiresolution Decomposition with an Embedded Zerotree coding. The aim of the proposed method is to compress images and to improve the quality simultaneously. Generally, for ultrasound images, by reducing speckle during compression, and for MRI by improving diagnostic ability.

The Embedded Zerotree MMD algorithm (EZ-MMD) uses the same principle of the Embedded Zerotree Wavelet (EZW) initially proposed by [Sha93]. The algorithm is based on the following EZW key concepts.

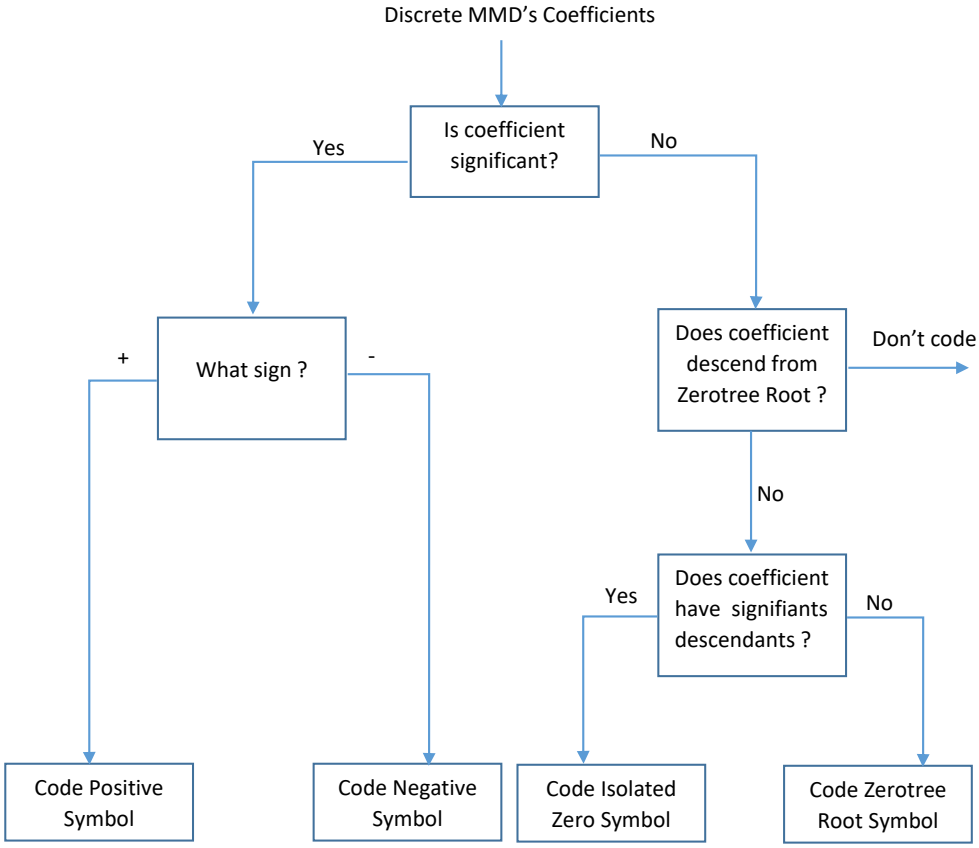

Figure 6.1: Zerotree coding of MMD's coefficient

- Divide the image into blocks of size 16×16 and for each block, apply the next steps.
- Multiplicative Multiresolution Decomposition.
- Zerotree coding which provides a compact multiresolution representation of significance maps.
- Prediction of the absence of significant information across scales by exploiting the self-similarity inherent in images.
- Entropy-coded successive-approximation quantization.
- Lossless data compression which is achieved via adaptive arithmetic coding.

The MMD's coefficients are real, in order to obtain discret coefficients, a *mp* parameter is used for truncation. Figure 6.1 illustrates the zerotree coding applied to MMD's coefficients, and is constructed as follows [Sha93]:

- Every MMD's coefficient at a given scale can be related to a set of coefficients at the next finer scale of similar orientation.

- Zerotree root (ZTR) is a low scale "zero-valued" coefficient. The magnitude of a coefficient is less than a threshold TZ for which all the related higher-scale coefficients (all its descendants) are also "zero-valued".
- Specifying a ZTR allows the decoder to "track down" and zero out all the related higher-scale coefficients.
- Isolated zero: if a coefficient has some significant descendants, and its the magnitude is less than the threshold TZ, then this coefficient is labeled as isolated zero.
- Positive significant: if a coefficient is greater than the threshold TZ at level k, and is positive, than it is labeled as positive significant.
- Negative significant: if a coefficient is greater than the threshold TZ at level k, and is negative, than it is labeled negative significant.

The reconstruction process involves applying the decoding followed by MMD reconstruction.

6.2 Experiment and validation of compression scheme

6.2.1 results

We have tested the proposed compression scheme on ultrasound (*c.f.* 5.14) and MR images (*c.f.* 4.2.3). To quantitatively evaluate the algorithm, the EZ-MMD is mainly based on 2 parameters that can be tunned. In this section we presen,t some results with different values of TZ and mp. Finaly, we will suggest a choice of parameter to perform the compression and to compare the proposed method to with ones standardized in DICOM: the JPEG compression.

For the assessment of quality, three evaluation metrics are used :

- NIQE: This metric has been widely used for quality assessments of different modalities of medical images. NIQE scores are often correlated to radiologist's opinion.
- NIQE-K: This metric detailed in chapter 4, was validated for assessing compressed MR image [OZD+16].

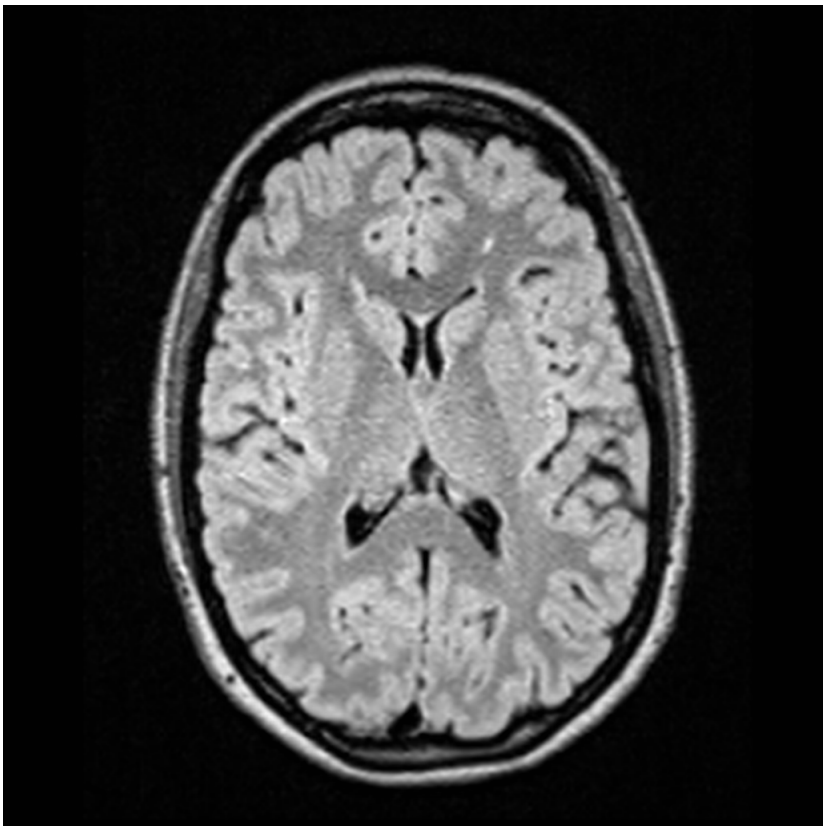

Figure 6.2: Original MR image

- SSIM: It has been demonstrated in [KUBW+14] that SSIM presents a high level of confidence considering the quality of the compressed image is diagnostically acceptable. Furthermore, a threshold values of 0.95 for the SSIM was defined and juged acceptable for compressed images, i.e. the compression is considered as "diagnostically lossless".

Ultrasound images

In this section, we present the results of EZ-MMD compression applied on US images (Figure 6.3). The US images are of diffrent size: for our test, we croped the images in order to obtain a size of 512×512. Table 6.1 shows the results for a threshol TZ of and different mp. For a bitrate of 1.16 bpp the PSNR value reflect a near-lossless compression. Furthermore, the SSIM, which is the closest metric to radiologists' assessments acoording to [KUBW+14], permitd to quaify the compression as "diagnostically lossless". Also, the EZ-MMD with its two parameters TZ and mp offers several possibilities of compression with low bitrate and potentially an enhancement of the quality to the user. One could see that for $mp = 100$ there is a good compromise between the

Figure 6.3: Original US image

quality and the bitrate, so we chosse this *mp* for testing various thresholds presented in Table 6.2. From this table, we conclude that the proposed scheme reached its limit of compression for $TZ = 2$. Indeed, for greater values of TZ, the quality of the image is degraded: the NIQE-K increases and the SSIM reaches the limit set in [KUBW+14].

Table 6.1: EZ-MMD compression with diffrent thresholds values with $TZ = 0.5$ US image with NR quality scores $NIQE_{original} = 4.72$ $NIQE - K_{original} = 17.93$

mp	BPP	PSNR	NIQE	NIQEK	SSIM
1000	1.36	93.28	4.72	18	1
500	1.21	75.14	4.72	17.86	1
400	1.16	71.28	4.72	17.99	1
300	1.10	66.23	4.71	17.46	1
200	1.01	61.23	4.71	17.35	0.99
100	0.85	54.69	4.6	17.24	0.99
50	0.69	49.02	4.41	16.03	0.99
40	0.63	47.29	4.31	15.84	0.99
30	0.56	44.87	4.07	14.09	0.99
20	0.45	41.70	3.89	14.14	0.98
10	0.27	36.31	4.11	15.19	0.93

Table 6.2: EZ-MMD compression with different thresholds values with $mp = 100$ US image with NR quality scores $NIQE_{original} = 4.72$ $NIQE - K_{original} = 17.93$

TZ	BPP	PSNR	NIQE	NIQEK	SSIM
0.25	1.01	61.29	4.70	17.33	0.99
0.5	0.85	54.69	4.60	17.24	0.99
1	0.68	49	4.4	16.05	0.99
2	0.5	43.33	4.12	14.91	0.98
4	0.32	37	3.98	15	0.95
5	0.15	33	5.89	22.83	0.87

The performance of the Embedded Zerotree MMD based scheme is compared to wavelet based one and represented in Figure 6.4. The curve shows that the image quality increases with the compression ratio and then decreases. Moreover, the quality of the compressed image is better than the original for given bitrates. This signify that the compression improved the quality and reduce the speckle.

MRI images

We present the results of EZ-MMD compression applied on MRI images of size 1024×1024 (Figure 6.2). Table 6.3 shows the scores obtained for different values of threshold with $mp = 100$ on compressed MRI shown in Figure 6.2 . One could see, as a preliminary step, that the quality is acceptable for a diagnostic task. In fact, considering the quality criterion formulated by [KUBW+14] in term of SSIM, the images are confidentially compressed in term of diagnostic as we obtain a SSIM of 0.99 for a bitrate of 0.49 BPP.

Table 6.3: EZ-MMD compression with diffrent thresholds values with $mp = 100$ MR image with NR quality scores $NIQE_{original} = 8.55$ $NIQE - K_{original} = 12.89$

Threshold TZ	BPP	PSNR	NIQE	NIQEK	SSIM
0.25	0.79	54.72	8.39	12.64	0.999
0.5	0.64	50.82	8.12	12.37	0.996
0.75	0.49	43.51	7.15	11.66	0.989
1	0.49	43.51	7.15	11.66	0.989

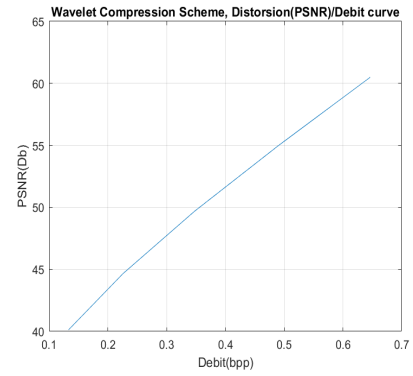

(a) PSNR

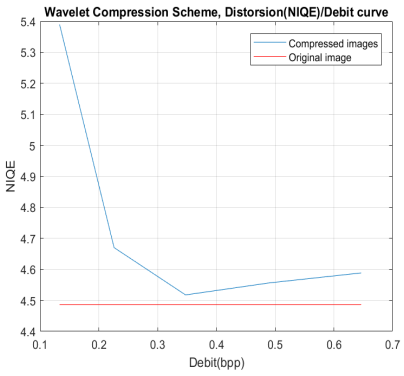

(b) NIQE

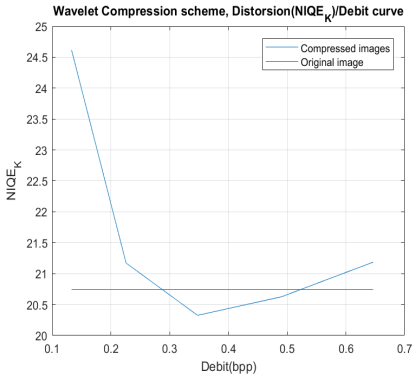

(c) NIQE-K

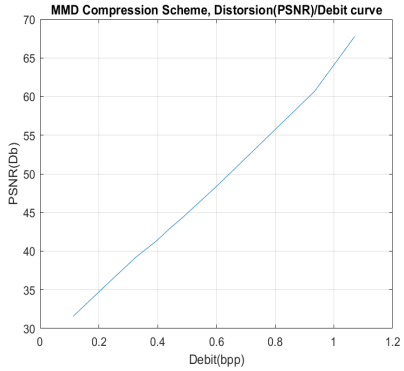

(d) PSNR

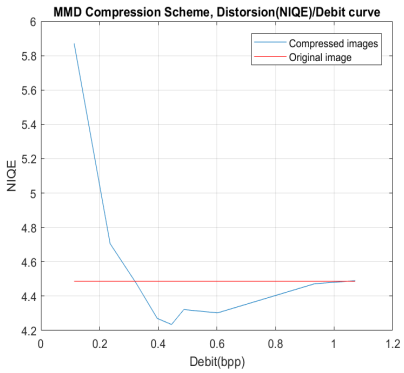

(e) NIQE

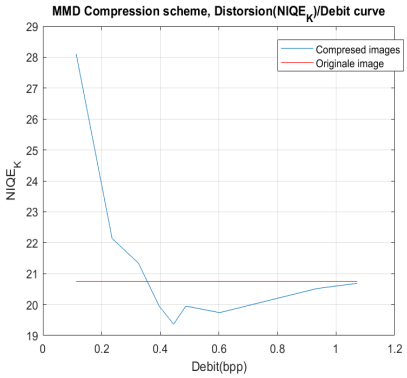

(f) NIQE-K

Figure 6.4: Plot wavelet compression scheme VS MMD compression scheme

Comparison with JPEG compression solutions

Table 6.5 summarizes the assessment of compressed MR images using JPEG, JPEG XR, and JPEG 2000. Notice that the result are obtained using Pixillion software. The image is compressed with intrinsic parameter of the software. The results show that the EZ-MMD offers an acceptable compression ratio with an improvement of the quality

Table 6.4: EZ-MMD compression with diffrent thresholds values with $mp = 10$ MR image with NR quality scores $NIQE_{original} = 8.55$ $NIQE - K_{original} = 12.89$

Threshold TZ	BPP	PSNR	NIQE	NIQEK	SSIM
0.125	0.46	41.69	6.6	11.16	0.98
0.25	0.33	36.46	5.7	11.4	0.95
0.5	0.22	31.85	6.02	14.75	0.90
0.75	0.11	28	5.93	17.37	0.84
0.75	0.11	28	5.93	17.37	0.84

Table 6.5: Quality assessment of compressed MR image

Method	BPP	PSNR	NIQE	NIQEK	SSIM
JPEG	1.9379	35.62	16.42	20.02	0.90
JPEGXR	0.8393	47.98	8.31	12.40	0.99
JPEG 2000	0.1391	35.47	16.42	20.02	0.90
EZ-MMD	0.4937	43.51	6.94	11.31	0.99

in term of diagnostic, with a NIQE-K of 11.31 (the lower it is, better is the quality). Indeed, from the results presented in chapter 4, the NIQE-K is valuable for assessing the quality of medical images in general, and for MRI in particular it is even more correlated to expert's opinion. Regarding the SSIM value it is 0.99 for EZ-MMD and JPEGXR wich means that the compression is acceptable, and that the compressed image permit a to establish a diagnosis as well as the original one. Otherwise, the image compressed by JPEG and JPEG 2000 returns an SSIM of 0.90 which cannot be acceptable for medical data compression.

Conclusion

In this chapter we have presented a compression scheme based on MMD for compression of medical images. The preliminary results of tests conducted using this scheme show that this method can be used confidently for diagnosis on medical data. However, the tests must be extended to a database with subjective evaluation involving medical expert or at least with model observer evaluation.

CHAPTER 7 Conclusion

7.1 Conclusion

In this thesis, a complete scheme to compress medical image with an efficient despeckling algorithm is proposed with demonstrations of its efficiency with respect of the diagnostic quality.

Firstly, we have investigated the image quality assessment in medical context. Therfore, we have study the possible usability of state-of-the-art no-reference IQA metrics originally designed for natural image, in the context of medical ones. We have also proposed a modified NIQE, called NIQE-K, inspired by some BIQES features and more adapted to medical images. Three experiments have proved the usability of the proposed metric in medical context. One was conducted on natural IQA database (LIVE-Release2 and CSIQ), the second on ultrasound image corrupted with noise and the last one includes tests on Magnetic Resonance images with compression distortions analyzed with quality scores evaluated by radiologists.

In a second time, we have proposed a Multi-Output filter based on Multi-Output Filter based on Multiplicative Multiresolution Decomposition (MOF-MMD) for reducing the speckle present US. A multi-scale approach that enhances different features and structures of the images previously extracted by mathematical morphology operators. We have demonstrated, trough objective and subjective evaluation of the diagnostic quality of the image, that the MOF-MMD effectively reduces the speckle and improves the quality of the US images by enhancing the boundaries of lesions and reducing the speckle in the echo texture of organs while preserving the pattern without neither over-smoothing nor artificial appearance. Moreover, subjective tests have shown that the MOF-MMD with its various output is more or less valuable according to different years of experience of the radiologists.

Finally, a compression scheme was built without compromising the diagnostic task, furthermore the image is enhanced and its quality is potentially more appropriate for diagnostic task.

As conclusion, in this thesis we have explored several issues related to medical imaging.This allows us to better understand challenges in the medical field of image processing. Furthermore, several research topics were also investigated such as objective quality assessment, preparing and conducting subjective tests, speckle reduction and compression of images in accordance with clinical needs.

7.2 Perspectives

7.2.1 Quality assessment

One of the main challenge in this thesis is the quality assessment of medical images. The NIQE [MSB13] approaches often radiologists' perception, despite it is based on natural scene statistics. Furthermore, the main achievement of our work is an ultrasound database. As a perspective, we aim to adapt the NIQE to medical images by extracting the features from own corpus of medical images and fitting them to a MVG model, which then serves as a reference model to assess the quality of the image.

7.2.2 Filtering

In medical context

The selection of optimal threshold is the main limitation of the thresholding filter. Hence, the thresholding may be improved particularly to adapt it to other imaging modalities. The statistical analysis suggests that the content of the image has a significant effect on the perceived quality. It would be beneficial to study the impact of the image content: healthy versus pathological, granular versus smooth on the diagnostic performance. Finally, one can note that the ultrasound examination is used in real time for a wide variety of clinical tasks. So, it would be of great interest to embed a speckle filter into ultrasound imaging systems. Also, further improved results can be expected by incorporating some feature learning based strategies into the proposed methods, such as dictionary learning or deep convolution learning [LHY+17, LMZ+17, YZY+17].

In holographic imaging

Despite the development of recently de-speckling methods, many have not yet attained the required level of effectiveness in digital holography. As a perspective we aim to apply our MOF-MMD to holographic imaging.

7.2.3 Compression

We have studied the lossy compression on US and MRI, however tests must be extended to a larger database with subjective evaluation. Moreover the peoposed scheme can be adapted to other modalities such as mammography.

Another perspective, is to apply and study the proposed method in telemdecine application: the tele-echography.

List of Publications

International Journals

1 Meriem Outtas, Lu Zhang, Olivier Deforges, Amina Serir, Wassim Hamidouche, and Yang Chen. Subjective and objective evaluations of feature selected multi output filter for speckle reduction on ultrasound images. Physics in Medicine and Biology, 2018 DOI: 10.1088/1361-6560/aadbc9.

International Conferences

1 M. Outtas, L. Zhang, O.Deforges, W. Hamidouche and A. Serir. "Evaluation of No-reference quality metrics for Ultrasound liver images". In Proceedings of the 10th International Conference on Quality of Multimedia Experience (QoMEX 2018), Sardinia, Italy, May 29-31, 2018.

2 L. Leveque, H. Liu, S. barakovic, J.B. Husic, A. Kumcu, L. Platisa, M. Martini, R. Rodrigues, A. Pinheiro, M. Outtas, L. Zhang, and A. Skodras. "On the subjective assessment of the perceived quality of medical images and videos". In Proceedings of the 10th International Conference on Quality of Multimedia Experience (QoMEX 2018), Sardinia, Italy, May 29-31, 2018.

3 M. Outtas, L. Zhang, Olivier Deforges, A. Serir, and Wassim Hamidouche. "Multioutput speckle reduction

lter for ultrasound medical images based on multiplicative multiresolution decomposition". In 2017 IEEE International Conference on Image Processing, ICIP.

4 M. Outtas, L. Zhang, O. Deforges, W. Hammidouche, A. Serir, and C. Cavaro-Menard. A study on the usability of opinion-unaware no-reference natural image quality metrics in the context of medical images. In 2016 International Symposium on Signal, Image, Video and Communications (ISIVC), pages 308-313, Nov 2016.

5 M. Outtas, A. Serir, and F. Kerouh. Speckle noise reduction in ultrasound image based on A Multiplicative Multiresolution Decomposition (MMD). In ISIVC 2014, The eighth edition of International Symposium on signal, Image, Video and Communications (ISIVC), Marrakech, Morocco, November 2014.

French Conferences

1 M. Outtas, O. Deforges, L. Zhang, A. Serir, and W. Hammidouche. "Filtre multisorties pour la rÈduction de bruit appliquÈ aux images mÈdicales ultrasons". In CORESA 2017, Caen, France, November 2017.

2 M. Outtas, A. Serir, O. Deforges, and L. Zhang. "Reduction de bruit multiplicatif dans les images ultrasons basÈes sur la decomposition multiplicative multiresolution (MMD)". In CORESA 2016, Nancy, France, May 2016.

Bibliography

[AAC+12] G. Andria, F. Attivissimo, G. Cavone, N. Giaquinto, and AML. Lanzolla. Linear filtering of 2-d wavelet coefficients for denoising ultrasound medical images. *Measurement*, 45:1792–1800, 2012. 29, 30

[ABT01] A. Achim, A. Bezerianos, and P. Tsakalides. Novel bayesian multiscale method for speckle removal in medical ultrasound images. *IEEE Trans. Med. Imaging*, 20(8):772–783, 2001. 28, 29, 35, 37

[AL06] S. Aja-Fernández and C. A. López. On the estimation of the coefficient of variation for anisotropic diffusion speckle filtering. *IEEE Transactions on Image Processing*, 15(9):2694–2701, 2006. 36

[AMC98] R. Ansari, N. Memon, and E. Ceran. Near-lossless image compression techniques. *Journal of eletronic imaging system*, 7(3):486–494, 1998. 38

[AMD08] Murtaza Ali, Dave Magee, and Udayan Dasgupta. Signal processing overview of ultrasound systems for medical imaging. 2008. 14, 15

[BCM05] Antoni Buades, Bartomeu Coll, and Jean-Michel Morel. A review of image denoising algorithms, with a new one. *Multiscale Modeling & Simulation*, 4(2):490–530, 2005. 37

[BT.00] ITU-R BT.500-10. *RECOMMENDATION ITU-R BT.500-10 METHODOLOGY FOR THE SUBJECTIVE ASSESSMENT OF THE QUALITY OF TELEVISION PICTURES*. 2000. 24, 26

[Bur78] C. B. Burckhardt. Speckle in ultrasound b-mode scans. *IEEE Transactions on Sonics and Ultrasonics*, 25(1):1–6, Jan 1978. 15, 28

[Can08] Canadian Association of Radiologists. CAR Standards for Irreversible Compression in Digital Diagnostic Imaging within Radiology. *Canadian Association of Radiologists*, pages 1–11, 2008. 20

[Cap02] Anne-Sophie Capelle. Segmentation d ' images IRM multi-échos tridimensionnelles pour la détection des tumeurs cérébrales par la théorie de l ' évidence. 2002. 20

[CCY+11] Yang Chen, Wufan Chen, Xindao Yin, Xianghua Ye, Xudong Bao, Limin Luo, Qianjing Feng, Yinsheng li, and Xiaoe Yu. Improving low-dose abdominal ct images by weighted intensity averaging over large-scale neighborhoods. *European Journal of Radiology*, 80(2):e42 – e49, 2011. 37

[CGL+14] Amine Chaabouni, Yann Gaudeau, Julien Lambert, Jean-Marie Moureaux, and Pierre Gallet. Subjective and objective quality assessment for H264 compressed medical video sequences. In *4th International Conference on Image Processing Theory, Tools and Applications, IPTA 2014, Paris, France, October 14-17, 2014*, pages 18–22, 2014. 26

[Cha11] Dev P Chakraborty. New developments in observer performance methodology in medical imaging. In *Seminars in nuclear medicine*, volume 41, pages 401–418. Elsevier, 2011. 52

[CHKB09] P. Coupé, P. Hellier, C. Kervrann, and C Barillot. Nonlocal means-based speckle filtering for ultrasound images. *IEEE Transactions on Image Processing*, 18:2221–2229, 2009. 31, 37, 68

[Cla48] Claude E. Shannon. A Mathematical Theory of Communication. *Bell System Technical Journal*, 27(July 1928):623–656, 1948. 40

[CMF+08] Yang Chen, Jianhua Ma, Qianjin Feng, Limin Luo, Pengcheng Shi, and Wufan Chen. Nonlocal prior bayesian tomographic reconstruction. *Journal of Mathematical Imaging and Vision*, 30(2):133–146, 2008. 38

[CYH+12] Yang Chen, Zhou Yang, Yining Hu, Guanyu Yang, Yongcheng Zhu, Yinsheng Li, Limin Luo, Wufan Chen, and Christine Toumoulin. Thoracic low-dose CT image processing using an artifact suppressed large-scale nonlocal means. *Physics in Medicine and Biology*, 57(9):2667–88, May 2012. 37

[CYV00] S G Chang, B Yu, and M Vetterli. Adaptive wavelet thresholding for image denoising and compression. *IEEE transactions on image processing*, 9(9):1532–1546, 2000. 37

[CZS+18] Y. Chen, Y. Zhang, H. Shu, J. Yang, L. Luo, J. L. Coatrieux, and Q. Feng. Structure-adaptive fuzzy estimation for random-valued impulse noise suppression. *IEEE Transactions on Circuits and Systems for Video Technology*, 28(2):414–427, Feb 2018. 38

[Dah11] Sonia Dahdouh Dahdouh. *Filtering, Segmentation and ultrasound images tracking. : clinical applications.* Theses, Université Paris Sud - Paris XI, September 2011. 15

[DNB13] O. Déforges, N. Normand, and M. Babel. Fast recursive grayscale morphology operators: from the algorithm to the pipeline architecture. *Journal of Real-Time Image Processing*, 8(2):143–152, 2013. 62, 63

[Don95] David L. Donoho. De-noising by soft-thresholding. *IEEE Transactions on Information Theory*, 41(3):613–627, 1995. 37

[DS98] Ingrid Daubechies and Wim Sweldens. Factoring wavelet transforms into lifting steps. *The Journal of Fourier Analysis and Applications*, 4(3):247–269, 1998. 41

[Els] Allen D. Elster. Mriquestions.com. 18

[FGJ11] S. Finn, M. Glavin, and E. Jones. Echocardiographic speckle reduction comparison. *Ultrasonics, Ferroelectrics, and Frequency Control, IEEE Transactions on*, 58(1):82–101, January 2011. 31

[FK05] E. Wyckens F. Kozamernik, P. Sunna. Subjective quality of internet video codecs: Evaluation using samviq. 2005. 27

[FMYS97] A. C. Frery, H. J. Müller, C. C. F. Yanasse, and S. J. S. Sant'Anna. A model for extremely heterogeneous clutter. *IEEE T. Geoscience and Remote Sensing*, 35(3):648–659, 1997. 15

[FSSH82] Victor S. Frost, Josephine Abbott Stiles, K. Sam Shanmugan, and Julian C. Holtzman. A model for radar images and its application to adaptive digital filtering of multiplicative noise. *IEEE Trans. Pattern Anal. Mach. Intell.*, 4(2):157–166, 1982. 34

[GBS14] P. Gifani, H. Behnam, and Z. Sani. Noise reduction of echocardiographic images based on temporal information. *Ultrasonics, Ferroelectrics, and Frequency Control, IEEE Transactions on*, 61(4):620–630, April 2014. 28, 30, 31

[GCS05] S. Gupta, R.C. Chauhan, and S.C. Saxena. Locally adaptive wavelet domain bayesian processor for denoising medical ultrasound images using speckle modelling based on rayleigh distribution. *Vision, Image and Signal Processing, IEE Proceedings* -, 152(1):129–135, Feb 2005. 27, 29, 30

[GG14] J. F. Gerstenmaier and R. N. Gibson. Ultrasound in chronic liver disease. *Insights into imaging*, 5(4):441–455, 2014. 16, 78

[Goo10] Bart Goossens. *Beeldmultiresolutiemodellen en schattingstechnieken Multiresolution Image Models and Estimation Techniques*. 2010. 23

[GPL+11] B. Goossens, A. Pižurica, H. Luong, J. Aelterman, and W. Philips. *Wavelet-based analysis and estimation of colored noise*. INTECH Open Access Publisher, 2011. 48

[GSP05] Nikhil Gupta, M N S Swamy, and Eugene I Plotkin. Despeckling of medical ultrasound images using data and rate adaptive lossy compression. *{IEEE} Trans. Med. Imaging*, 24(6):743–754, 2005. 27, 37, 42

[GTC+15] Vijay PB Grover, Joshua M Tognarelli, Mary ME Crossey, I Jane Cox, Simon D Taylor-Robinson, and Mark JW McPhail. Magnetic resonance imaging: principles and techniques: lessons for clinicians. *Journal of clinical and experimental hepatology*, 5(3):246–255, 2015. 18

[GZYY18] Shan Gai, Boyu Zhang, Cihui Yang, and Lei Yu. Speckle noise reduction in medical ultrasound image using monogenic wavelet and Laplace mixture distribution. *Digital Signal Processing: A Review Journal*, 72:192–207, 2018. 37

[HPN+10] Martin Christian Hemmsen, Mads Møller Pedersen, Svetoslav Nikolov, Michael Bachmann Nielsen, and Jørgen Arendt Jensen. Ultrasound image quality assessment: A framework for evaluation of clinical image quality. In *SPIE*, 2010. 26

[IL08] Telephone Installations and Local Line. ITU-T. 2008. 25

[Jen07] J. A. Jensen. Medical ultrasound imaging. *Progress in Biophysics and Molecular Biology*, 93(13):153 – 165, 2007. Effects of ultrasound and infrasound relevant to human health. 13, 15

[KBB+09] David Koff, Peter Bak, Paul Brownrigg, Danoush Hosseinzadeh, April Khademi, Alex Kiss, Luigi Lepanto, Tracy Michalak, Harry Shulman, and Andrew Volkening. Pan-Canadian evaluation of irreversible compression ratios ("Lossy" Compression) for development of national guidelines. *Journal of Digital Imaging*, 22(6):569–578, 2009. 20, 38, 83

[KBP+17] A. Kumcu, K. Bombeke, L. Platisa, L. Jovanov, J. Van Looy, and W. Philips. Performance of four subjective video quality assessment protocols and impact of different rating preprocessing and analysis methods. *IEEE Journal of Selected Topics in Signal Processing*, 11(1):48–63, Feb 2017. 70

[KKJ+10] Ashish Khare, Manish Khare, Yongyeon Jeong, Hongkook Kim, and Moongu Jeon. Despeckling of medical ultrasound images using Daubechies complex wavelet transform. *Signal Processing*, 90(2):428–439, 2010. 27, 28

[KLY16a] Jinbum Kang, Jae Young Lee, and Yangmo Yoo. A New Feature-Enhanced Speckle Reduction Method Based on Multiscale Analysis for Ultrasound B-Mode Imaging. *IEEE Transactions on Biomedical Engineering*, 63(6):1178–1191, 2016. 16

[KLY16b] Jinbum Kang, Jae Young Lee, and Yangmo Yoo. A new feature-enhanced speckle reduction method based on multiscale analysis for ultrasound b-mode imaging. *IEEE Trans. Biomed. Engineering*, 63(6):1178–1191, 2016. 37, 69

[KOK+98] Juha Kivijärvi, Tiina Ojala, Timo Kaukoranta, Attila Kuba, László Nyúl, and Olli Nevalainen. A comparison of lossless compression methods for medical images. *Computerized Medical Imaging and Graphics*, 22(4):323–339, 1998. 41, 42

[KSSC85] Darwin T. Kuan, Alexander A. Sawchuk, Timothy C. Strand, and Pierre Chavel. Adaptive noise smoothing filter for images with signal-dependent noise. *IEEE Trans. Pattern Anal. Mach. Intell.*, 7(2):165–177, 1985. 34

[KUBW+14] Ilona Kowalik-Urbaniak, Dominique Brunet, Jiheng Wang, David Koff, Nadine Smolarski-Koff, Edward R. Vrscay, Bill Wallace, and Zhou Wang. The quest for 'diagnostically lossless' medical image compression: a comparative study of objective quality metrics for

compressed medical images. 9037:903717, 2014. 30, 38, 42, 83, 86, 87, 88

[KWKV07] Karl Krissian, Carl-Fredrik Westin, Ron Kikinis, and Kirby G. Vosburgh. Oriented speckle reducing anisotropic diffusion. *IEEE Trans. Image Processing*, 16(5):1412–1424, 2007. 36

[LB13] Harald Lutz and Elisabetta Buscarini. *Manual of diagnostic ultrasound*, volume 2. World Health Organization, 2013. 13, 14

[LC10] E. C. Larson and D. M. Chandler. Most apparent distortion: full-reference image quality assessment and the role of strategy. *Journal of Electronic Imaging*, 19(1):011006, 2010. 48

[Lee] Jong-Sen Lee. Speckle analysis and smoothing of synthetic aperture radar images. 34

[Lee80] Jong-Sen Lee. Digital image enhancement and noise filtering by use of local statistics. *IEEE Trans. Pattern Anal. Mach. Intell.*, 2(2):165–168, 1980. 34

[LHY+17] J. Liu, Y. Hu, J. Yang, Y. Chen, H. Shu, L. Luo, Q. Feng, Z. Gui, and G. Coatrieux. 3d feature constrained reconstruction for low dose ct imaging. *IEEE Transactions on Circuits and Systems for Video Technology*, PP(99):1–1, 2017. 92

[LLM+18] Lucie Lévêque, Hantao Liu, Maria Martini, Meriem Outtas, and Lu Zhang. On the Subjective Assessment of the Perceived Quality of Medical Images and Videos. 2018. 25

[LMA89] T Loupas, WN McDicken, and PL Allan. An adaptive weighted median filter for speckle suppression in medical ultrasonic images. *Circuits and Systems, IEEE Transactions on*, 36(1):129–135, 1989. 28

[LMP+14] C. P. Loizou, V. Murray, M. S. Pattichis, M Pantziaris, A. Nicolaides, and C. S. Pattichis. Despeckle filtering for multiscale amplitude-modulation frequency-modulation (AM-FM) texture analysis of ultrasound images of the intima-media complex. *Int. J. Biomedical Imaging*, 2014, 2014. 26, 32, 45

[LMZ+17] J. Liu, J. Ma, Y. Zhang, Y. Chen, J. Yang, H. Shu, L. Luo, G. Coatrieux, W. Yang, Q. Feng, and W. Chen. Discriminative feature representation to improve projection data inconsistency for low dose ct

imaging. *IEEE Transactions on Medical Imaging*, 36(12):2499–2509, Dec 2017. 92

[LP13] Yves Vander Haeghen Cedric Marchessoux Ewout Vansteenkiste Wilfried Philips Ljiljana Platisa, Leen Van Brantegem. Psycho-visual evaluation of image quality attributes in digital pathology slides viewed on a medical color lcd display, 2013. 25

[LPC+05] C. P. Loizou, C. S. Pattichis, C. I. Christodoulou, R. SH. Istepanian, M. Pantziaris, and A. Nicolaides. Comparative evaluation of despeckle filtering in ultrasound imaging of the carotid artery. *Ultrasonics, Ferroelectrics, and Frequency Control, IEEE Transactions on*, 52(10):1653–1669, 2005. 16, 26, 28, 29, 30, 33

[LTN90] A. Lopes, R. Touzi, and E. Nezry. Adaptive speckle filters and scene heterogeneity. *IEEE Transactions on Geoscience and Remote Sensing*, 28(6):992–1000, Nov 1990. 35

[MB11] Anush K. Moorthy and Alan Conrad Bovik. Blind image quality assessment: From natural scene statistics to perceptual quality. *IEEE Trans. Image Processing*, 20(12):3350–3364, 2011. 31

[MKAK] Jieming Ma, Kerem Karadayi, Murtaza Ali, and Yongmin Kim. Software-based Ultrasound Phase Rotation Beamforming on Multicore DSP. 14, 111

[MMB12] Anish Mittal, Anush Krishna Moorthy, and Alan Conrad Bovik. No-Reference Image Quality Assessment in the Spatial Domain. *{IEEE} Trans. Image Processing*, 21(12):4695–4708, 2012. 31, 32

[MRC14] Fernando C. Monteiro, José Rufino, and Vasco Cadavez. Towards a comprehensive evaluation of ultrasound speckle reduction. In *Image Analysis and Recognition - 11th International Conference, ICIAR 2014, Vilamoura, Portugal, October 22-24, 2014, Proceedings, Part I*, pages 141–149, 2014. 31

[MSB13] A. Mittal, R. Soundararajan, and A. C. Bovik. Making a "completely blind" image quality analyzer. *IEEE Signal Process. Lett.*, 20(3):209–212, 2013. 32, 43, 45, 48, 70, 92

[MT06a] Oleg Michailovich and Allen Tannenbaum. Despeckling of medical ultrasound images. *IEEE Trans. Ultrason., Ferroelect., Freq. Contr*, 53:64–78, 2006. 28, 29

[MT06b] O.V. Michailovich and A. Tannenbaum. Despeckling of medical ultrasound images. *IEEE Transactions on Ultrasonics, Ferroelectrics and Frequency Control*, 53(1):64–78, 2006. 16

[OSK14] M. Outtas, A. Serir, and F. Kerouh. Speckle noise reduction in ultrasound image based on A Multiplicative Multiresolution Decomposition (MMD). In *ISIVC 2014*, The eighth edition of International Symposium on signal, Image, Video and Communications (ISIVC), Marrakech, Morocco, November 2014. 10, 57

[OZD+16] M. Outtas, L. Zhang, O. Deforges, W. Hammidouche, A. Serir, and C. Cavaro-Menard. A study on the usability of opinion-unaware no-reference natural image quality metrics in the context of medical images. In *2016 International Symposium on Signal, Image, Video and Communications (ISIVC)*, pages 308–313, Nov 2016. 10, 70, 85

[OZD+17] M. Outtas, L. Zhang, O. Deforges, A. Serir, and W. Hamidouche. Multi-output speckle reduction filter for ultrasound medical images based on multiplicative multiresolution decomposition. In *IEEE International Conference on Image Processing ICIP 2017, Beijing, China.* IEEE, 2017. 10, 55

[OZD+18] Meriem Outtas, Lu Zhang, Olivier Deforges, Amina Serir, Wassim Hamidouche, and Yang Chen. Subjective and objective evaluations of feature selected multi output filter for speckle reduction on ultrasound images. *Physics in Medicine and Biology*, 2018. 10, 55

[PM90] Pietro Perona and Jitendra Malik. Scale-Space and Edge Detection Using Anisotropic Diffusion. *{IEEE} Trans. Pattern Anal. Mach. Intell.*, 12(7):629–639, 1990. 35

[PPLA03] A. Pizurica, W. Philips, I. Lemahieu, and M. Acheroy. A versatile wavelet domain noise filtration technique for medical imaging. *IEEE Trans. Med. Imaging*, 22(3):323–331, 2003. 27, 37

[Pra77] W. K. Pratt. In Wiley, editor, *Digital Signal Processing*. New York, 1977. 30

[Ral08] VP Subramanyam Rallabandi. Enhancement of ultrasound images using stochastic resonance-based wavelet transform. *Computerized medical imaging and graphics*, 32(4):316–320, 2008. 51

[RDM99] Giovanni Ramponi, Raffaele D'Alvise, and Cecilia Moloney. Automatic estimation of the noise variance in SAR images for use in speckle filtering. In *Proceedings of the IEEE-EURASIP Workshop on Nonlinear Signal and Image Processing (NSIP'99), Antalya, Turkey, June 20-23, 1999*, pages 835–838, 1999. 63

[Rec02] ITURBT Recommendation. 500-11,"Methodology for the Subjective Assessment of the Quality of Television Pictures," Recommendation ITU-R BT. 500-11. *ITU Telecom. Standardization Sector of ITU*, pages 1–48, 2002. 25

[RJ91] Majid Rabbani and Paul W Jones. *Digital image compression techniques*, volume 7. SPIE Press, 1991. 39

[RLVSFMF+14] G. Ramos-Llorden, G. Vegas-Sanchez-Ferrero, M. Martin-Fernandez, C. Alberola-Lopez, and S Aja-Fernández. Anisotropic diffusion filter with memory based on speckle statistics for ultrasound images. 2014. 31, 36, 68

[RM16] Manzoor Razaak and Maria G Martini. Cuqi: cardiac ultrasound video quality index. *Journal of Medical Imaging*, 3(1):011011–011011, 2016. 79

[RMS14] Manzoor Razaak, Maria G. Martini, and Ketty Savino. A Study on Quality Assessment for Medical Ultrasound Video Compressed via HEVC. *IEEE Journal of Biomedical and Health Informatics*, 18(5):1552–1559, 2014. 26

[RNR84] E. Russell Ritenour, T. R. Nelson, and U. Raff. Applications of the median filter to digital radiographic images. In *IEEE International Conference on Acoustics, Speech, and Signal Processing, ICASSP '84, San Diego, California, USA, March 19-21, 1984*, pages 251–254, 1984. 33

[RPCH10] David M. Rouse, Romuald Pépion, Patrick Le Callet, and Sheila S. Hemami. Tradeoffs in subjective testing methods for image and video quality assessment. In *Human Vision and Electronic Imaging XV, part of the IS&T-SPIE Electronic Imaging Symposium, San Jose, CA, USA, January 18-21, 2010, Proceedings*, page 75270, 2010. 25, 26, 70

[RV12] V. Naga Prudhvi Raj and T. Venkateswarlu. Denoising of medical images using dual tree complex wavelet transform. *Procedia Technology*, 4(0):238 – 244, 2012. 2nd International Conference on Computer,

Communication, Control and Information Technology(C3IT-2012) on February 25 - 26, 2012. 30

[RV13] P. Renbin and P.K. Varshney. Noise-refined image enhancement using multi-objective optimisation. *Image Processing, IET*, 7(3):191–200, 2013. 51

[SB04] A. Serir and A. Belouchrani. Multiplicative multiresolution decomposition for 2d signals: application to speckle reduction in sar images. In *Image Processing, 2004. ICIP '04. 2004 International Conference on*, volume 1, pages 657–660 Vol. 1, Oct 2004. 57

[SB13] T G Shirsat and V K Bairagi. Lossless Medical Image Compression by Integer Wavelet and Predictive Coding. *ISRN Biomedical Engineering*, 2013(4):143–150, 2013. 42

[SBC05] Hamid R. Sheikh, Alan C. Bovik, and Lawrence K. Cormack. No-reference quality assessment using natural scene statistics: JPEG2000. *IEEE Trans. Image Processing*, 14(11):1918–1927, 2005. 77

[SBC12] Michele A. Saad, Alan C. Bovik, and Christophe Charrier. Blind image quality assessment: A natural scene statistics approach in the DCT domain. *IEEE Trans. Image Processing*, 21(8):3339–3352, 2012. 31

[SBK13] A. Serir, A. Beghdadi, and F. Kerouh. No-reference blur image quality measure based on multiplicative multiresolution decomposition. *Journal of Visual Communication and Image Representation*, 24(7):911 – 925, 2013. 57

[SFSL97] F. Sattar, L. Floreby, G. Salomonsson, and B. Lövström. Image enhancement based on a nonlinear multiscale method. *IEEE Transactions on Image Processing*, 6(6):888–895, 1997. 30

[Sha93] J. M. Shapiro. Embedded image coding using zerotrees of wavelet coefficients. *IEEE Transactions on Signal Processing*, 41(12):3445–3462, Dec 1993. 83, 84

[SHB07] M. Sonka, V. Hlavac, and R. Boyle. *Image Processing, Analysis, and Machine Vision*. Thomson-Engineering, 2007. 62

[SiVS+18] V. Sa-ing, P. Vorasayan, N. C. Suwanwela, S. Auethavekiat, and C. Chinrungrueng. Multiscale adaptive regularisation savitzky golay method for speckle noise reduction in ultrasound images. *IET Image Processing*, 12(1):105–112, 2018. 37

[SPR+16] P.V. Sudeep, P. Palanisamy, Jeny Rajan, Hediyeh Baradaran, Luca Saba, Ajay Gupta, and Jasjit S. Suri. Speckle reduction in medical ultrasound images using an unbiased non-local means method. *Biomedical Signal Processing and Control*, 28:1 – 8, 2016. 37

[SVCK97] S Sahni, B C Vemuri, F Chen, and C Kapoor. State of the art lossless image compression algorithms. *IEEE Proceedings of . . .*, 1997. 41

[SW15] A. Saha and Qing Ming Jonathan Wu. Utilizing image scales towards totally training free blind image quality assessment. *Image Processing, IEEE Transactions on*, 24(6):1879–1892, 2015. 32, 45, 46, 48, 70

[SWCB05] H. R. Sheikh, Z. Wang, L. Cormack, and A. C. Bovik. Live image quality assessment database release 2, 2005. 48

[Sza04] Thomas L Szabo. *Diagnostic ultrasound imaging: inside out*. Academic Press, 2004. 13

[TAH06] Peter C. Tay, Scott T. Acton, and John A. Hossack. Ultrasound despeckling using an adaptive window stochastic approach. In *Proceedings of the International Conference on Image Processing, ICIP 2006, October 8-11, Atlanta, Georgia, USA*, pages 2549–2552, 2006. 31, 35

[Taq11] Jonathan Taquet. *Advanced techniques for compression of biomedical images*. Theses, Université Rennes 1, December 2011. 18

[Taq12] Jonathan Taquet. Techniques avancées pour la compression d ' images médicales. 2012. 20

[TC08] Bengisu Tulu and Samir Chatterjee. Internet-based telemedicine: An empirical investigation of objective and subjective video quality. *Decision Support Systems*, 45(4):681–696, 2008. 25

[TC11] Jing Tian and Li Chen. Image despeckling using a non-parametric statistical model of wavelet coefficients. *Biomedical Signal Processing and Control*, 6(4):432 – 437, 2011. 29

[TJK11] Huixuan Tang, Neel Joshi, and Ashish Kapoor. Learning a blind measure of perceptual image quality. In *The 24th IEEE Conference on Computer Vision and Pattern Recognition, CVPR 2011, Colorado Springs, CO, USA, 20-25 June 2011*, pages 305–312, 2011. 31

[VA18] C. Vimala and P. Aruna Priya. Double Density Dual Tree Discrete Wavelet Transform implementation for Degraded Image Enhancement. *Journal of Physics: Conference Series*, 1000(1), 2018. 37

[VS08] Arash Vosoughi and Mohammad Bagher Shamsollahi. Speckle noise reduction of ultrasound images using m-band wavelet transform and wiener filter in a homomorphic framework. In *Proceedings of the 2008 International Conference on BioMedical Engineering and Informatics, BMEI 2008, May 28-30, 2008, Sanya, Hainan, China - Volume 2*, pages 510–515, 2008. 28, 30

[WFC+13] Y. Wang, X. Fu, L. Chen, S. Ding, and J. Tian. DTCWT based medical ultrasound images despeckling using LS parameter optimization. In *IEEE International Conference on Image Processing, ICIP 2013, Melbourne, Australia, September 15-18, 2013*, pages 805–809, 2013. 27, 29

[WLB04] Z. Wang, L. Lu, and A. C. Bovik. Video quality assessment based on structural distortion measurement. *Sig. Proc.: Image Comm.*, 19(2):121–132, 2004. 30

[WMSS00] Marcelo J Weinberger, Senior Member, Gadiel Seroussi, and Guillermo Sapiro. The LOCO-I Lossless Image Compression Algorithm : Principles and Standardization into JPEG-LS. 9(8):1309–1324, 2000. 41

[WRA+13] Andreas Weinlich, Johannes Rehm, Peter Amon, Andreas Hutter, and André Kaup. Massively parallel lossless compression of medical images using least-squares prediction and arithmetic coding. *2013 IEEE International Conference on Image Processing, ICIP 2013 - Proceedings*, pages 1680–1684, 2013. 41

[WSSL83a] R. F. Wagner, S. W. Smith, J. M. Sandrik, and H. Lopez. Statistics of speckle in ultrasound b-scans. *IEEE Transactions on Sonics and Ultrasonics*, 30(3):156–163, May 1983. 15, 28

[WSSL83b] R. F. Wagner, S. W. Smith, J. M. Sandrik, and H. Lopez. Statistics of speckle in ultrasound b-scans. *IEEE Transactions on Sonics and Ultrasonics*, 30(3):156–163, May 1983. 16

[WZX13a] S. Wu, Q. Zhu, and Y. Xie. Evaluation of various speckle reduction filters on medical ultrasound images. In *2013 35th Annual International Conference of the IEEE Engineering in Medicine and Biology Society (EMBC)*, pages 1148–1151, July 2013. 17

[WZX13b] Shibin Wu, Qingsong Zhu, and Yaoqin Xie. Evaluation of various speckle reduction filters on medical ultrasound images. In *Engineering in Medicine and Biology Society (EMBC), 2013 35th Annual International Conference of the IEEE*, pages 1148–1151. IEEE, 2013. 29

[WZX13c] Shibin Wu, Qingsong Zhu, and Yaoqin Xie. Evaluation of various speckle reduction filters on medical ultrasound images. In *Engineering in Medicine and Biology Society (EMBC), 2013 35th Annual International Conference of the IEEE*, pages 1148–1151, July 2013. 32

[XM96] Xiaolin Wu and N. Memon. CALIC-a context based adaptive lossless image codec. *1996 IEEE International Conference on Acoustics, Speech, and Signal Processing Conference Proceedings*, 4(June):1890–1893, 1996. 41

[YA02a] Yongjian Yu and Scott T. Acton. Speckle reducing anisotropic diffusion. *IEEE Trans. Image Processing*, 11(11):1260–1270, 2002. 34, 36

[YA02b] Yongjian Yu and Scott T. Acton. Speckle reducing anisotropic diffusion. *IEEE Trans. Image Processing*, 11(11):1260–1270, 2002. 36

[YD12] Peng Ye and David S. Doermann. No-reference image quality assessment using visual codebooks. *IEEE Trans. Image Processing*, 21(7):3129–3138, 2012. 31

[YZY+17] W. Yang, H. Zhang, J. Yang, J. Wu, X. Yin, Y. Chen, H. Shu, L. Luo, G. Coatrieux, Z. Gui, and Q. Feng. Improving low-dose ct image using residual convolutional network. *IEEE Access*, 5:24698–24705, 2017. 92

[ZW04] Li-bao Zhang and Ke Wang. Efficient Lossy to Lossless Medical Image Compression Using Integer Wavelet Transform and Multiple Subband

Decomposition. *Medical Imaging and Augmented Reality*, pages 86–93, 2004. 41

[ZWC15] J. Zhang, C. Wang, and Y. Cheng. Comparison of despeckle filters for breast ultrasound images. *Circuits, Systems, and Signal Processing*, 34(1):185–208, 2015. 26, 28, 29, 30, 31, 32, 45, 55

[ZYKK07] Fan Zhang, Yang Mo Yoo, Liang Mong Koh, and Yongmin Kim. Nonlinear diffusion in laplacian pyramid domain for ultrasonic speckle reduction. *IEEE Trans. Med. Imaging*, 26(2):200–211, 2007. 37

[ZZB15] Lin Zhang, Lei Zhang, and Alan C. Bovik. A feature-enriched completely blind image quality evaluator. *IEEE Trans. Image Processing*, 24(8):2579–2591, 2015. 31

List of Figures

List of Tables